UNIVERSITA' DEGLI STUDI DI MILANO

FACOLTA' DI MEDICINA VETERINARIA

CORSO DI DOTTORATO DI RICERCA

IN IGIENE VETERINARIA E PATOLOGIA ANIMALE

XXV CICLO

A preclinical investigative platform set up, as a tool for evaluating the efficacy of cetuximab in addition to the standard human malignant mesothelioma chemotherapy protocol

SSD VET 03

DOCENTE GUIDA

Prof. Eugenio SCANZIANI

COORDINATORE

Prof. Giuseppe SIRONI

TESI DI DOTTORATO DI RICERCA:

Dr. Michele Ardizzone

Matr. N. R08529

Anno Accademico 2011-2012

PREFACE

The diagnosis of "mesothelioma" is dreaded because it is, in fact, still today a death sentence. The onset of mesothelioma is not always connected with a pleural effusion, sometimes appearing only with pain and breathlessness. Diagnostic tests may range from chest X-rays, to CT scans of the chest-abdominal area and, in the event of a pleural effusion, to cytological analysis of the fluid in order to detect any tumour cells, to pleuroscopy with a pleural tissue biopsy and consequent histological examination. All these tests are completed by carrying out a PET scan that provides information not only on the presence of a tumour in various locations, but also on how active it is. Having reached a diagnosis, nowadays the first treatment is chemotherapy aimed at reducing the tumour mass and slowing down the evolution of the cancer. In some particular cases surgery may be attempted, removing the lung, the pleura, the diaphragm or, in a less demolitive form, resection of just the pleura: the main goal is to reduce pain and the pleural effusion. There is also another procedure known as "talc pleurodesis" that aims to contain or prevent pleural effusion. When the so-called "first line" standard chemotherapy gives no response, the next step may be experimental treatment. The objective is to stop development of the tumour by means of different methods, mainly using biotech drugs or immunotherapeutics which, on the one hand, inhibit cancer cell growth, and on the other hand, boost the immune system. It is still premature today to give ourselves false hopes about mesothelioma. As well as the willingness to make a commitment, considerable financial resources are needed. We place our hope in only one faith, science, and in only one method, research done in a network, that is, carried out by researchers from research institutes in several continents, working to find drugs that doctors can then administer to patients in treatment centres. Research has now started in earnest. Unfortunately, treatments for mesothelioma are only partially successful and do not significantly improve survival, although more cases are being recorded in which the patient lives with the illness for years rather than the few months expected some time ago. Today researchers are concentrating on therapies that allow the illness to become chronic, that is, seeking a sequence of therapeutic lines that allow people to live with the illness for longer. The scrupulous steps of research – the in vitro testing phase on cell cultures, the testing phase on animals and, later, on terminal patients, the phase of comparison between a certain number of patients treated with the new product and others not treated – are the guarantee of the thoroughness of research.

In the mid 1940s, Marlene Dietrich almost died of pneumonia. She was saved thanks to penicillin, discovered by chance when moulds were being studied. The people of Casale (but not only us) have a dream: that mesothelioma, like pneumonia today, will soon be nothing to fear. That we can say: I was ill, I was treated and I am cured. It is not only a plea; it is a secular prayer in chorus to researchers and doctors of good will and to all those who have the means to give financial support to this project for mankind.

Based on: Malapolvere - una città si ribella ai "signori" dell'amianto –
Silvana Mossano - Edizioni Sonda, 2010, pag. 185-188

ACKNOWLEDGEMENTS

Before describing the PhD project carried out over the last three years, it is only right for me to thank, in addition to Professor Eugenio Scanziani, my supervisor and mentor, for his valuable support, all those who have contributed to the success of the work.

Heartfelt thanks therefore go to:

Dr. Enrico Radaelli - Mouse and Animal Pathology Laboratory, Milano - my colleague and friend, for his constant, constructive help during this exciting task.

Dr. Laura Moro and Dr. Giulia Pinton - Dipartimento di Scienze del Farmaco, University of Piemonte Orientale A. Avogadro, Novara - for their part in carrying out *in vitro* activities.

Dr. Michele Cilli, Dr. Laura Emionite and Dr. Antonio Daga - National Institute for Cancer Research, Genova - for their help in carrying out *in vivo* activities and imaging diagnostics.

Dr. Elisabetta Sala - Università degli Studi di Milano - for her support in processing data acquired for imaging diagnostics.

Dr. Silvia Pompili - Merck Serono, Colleretto Giacosa - for preparing drugs to be tested in the main study.

Dr. Luciano Mutti - Presidente Gruppo Italiano Mesotelioma (GIMe) - for his crucial advice in setting up an experimental protocol in line with the needs of research into malignant mesothelioma.

Dr. Massimo Pastormerlo - Department of Pathological Anatomy, Ospedale Santo Spirito di Casale Monferrato - for his help in carrying out part of the immunohistochemistry panel for diagnostic markers of malignant mesothelioma.

Dr. Christopher Stroh, and Merck Serono as a whole, for their financial support and encouragement over these three years to bring the project to a successful conclusion.

INDEX

1 INTRODUCTION

Malignant mesothelioma and asbestos exposure

Mesothelioma is a malignant tumour that arises from mesothelial cells lining the serosal cavities; in most cases it originates in the pleura and in very few cases in the peritoneum; other sites of origin (pericardium and tunica vaginalis of the testis) are extremely rare. The tumour itself is rare with regard to spontaneous occurrence, however it is universally recognized that exposure to asbestos fibres is harmful to human health, since as well as causing an occupational illness known for many years, *asbestosis*, it also causes malignant pleural and peritoneal mesothelioma as well pulmonary carcinoma, as proven in many epidemiological studies published since the early 1960s (Wagner et al., 1960; Magnani et al., 2000, 2001, 2008; Ferrante et al., 2007).

Epidemiology of malignant mesothelioma

Asbestos was widely used in the past in many Countries, for its resistance to heat and its fibrous structure making it suitable for a broad range of uses, ***1)*** as insulation for roofs, ships and trains ***2)*** in the building sector, in particular for the production of tiles, and also ***3)*** to manufacture paints for motor vehicles, work overalls and many other items. Although past exposure to asbestos was more common in primary asbestos workers (handling raw asbestos material), however, over the last decades, a shift has been observed in the exposure history of human malignant pleural mesothelioma cases, to end-users often exposed when installing asbestos products or handling asbestos materials that are still in place, (e.g. construction workers, electricians, plumbers and heating workers). Even if the occupations with the highest risk of malignant mesothelioma belong to the first group (primary asbestos workers), the number of subjects at risk is presently much larger in the latter group (end-users). Environmental mesotheliomas are either linked to ‘‘natural’’ exposure in areas of the world where asbestos exists as a geological component of the soil (Turkey, Corsica, Cyprus and New Caledonia) or where it is often used for white-washing walls of houses, or to neighborhood exposures in people living close to asbestos mines or factories. Para-occupational cases are described in households of asbestos workers, mainly because of domestic exposure via clothes used at work.

There are prominent differences in incidences reported from different countries worldwide, varying from 7 per million (Japan) to 40 per million (Australia) inhabitants per year; in Europe, the incidence is 20 per million (Fig.1). It is reasonable to accept that these differences are mainly due to differences in historical asbestos import and consumption but an influence of diagnostic practices and awareness may also interfere (Scherpereel, 2010). Unfortunately, for very large parts of the world no data on malignant mesothelioma incidence and mortality are available, constituting a serious obstacle to the progress of knowledge on it; moreover, lack of data does not allow that a sufficient perception of the risk is reached. Therefore, even though diffusely and erroneously considered a “rare” tumour, because of its low incidence recorded in the worldwide population, if compared to other tumours, a dramatic increase of incidence is expected to occur in the next decades throughout the world

given the fact that also if the number of the countries that have banned the use of asbestos are growing, however it is still mined or used over the world (i.e. Canada, Brazil, Russia, India, China, Kazakhstan) (The Mesothelioma Center, 2012).

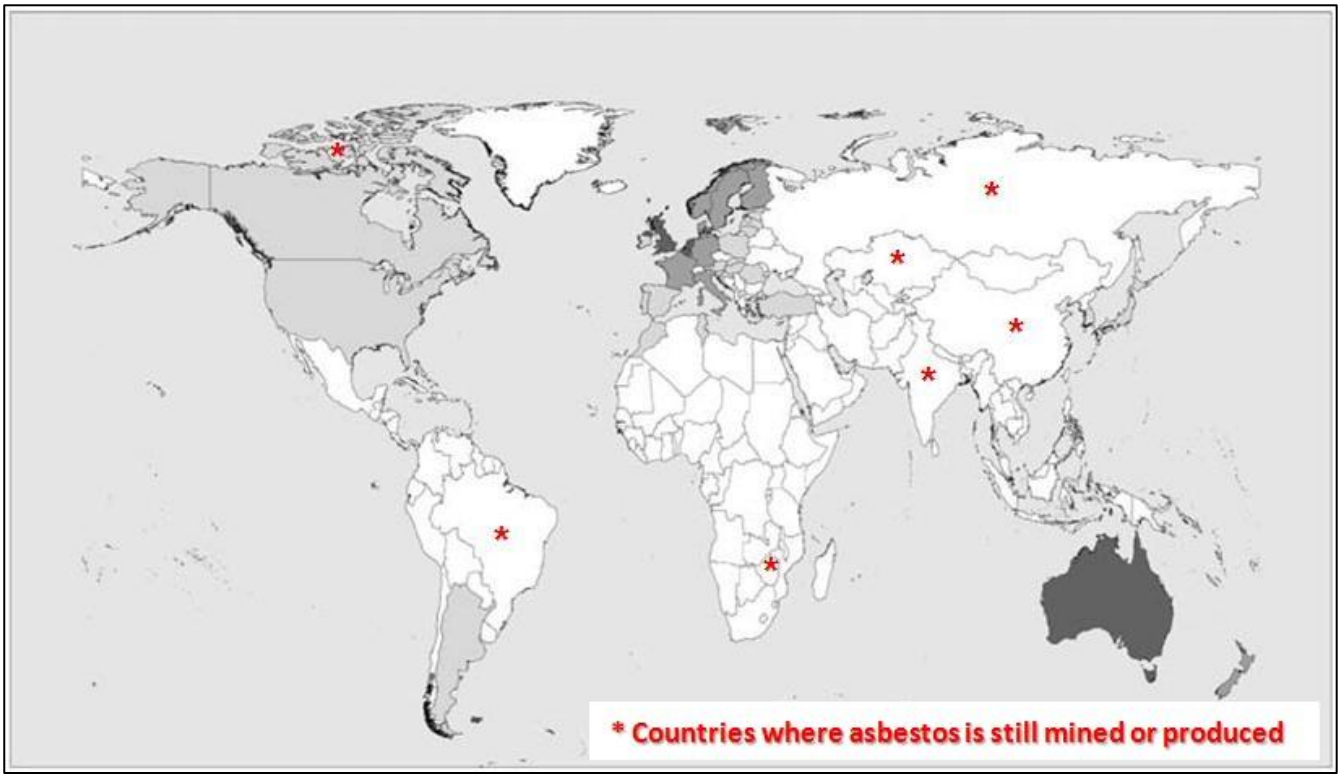

Fig.1: Estimated annual crude incidence rates of malignant mesothelioma in the world (modified from: Bianchi and Bianchi, 2007) ■ >20 cases per million; ■ 11–20 cases per million; ■ <11 cases per million; [ ] not available data

Expected peak incidences of malignant mesothelioma in the next future

Epidemiologists expect peak incidences of malignant mesothelioma in the very next decades, with differences between countries, which mainly reflect differences in asbestos consumption over the past decades. Because of the long latency of malignant mesothelioma and the national differences in the timing of reduction or ban of asbestos use, the timing of the peak incidence may vary from one country to another. Epidemiological projections have suggested that the incidence of malignant mesothelioma could still increase in Europe for the next 10 years, is expected to peak between 2015 and 2020, and may already have been reached in some countries (USA and Sweden). However, in countries that continue to use asbestos in the 21st century, the incidence of malignant mesothelioma is expected to increase in the forthcoming decades (Scherpereel, 2010).

Asbestos and malignant mesothelioma in Italy (with particular reference to Casale Monferrato)

Italy was one of the major producer and exploiter of asbestos until the end of 1980s. In the period between the end of the second world war until 1992, when asbestos was banned, almost 4 million tons of raw asbestos were produced and other 50 thousand tons every year were imported.

In Casale Monferrato, a small city of 35 thousand people, situated in the eastern part of Piedmont region, a factory working asbestos products (Eternit) was active from 1907 until 1986, with all the known consequences on workers, people and environmental contamination over a long period of time. At present the greatest problem of environmental contamination in Casale Monferrato and surrounding areas is the presence of latent products or waste resulting from the working of asbestos in the past, the so-called "*polverino (dust)*", used to fill courtyards, pavements and roads, to lag gas and water pipes and, to a much lesser extent, worn roof-covering slabs and tiles.

Taking into account that the risk of malignant mesothelioma onset is directly related to the dose and that it is impossible to define a threshold of cumulative exposure below which there is no increased risk, and considering the long latency of 20-30 years between exposure and mesothelioma onset, it is evident that all individuals who have been exposed to asbestos are still considered to be a population at risk (Iwatsubo, 1998), as demonstrated by the high incidence of this illness among the inhabitants of Casale Monferrato and surrounding areas. Currently about 35 new cases of malignant mesothelioma occur every year, corresponding to a crude incidence of 86 and 89 cases per 100.000 person/years in men and women, respectively (2005-2009 statistics from the Piedmont Malignant Mesothelioma Registry).

Malignant mesothelioma and the translational medicine therapeutic approach.

Over the last 15 years, our knowledge of the biology of malignant mesothelioma has increased considerably, in parallel with improvement in the accuracy and standardization of cyto-histopathological characterization and diagnostic imaging. Nevertheless, no curative treatments are available at present and the standard "multimodal" therapeutic approach consists of a combination of chemotherapy, surgery and radiation with a poor prognosis. The median survival is commonly estimated to be between 9 and 12.4 months, depending on many factors, including the stage, the location and the spread of the cancer and the morphological appearance. Indeed malignant pleural mesothelioma exhibits a high resistance to chemotherapy and only a few patients are candidates for radical surgery.

New chemotherapies and therapeutic strategies are continuously under review and because of limited data on the best combination treatment; patients who are considered candidates for a multimodal approach should be included in a prospective trial at a specialized center (Scherpereel, 2010). The unmet medical need for malignant mesothelioma therapy turns researchers' attention to *translational medicine*, a scientific approach that facilitates the translation of findings from basic science to practical applications that enhance human health and well-being, turning appropriate biological discoveries into new drugs or medical strategies in the treatment of patients.

Malignant Pleural Mesothelioma: diagnostic in human

The clinical manifestations of human malignant pleural mesothelioma (hMPM) are usually nonspecific and insidious and should not be used alone as diagnostic criteria, even in case of previous asbestos exposure. An early chest radiograph, usually shows pleural effusion or thickening, however this alone should not be consider sufficient for the diagnosis of hMPM. When a mesothelioma is suspected on clinical or radiological data, thoracoscopy is the best method to obtain the diagnosis. A chest CT scan is unsuitable for definitive diagnosis of hMPM, but diffuse or nodular pleural thickening are suggestive of the disease. MRI and PET scanning unfortunately are not relevant for the diagnosis of all mesothelioma types. As pleural effusion is usually the first clinical sign of hMPM, cytology is often the first diagnostic examination to be carried out, even if it is not recommended to make a diagnosis based on cytology alone because of the high risk of diagnostic error. Therefore it is recommended that a cytological suspicion of mesothelioma is followed by tissue confirmation. Thoracoscopy should be preferred for diagnostic investigation, allowing complete visual examination of the pleura and multiple, deep and large biopsies, providing a diagnosis in 90% of cases. Finally, the accurate diagnosis of hMPM, is made on histopathological examination which can be difficult because of its heterogeneous morphology; however the microscopic characteristics of hMPM are now well defined in the new international classification of pleural tumours and it is strongly suggested that a final diagnosis of hMPM always be based on immunohistochemical examination.

For this purpose the International Mesothelioma Panel has put forward various recommendations and the proposed immunohistochemical approach depends on whether the tumour subtype of hMPM is epithelioid or sarcomatoid. To separate epithelioid subtype from adenocarcinoma (Fig.2), it is recommended that two markers with positive diagnostic value for mesothelioma (e.g. anticalretinin and anti-Wilms tumour antigen-1 or anti-cytokeratin 5/6 etc.) and two markers with negative diagnostic value (e.g. anti-Ber-EP4, or monoclonal anti-carcinoembryonic antigen) be used to validate the diagnosis. To separate sarcomatoid subtype from squamous and transitional cell carcinoma (Fig.3), it is recommended to use two broad-spectrum anti-cytokeratin antibodies and two markers with negative predictive value to confirm the diagnosis. Lastly, electron microscopy and molecular biology should not be carried out routinely to confirm the diagnosis of Mesothelioma (Scherpereel, 2010).

Antibody	Current value	Mesothelioma	Positivity	Adenocarcinoma	Positivity
Mesothelioma					
Calretinin	Essential	Positive (nuclear and cytoplasmic)	80-100%	Usually negative	5-10% cytoplasmic positivity of lung adenocarcinoma
Keratin CK 5/6	Useful	Positive (cytoplasmic)	60-100%	Usually negative	2-10%focal positivity
WT-1	Useful	Positive (nuclear)	43-93%	Lung adenocarcinoma are negative	0%
EMA	Useful	Positive (membranous)	60-100%	Positive (cytoplasmic)	70-100%
Podoplanin	Useful	Positive (membranous)	80-100%	Usually negative	7% focal positivity
Lung adenocarcinoma					
CEA monoclonal	Very useful	Almost invariably negative	0%	Positive (cytoplasmic)	50-90%
CD15	Useful	Never expressed in mesothelioma	0%	Positive (membranous)	50-70% focally positive
Ber-EP4	Very useful	Positive or negative (membranous)	Up to 20% can be focally positive	Positive (membranous)	95-100%
TTF-1	Very useful	Never expressed	0%	Positive (nuclear)	70-85% of lung adenocarcinoma
B72.3	Very useful	Rarely positive	<1%	Positive (cytoplasmic)	70-85% of lung adenocarcinoma
Breast carcinoma					
ER	Very useful	Never expressed in mesothelioma	0%	Positive nuclear staining	~70%
CK 5/6: cytokeratin 5/6; WT-1: Wilms tumour antigen-1; EMA: epithelial membrane antigen; CEA: carcinoembryonic antigen; TTF-1: thyroid transcription factor-1; ER: endoplasmic reticulum marker.					

Fig.2: IHC to distinguish epithelioid mesothelioma from adenocarcinoma (modified from Scherpereel, 2010)

Antibody	Current value	Mesothelioma	Positivity	Squamous and transitional cell carcinoma	Positivity
Mesothelioma					
Calretinin	Useful	Positive (strong nuclear and cytoplasmic)	80-100%	Usually cytoplasmic positivity	5-40%
Keratin CK 5/6	Not useful	Positive (cytoplasmic)	60-100%	Cytoplasmic positivity	100%
WT-1	Very useful	Positive (nuclear)	43-93%	Negative	0%
Lung adenocarcinoma					
P63	Very useful	Almost always negative	0%	Positive (nuclear)	~100%
Ber-EP4	Useful	Positive or negative	Up to 20% are positive	Positive (cytoplasmic)	80-100%
MOC 31	Useful	Positive or negative (focal membranous staining)	2-10%	Positive (membranous)	97-100%
CK 5/6: cytokeratin 5/6; WT-1: Wilms tumour antigen-1;					

Fig.3: IHC to distinguish sarcomatoid mesothelioma from squamous and transitional cell carcinoma (modified from Scherpereel, 2010)

Malignant mesothelioma: animal models

Spontaneous mesotheliomas occur rarely in humans and similarly way occur very rarely in rats and mice; however it is now well established that asbestos fibres induce pleural and peritoneal mesotheliomas also in rodents.

Since the 1950-60s epidemiological studies in human have suggested that the risk of pleural and peritoneal mesothelioma was related to past exposure to asbestos dust, in particular for miners and workers occupationally exposed to asbestos fibres. This knowledge moved the interest of researchers to investigate the potential mechanisms at the basis of this relationship. Numerous animal models have been developed over the years to study mesotheliomas and to deeply investigate the factors involved in malignant transformation, invasion and metastasis, as well as to examine response to therapy.

A first large scale experiment conducted to study potential cancerogenicity of asbestos by intra-pleural injection in specific pathogen-free (SPF) and standard rats, was started in November 1962; a preliminary report on the tumours arising in the SPF rats was given by Wagner in 1965, including detailed descriptions of the material, methods and histological findings. At the Second International Congress on the Biological Effects of Asbestos held in Dresden in 1968, the results of both experiments (SPF and standard rats) were presented and in a final paper in 1969, the statistical basis of these experiments and the results were considered. This study was an important first step in the research for mesothelioma demonstrating with scientific evidence that pleural mesotheliomas can be easily induced in animals by intra-pleural injection of asbestos fibres (Wagner and Berry, 1969).

Even though this study established factors influencing the occurrence of these tumours, such as the type of fibre, the mechanism of access to the pleura and peritoneal surfaces, and the importance of particle size, however the mechanism by which asbestos induced tumours in humans and animals still remained unknown.

In the following decades researchers exploited the possibility to induce mesothelioma in rodents together with the new technologies having become available in the meantime, building new animal models to be used in the field of mesothelioma research. Syngenic models were therefore obtained by injecting rodent mesothelioma cell lines both in wild type (Shi et al., 2011) and in genetically engineered rodents (GEM). GEM syngenic mice such as Heterozygous $p53^{+/-}$ knockout mice (Jackaman et al., 2003) or $Nf2^{+/-}$ knockout mice (Vaslet et al., 2002; Altomare et al., 2005) allowed the development of asbestos-induced mesothelioma more rapidly and at a higher incidence than wild-type littermates, resulting therefore useful to investigate the biology and the molecular features of the tumour. Although GEM or syngenic rodent tumour models are useful in many cases, they usually cannot fully reproduce the genetic complexity of human tumours and do not often predict exactly what will happen in the human tumour with regard to therapeutic response. In this case, to know whether a patient's tumour will respond to a specific therapeutic regimen, the best approach is to examine the response of that human tumour, not a mouse or rat tumour, to the therapy. This is where the human malignant mesothelioma xenograft on athymic nude severe combined immunodeficiency mice (SCID), or non-obese diabetic (NOD)/SCID humanized mice, become extremely helpful.

Human malignant mesothelioma xenograft and in-vivo bioluminescence imaging in research

Human tumour xenograft mouse model is widely used in research particularly to examine biological responses of tumours to drugs, featuring the complexity of genetic and epigenetic abnormalities that exist in the human tumour population. In xenograft models, human tumour cells are transplanted into immunocompromised mice that do not reject human cells, either under the skin (subcutaneous transplant) or into the organ type in which the tumour originated (orthotopic transplant); compared to subcutaneous xenografts, orthotopic xenografts better reproduce the organ environment in which the tumour grows, including tumour stroma, so that the effect of the tumour on its microenvironment can be reproduced and modulated, albeit with the exception of certain T-cell populations (athymic mice). By using this model, multiple therapies or therapeutic procedures can be therefore tested and the biological response of tumoural cells evaluated on the basis of tumour growth rate, shrinkage/regression and animal survival (Bertino et al., 2008; Yanagihara et al., 2010; Silberhumer et al., 2010; Mingqian et al., 2011; Au et al., 2012).

A challenge presented with orthotopic models is the difficulty of following tumour growth, as compared with subcutaneous models where tumour dimension is easily measurable with non-invasive methods. However, the recent development of new imaging techniques such as micro-PET or bioluminescent imaging may minimize this problem. Indeed bioluminescence imaging is a highly sensitive, non-toxic analytical technique that is particularly well suited to long-term studies in living organisms with a particularly strong impact in studies of tumour progression. Neoplastic cells are pre-labeled by transfection with a luciferase reporter gene and then transplanted in mice; when required, mice are immobilized by anesthesia and imaged non-invasively with a highly sensitive, low-noise camera after being administered luciferin a few minutes before imaging. The camera measures the intensity of light emitted by the reaction between endogenous luciferase and the luciferin injected and the amount of photons emitted is representative of the neoplastic cell activity.

Combination of a xenograft model with bioluminescence imaging is also important from an ethical point of view as in accordance with Animal Welfare standards as regards the 3R's, by reducing both the number of animals used in the experiment and the stress or discomfort induced by using non invasive diagnostic techniques.

All these aspects which are certainly positive from different points of view were considered extremely useful and suited to the purposes of the PhD program and will therefore be better described in the next chapters.

2 PURPOSES OF THE PhD PROGRAM

The purposes of the overall PhD program were on the one hand ***1)*** to set up a preclinical investigative platform screening the efficacy of anticancer drugs in human malignant mesothelioma cell lines, based on the integration of data from *in vitro* and *in vivo* activities, and on the other hand ***2)*** to adopt this platform investigating the potential benefit of an anticancer monoclonal antibody (cetuximab) in the treatment of human malignant mesothelioma, both as single agent or in adjunct to the standard first line chemotherapy protocol with folate antimetabolite (pemetrexed) and platinum (cisplatin) compounds.

The experimental phases conducted during the overall PhD program and the outline of the final draft of the thesis reflect this dual objective as shown in Tab.1:

Tab.1: Summary of experimental phases

PLATFORM SETUP
In Vitro Tumour Growth Assays (REN and MSTO-211H cells) o cell proliferation as determined by direct counting o assay for anchorage-independent cell growth (colony formation assay) o phosphorylation analysis (EGFR, AKT and ERK)
In Vitro Bioluminescence Imaging (REN luc$^{+/+}$ and MSTO-211H luc$^{+/+}$ cells) o bioluminescence quantification
In Vivo Pilot Study (REN luc$^{+/+}$ and MSTO-211H luc$^{+/+}$ cells) o first phase o second phases
EFFICACY EVALUATION
In Vivo Main Study (REN luc$^{+/+}$ and MSTO-211H luc$^{+/+}$ cells)

Preclinical investigative platform setup

The use of cell lines in scientific research, whether healthy or diseased (i.e. tumoural), is closely connected with the possibility of studying their response to the experimental conditions applied, such as, for example, treatment with chemical, physical or biological agents. Although several mesothelioma cell lines have been immortalized over the last few years starting from primary tumours, and are nowadays commonly used in the conduct of preclinical *in vitro* and *in vivo* studies to discover new therapies for human malignant mesothelioma, most of the works published tend to focus on specific endpoints, according to the field of interest of the researcher.

In this PhD program we combined different methodologies published in literature, to generate a single preclinical investigative platform, consisting of *in vitro* and *in vivo* models, bioluminescence imaging and histopathology investigations, with the aim of creating a "*tool*" easily usable to investigate the response of human mesothelioma cells to drug compounds, based on a step-wise approach.

Efficacy evaluation of cetuximab in animal models

The rationale behind the interest for cetuximab is based on the knowledge that *epidermal growth factor receptor* (EGFR) is expressed on normal mesothelial cells, being involved in the response to asbestos fibres exposure and that it is also responsible for the proliferative effects induced by the *epidermal growth factor* (EGF)-dependent autocrine loop in malignant mesothelioma cells. Indeed EGFR is often autophosphorylated in mesothelial cells and overexpressed after exposure to asbestos fibres in malignant mesothelioma cells, leading to the hypothesis that its inhibition by specific molecules could significantly impact on therapeutic success.

Cetuximab is a monoclonal antibody inhibitor which binds specifically to EGFR on both normal and tumour cells, and competitively inhibits the binding of this and other ligands (i.e. Transforming Growth Factor-alpha), preventing EGFR activation and dimerization and ultimately inducing receptor internalization and downregulation. This interference with EGFR signalling (i.e. increases in cellular proliferation, motility, angiogenesis and apoptosis inhibition) could play a pivotal role in the inhibition of malignant mesothelioma cell growth, both as a single agent or in adjunct to the standard first line chemotherapy protocol with multi-targeted antifolate drugs which block the enzymes necessary for DNA copying and cell division and platinum compounds which kill cancer cells by binding to DNA and interfering with its repair mechanism, eventually leading to cell death.

The efficacy of cetuximab inhibition of human malignant pleural mesothelioma (hMPM) cells growth *in vitro* and also *in vivo* was tested both as a single agent and in combination with pemetrexed and cisplatin. Bioluminescence imaging and histopathology data were used to characterize tumour growth and behaviour in response to the treatment regimens in hMPM xenograft mice.

3 MATERIALS AND METHODS

3.1 IN VITRO STUDIES

Two studies were conducted *in vitro* ***1)*** to test the response of human malignant pleural mesothelioma (hMPM) cell lines to treatment with cetuximab (tumour growth assays) and ***2)*** to assess their luciferase activity after retroviral infection (bioluminescence quantification).

3.1.1 Cell lines

Two hMPM cell lines made available by the University of Piemonte Orientale A. Avogadro were used in the Tumour Growth Assay: the biphasic derived MSTO-211H cell line obtained from the National Institute for Cancer Research, Genova - Cell-bank and the epithelioid derived REN cell line, isolated, characterized (Smythe et al., 1994) and kindly provided by Dr. Albelda S.M. (University of Pennsylvania, Philadelphia; PA). Cells were cultured in standard conditions.

Both the MSTO-211H and REN cells were then infected at the National Institute for Cancer Research of Genova with a bicistronic retrovirus expressing the Luciferase gene (Luciferase synthesis) and the Neomycin phosphotransferase gene (aminoglycoside 3'-phosphotransferase synthesis) for Geneticin-resistant selection. The newly generated MSTO-211H $luc^{+/+}$ and the REN $luc^{+/+}$ cell lines were used to perform bioluminescence quantification *in vitro*.

3.1.2 Tumour Growth Assays

REN and MSTO-211H were seeded and tested in vitro as follows:

Cell proliferation assay: MSTO-211H or REN cells were seeded at a density of $1x10^5$ cells/well into six-well plates in growth medium supplemented with FBS and incubated overnight at 37°C in a humidified environment containing 5% CO2 to allow the cells to become adherent. After 24 hours the cells were grown as indicated in complete medium or treated with 0.1mM cetuximab and/or EGF 5 ng/ml for a further 24 hours. Cells were then trypsinized and stained with Trypan blue. The number of viable cells was counted in a Burker chamber within 5 minutes of staining.

Colony formation assay: a base layer of 0.6% agar in complete medium was plated in six-well plates and allowed to solidify. Next, wells were overlaid with 5×10^3 cells per well in a 0.3% agar. A growth control well was also included with 5×10^3 cells in medium alone (no agar) for each cell line. The plates were incubated at 37°C, 5% CO_2 for 15 days and checked every 2 days for colony formation. The treatment with 0.1mM cetuximab

and/or 1mg/ml Doxorubicin was performed every 2 days. At day 14, individual colonies (defined as clusters of 15 or more cells) were counted in 10 random fields.

Phosphorylation analysis: analysis of pEGFR, pAkt and pERK phosphorylation was performed 5 minutes after treatment with EGF 5 ng/ml and/or Erbitux 0.1mM. Cells were extracted with NP-40 lysis buffer (1% NP-40, 150 mM NaCl, 50 mM Tris-HCl pH 8, 5 mM EDTA, 10 mM NaF, 10 mM Na4P2O7, 0.4 mM Na3VO4, 10 mg/ml leupeptin, 4 mg/ml pepstatin and 0.1 Unit/ml aprotinin). Cell lysates were centrifuged at 13000 x g for 10 minutes and the supernatants were collected and assayed for protein concentration using the Bradford protein assay reagent (Bio-Rad). Proteins were separated by SDS-PAGE under reducing conditions. Following SDS-PAGE, proteins were transferred to nitrocellulose, reacted with the specific antibodies indicated and then detected with horseradish peroxidase-conjugated secondary antibodies and the chemioluminescent ECL reagent. Densitometric analysis was performed using the GS 250 Molecular Imager (Bio-Rad).

Drugs: drugs and compounds used in the *in vitro* tumour growth assays were cetuximab, a monoclonal antibody provided by Merck Serono; Doxorubicin, an anthracycline antibiotic used in cancer chemotherapy and Epidermal Growth Factor compound, both provided by the University of Piemonte Orientale A. Avogadro.

3.1.3 Bioluminescence Quantification

Luciferase activity of retrovirally infected and selected MSTO-211H $luc^{+/+}$ and REN $luc^{+/+}$ cells was assessed after a 10-minutes incubation with 150 microg/mL D-luciferin diluted in tissue culture medium with 30 thousand cells/well, to confirm and quantify their base-line signals. Bioluminescence signals were monitored using the IVIS system 100 series (Caliper Corp.); regions of interest (ROI) were quantified as total photon counts using Living Image software (Caliper Corp.).

3.2 IN VIVO STUDIES

Two studies were conducted *in vivo* in human malignant pleural mesothelioma (hMPM) xenograft mice: ***1)*** on the one hand to define the preclinical investigative platform setup (Pilot Study) and ***2)*** on the other hand to assess the potential additional benefit of cetuximab in the treatment of malignant mesothelioma in adjunct to the standard chemotherapy protocol with pemetrexed and cisplatin (Main Study).

In both studies the test system, the hMPM cell lines and the bioluminescence imaging procedures used were the same.

3.2.1 Test system

Female CD1-Foxn1$^{nu/nu}$ athymic nude mice (CD1-Foxn1$^{nu/nu}$ mice) were chosen as, in this model, transplanted human tumour cells are readily accepted and not rejected. Mice were maintained and handled at the National Institute for Cancer Research of Genova under aseptic conditions in rooms of a limited access, barrier rodent facility having the following environmental conditions: temperature 22° C ± 2°C, relative humidity 55% ± 15%, about 12 air changes per hour filtered on HEPA, artificial lighting with a circadian cycle of 12 hours of light (7 a.m. - 7 p.m.). The mice were kept in polycarbonate cages with stainless steel mesh tops and soft wood chip bedding. On arrival, the mice were about 4 to 5 weeks old and their health status was assessed. The mice were weighed, to ascertain that their weight conforms to that required (about 16-20 g on arrival). Before commencement of the experimental phase, an acclimatization period (at least 7 days) was performed during which the health status of the mice was assessed by daily observation. A certified diet, analyzed for nutrients, was offered to the animals “ad libitum”. Filtered and autoclaved water was distributed in sterilized plastic bottles. The drinking water was offered to the animals "ad libitum". During the experiments mice were inspected daily for mortality.

3.2.2 Cell lines

Retrovirally infected and selected MSTO-211H luc$^{+/+}$ and REN luc$^{+/+}$ cell lines, both expressing the *Luciferase gene* (Luciferase synthesis) and the *Neomycin phosphotransferase gene* (aminoglycoside 3'-phosphotransferase synthesis) for Geneticin-resistant selection, were transplanted in mice by intraperitoneal injection (orthotopic xenograft), in 0.5 mL of Ham’s F-12 medium. The amount of cells injected varied between cell lines and studies and is detailed in the respective sections.

3.2.3 Bioluminescence quantification

MSTO-211H luc$^{+/+}$ or REN luc$^{+/+}$ activity was assessed 10-minutes after incubation with 150 microg/mL D-luciferin, injected intraperitoneally. Bioluminescence signals were monitored using the IVIS system 100 series (Caliper Corp.); regions of interest (ROI) were identified around the tumour sites and were quantified as total photon counts using Living Image software (Caliper Corp.).

3.3 PILOT STUDY

The pilot study to define the preclinical investigative platform setup was conducted in two different phases, as outlined in Fig.4:

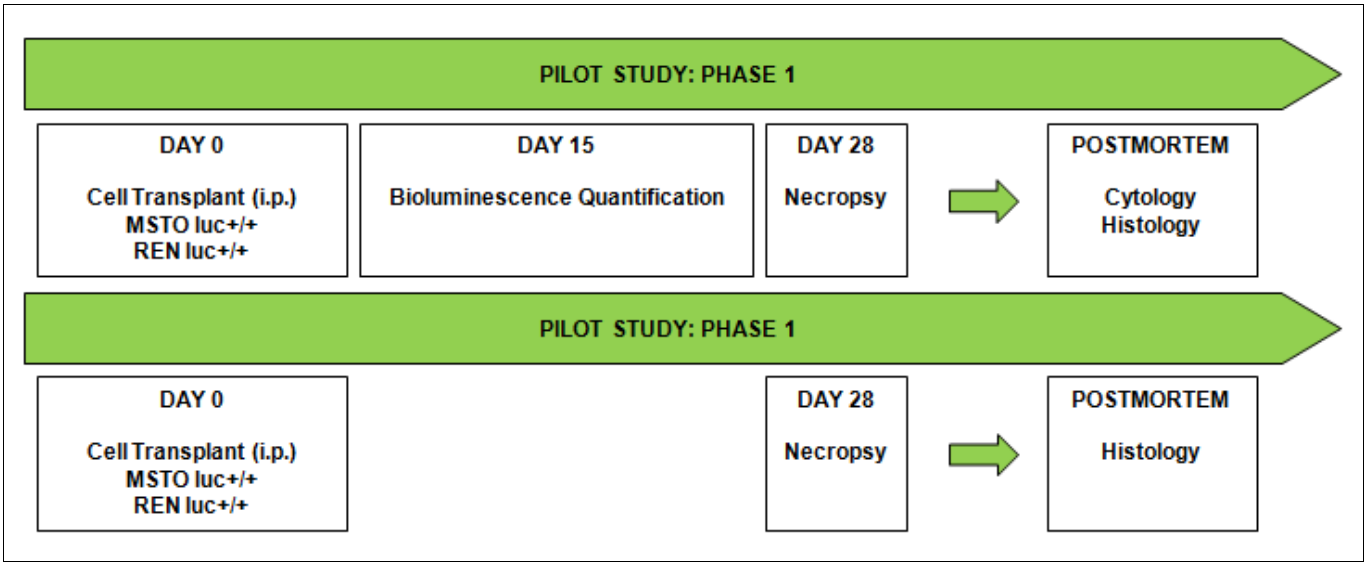

Fig.4: Pilot study outline

3.3.1 First phase pilot study

Orthotopic transplant: on day 0, three CD1-Foxn1$^{nu/nu}$ mice received i.p. injections of 0.5, 1 and 5 million/animal MSTO-211H luc$^{+/+}$ cells or REN luc$^{+/+}$ cells.

Bioluminescence quantification: was conducted 15 days after tumour cell inoculation ***1)*** to confirm tumour growth and ***2)*** to select the number of injected cells in the main study.

Necropsy: was conducted 28 days after tumour cell inoculation; mice underwent CO_2 anaesthesia shortly before being sacrificed by exsanguination.

Cytological evaluation: at necropsy, ascitic fluid in the abdominal cavity was collected in all sacrificed animals, to assess any possible added value of this data in the main study. Due to the scant amount collected, aspiration was performed by microcapillary tubes and smears were immediately prepared on glass slides. May Grunwald Giemsa staining was performed.

Sampling and fixation: at necropsy, tissues sampled were fixed “wholebody” in 10% Neutral Buffered Formalin (NBF) for 72 hours and then stored in 70% alcohol solution (see appendix 4). Wholebody fixation was chosen to

shorten the time between sacrifice and beginning of fixation while long-term storage was in alcohol solution to protect tissues from the risk of epitope formalin-related masking, with a view to further immunohistochemistry evaluation.

Histotechnique (routine): selected organs and tissues (i.e. ovaries, uterus, vagina, kidneys, adrenals, diaphragmatic muscle, lungs, heart, stomach, small and large intestines, spleen, pancreas and liver), were trimmed and embedded in paraffin blocks according to the International Guidelines jointly published by the Registry of Industrial Toxicology Animal-data (RITA) and the North American Control Animal Database (NACAD) groups (Ruehl-Fehlert et al., 2003; Kittel et al., 2004; Morawietz et al., 2004) and slides were stained with hematoxylin and eosin.

Histology evaluation: hematoxylin & eosin-stained sections were evaluated ***1)*** to qualify "wholemount" fixation of tissues and ***2)*** to assess the amount of tumour in all animals.

3.3.2 Second phase pilot study

Orthotopic transplant: on day 0, ten CD1-Foxn1$^{nu/nu}$ mice received i.p. injection of 1 million/animal MSTO-211H luc$^{+/+}$ cells or i.p. injection of 2 million/animal REN luc$^{+/+}$ cells.

Necropsy: was conducted 28 days after tumour cell inoculation; mice underwent CO_2 anaesthesia shortly before being sacrificed by exsanguination.

Sampling and fixation: at necropsy, tissues sampled were fixed "wholebody" in 10% Neutral Buffered Formalin (NBF) for 72 hours and then stored in 70% alcohol solution (see appendix 4).

Histotechnique (wholebody): abdominal organs and tissues (i.e. liver, GI tracts, pancreas, spleen, mesentery and mesenteric lymph nodes) were trimmed "en bloc", embedded in paraffin blocks (see appendix 5) and slides were stained with hematoxylin and eosin. Wholebody histotechnique was chosen since the routine histotechnique previously used did not permit an adequate evaluation of the smallest tumoural masses scattered around the peritoneum and unrelated to parenchymal structures.

Histology evaluation: to test and standardize the "wholebody histotechnique" as a potentially useful tool for histological data interpretation in the main study, and to assess the reproducibility of the sampling procedure, hematoxylin & eosin-stained sections of the "en bloc" abdominal organs collected were evaluated, scoring the presence or absence of the tumour at the first cut section level obtained.

3.4 MAIN STUDY

Once the preclinical investigative platform had been setup, a main study was started to investigate the potential benefit of a monoclonal antibody (cetuximab) in the treatment of human malignant mesothelioma, both as a single agent or in adjunct to the standard first line chemotherapy protocol with a folate antimetabolite (pemetrexed) and a platinum compound (cisplatin), outlined as shown in Fig.5:

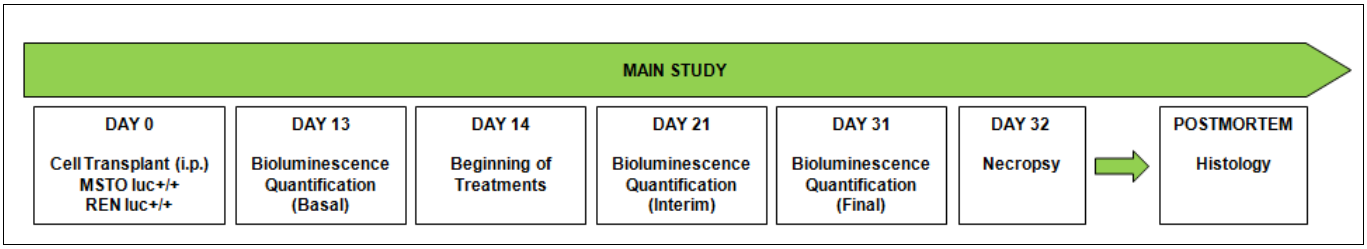

Fig.5: Main Study outline

3.4.1 Orthotopic transplant

On day 0, thirty five CD1-Foxn1$^{nu/nu}$ mice received i.p. injections of 1 million/animal MSTO-211H luc$^{+/+}$ cells and forty CD1-Foxn1$^{nu/nu}$ mice received i.p. injections of 2 million/animal REN luc$^{+/+}$ cells.

3.4.2 Bioluminescence quantification

Thirteen days after tumour cell inoculation, during the post-transplant period before the beginning of treatments, on all seventy five mice, to confirm the presence of tumour, to select and allocate animals to the dose groups by randomization based on ROI intensity (see appendix 1) and to define reference values for each animal (basal quantification);

Twenty one days after tumour cell inoculation, between the first and second cycle of treatments, on the sixty one mice randomized for the entire experiment (interim quantification);

Thirty one days after tumour cell inoculation, at the end of the second cycle of treatments, to evaluate tumour growth response at the end of treatment periods (final quantification).

3.4.3 Study design

Treatments started 14 days after orthotopic transplant; cetuximab provided by Merck Serono, pemetrexed provided by Ely Lilly, cisplatin and PBS solution provided by the National Institute for Cancer Research, were administered according to the scheme reported in Tab.2:

Tab.2: treatment scheme – main study

Group	No. of animals		Drug	Dose mg/kg	Volume administered mL/animal (i.p.)	Treatment scheme
	MSTO 211H	REN				
1	5	5	PBS solution	-	0.15	day 17, 24
2	5	5	cisplatin pemetrexed	5 150	0.15 0.15	days 17, 24 days 17 to 21 & 24 to 28
3	5	5	cetuximab	3	0.15	days 14, 20, 27
4	5	5	cetuximab	10	0.15	days 14, 20, 27
5	5	5	cetuximab	30	0.15	days 14, 20, 27
6	6	5	cetuximab cisplatin pemetrexed	30 5 150	0.15 0.15 0.15	days 14, 20, 27 days 17, 24 days 17 to 21 & 24 to 28

3.4.4 Pathology

Necropsy: was conducted 32 days after tumour cell inoculation; mice underwent CO_2 anaesthesia shortly before being sacrificed by exanguination.

Sampling and fixation: tissues sampled at necropsy were fixed "wholebody" in 10% Neutral Buffered Formalin (NBF) for 72 hours and then stored in 70% alcohol solution (see appendix 4).

Histotechnique (wholebody): abdominal organs and tissues (i.e. liver, GI tracts, pancreas, spleen, mesentery and mesenteric lymph nodes), thoracic organs and tissues (i.e. trachea, lungs, heart and tracheobronchial lymph nodes) and diaphragm were sampled "en bloc", embedded in paraffin blocks and a set of three slides per each animal was prepared including abdominal and thoracic organs and tissues and diaphragm muscle.

Histology evaluation: hematoxylin and eosin (H&E) and immunohistochemistry (IHC) stainings were performed on neoplastic samples for the following purposes:

a) ***H&E*** was focused on the comparison between the two cell lines together or between groups within each cell line as regards ***1)*** the morphological description of the tumour growth pattern and ***2)*** the characterization of its biological behavior, measured as the tendency of the tumour to growth and spread within the abdominal cavity and its surroundings.

b) ***IHC*** was carried out with the following indications:

   i. A first panel of antibodies (Tab.3) was used in two untreated control animals injected both with MSTO-211H luc$^{+/+}$ or REN luc$^{+/+}$ cell lines, to confirm their mesothelial origin. According to the indication of the European Respiratory Society and the European Society of Thoracic Surgeons for the management of malignant pleural mesothelioma (Scherpereel, 2010), since the two subtypes used in the main study are epithelioid for the REN luc$^{+/+}$ cells and mixed epithelioid/sarcomatoid for the MSTO-211H luc$^{+/+}$ cells, the markers used were carcinoembryonic antigen (CEA) and Ber-EP4 with negative diagnostic value for mesothelioma and Calretinin, Wilm's tumour (WT1) and cytokeratin 5/6 with positive diagnostic value for mesothelioma:

Tab.3: Antibodies used in IHC assay – mesothelial origin confirmation (diagnostic marker)

ANTIBODY	COMPANY	CLONE/COMPANY CODE	WORKING DILUTION	INCUBATION TIME	SECONDARY ANTIBODY
Carcinoembryonic antigen (CD66e)	Novocastra Liquid	12-140-10 / NCL-L-CEA-2	NA	NA	NA
Epithelial antigen	Dako	Ber-EP4 / M0804	NA	NA	NA
Calretinin	Dako	DAK Calret1 / M7245	NA	NA	NA
Wilms' Tumour antigen 1	Epitomics	CAN-R9(IHC)-56-2 / 2797-1	1:100	1h RT	Biotinylate anti-rabbit
Cytokeratin 5/6	Dako	D5-16 B4 / M7237	NA	NA	NA

NA: not applicable (IHC performed at the Department of Pathological Anatomy at the Santo Spirito Hospital of Casale Monferrato (AL) - Internal standardized protocols were used. RT: room temperature

ii. A second panel of antibodies (Tab.4) was used in two animals per group injected with MSTO-211H luc$^{+/+}$ or REN luc$^{+/+}$ cell lines, both in untreated control and treated animals given pemetrexed and cisplatin alone (group 2) or in combination with cetuximab (group 6), to better characterize the tumour biology as regard the evidence of apoptosis, proliferation and angiogenesis changes:

Tab.4: Antibodies used in IHC assay – angiogenesis, apoptosis and proliferation (biological tumour parameters)

ANTIBODY	COMPANY	CLONE/COMPANY CODE	WORKING DILUTION	INCUBATION TIME	SECONDARY ANTIBODY
Cleaved Caspase-3	Cell Signaling	Asp175/ 9661	1: 2000	1h RT	Biotinylate anti-rabbit
Ki67	Thermo Scientific	SP6 / RM-9106-5	1: 150	1h RT	Envision rabbit HRP
Anti-mouse CD31	Dianova	SZ31 / DIA 310	1: 50	1h RT	Biotinylate anti-rabbit

RT: room temperature

For Caspase 3 and Ki-67, three different fields (400x magnification) from each animal were chosen, consisting of well representative neoplastic nodules. The number of immunopositive nuclei was counted over the total number of neoplastic cells and the mean percentages of the three fields were calculated in each untreated control and treated animal.

For CD31 three different fields (400x magnification) from each animal were chosen, consisting of well representative neoplastic nodules. Each field had a maximum area of 198918.8 μm^2. The number of small immunopositive vessels was determined and related to the total area of the tumour examined, to calculate the number of vessels in 500μm^2.

iii. A third panel of antibodies (Tab.5) was used in one animal per group injected with MSTO-211H luc$^{+/+}$ cell line, both in untreated control and treated animals given pemetrexed and cisplatin alone (group 2) or in combination with cetuximab (group 6), to characterize changes in selected markers representative of the major signaling transduction pathways involved in the pathogenesis of mesothelioma:

Tab.5: Antibodies used in IHC assay – signal transduction patways

ANTIBODY	COMPANY	CLONE/COMPANY CODE	WORKING DILUTION	INCUBATION TIME	SECONDARY ANTIBODY
EGF Receptor	Cell Signaling	D38B1 / 4267	1: 150	1h RT	Biotinylate anti-rabbit
Phospho-EGF Receptor (Tyr1068)	Cell Signaling	D7A5 / 3777	1: 200	1h RT	Biotinylate anti-rabbit
Phospho-EGF Receptor (Tyr1173)	Cell Signaling	53A5 / 4407	1: 150	1h RT	Biotinylate anti-rabbit
Akt (pan)	Cell Signaling	11E7 / 4685	1: 350	1h RT	Biotinylate anti-rabbit
Phospho-Akt (Ser473)	Cell Signaling	D9E / 4060	1: 50	1h RT	Biotinylate anti-rabbit
p44 MAPK (Erk1) (N-Term)	Epitomics	Y72 / 1172-1	1: 150	1h RT	Biotinylate anti-rabbit
Phospho-p44/42 MAPK (Erk1/2) (thr202/Tyr204)	Cell Signaling	- / 4370	1: 350	1h RT	Biotinylate anti-rabbit

RT: room temperature

Image analysis was carried out using IMAGE J software, a public domain, Java-based image processing program developed at the National Institutes of Health (NIH). Three to four different fields (400x magnification) from each animal were chosen, consisting of well representative neoplastic nodules. Each field had a maximum area of 198918.8 μm^2. A threshold of intensity for each marker was defined using a field from the untreated control animal as reference; the percentage of the total immunopositive area was then calculated in untreated control and treated animals.

3.4.5 Statistical analyses on bioluminescence imaging

Statistical analysis was carried out using IBM SPSS Statistics software, version 19; generalized estimated equation (GEE) was used both to analyze ROI (Region of Interest) variable in MSTO and REN cell lines. Two models were built: the first with Roi as response variable for MSTO cell line, the second with ROI as response variable for REN cell line. For each of the two models Gamma was used as distribution of the variable response, “log” as link function and AR(1) as working correlation matrix. In each of the two models the independent variables were time (taking into account that the measurements were done at two different times – one at the beginning and the other at the end of treatment) and group.

4 RESULTS

4.1 IN VITRO STUDIES

Results *in vitro* showed an inhibiting effect of cetuximab in MSTO-211H cell line tumour growth assays and confirmed successful cell selection of both MSTO-211H and REN cell lines tested with bioluminescence imaging.

4.1.1 Tumour Growth Assays

Cell proliferation assay

The proliferation assay was conducted ***1)*** on both REN and MSTO-211H cell lines (Fig.6), to compare the inhibitory effect of cetuximab 0.1mM alone and ***2)*** on MSTO-211H cell line (Fig.7), to compare cetuximab 0.1mM inhibitory effect alone or supplemented with 5ng/ml EGF.

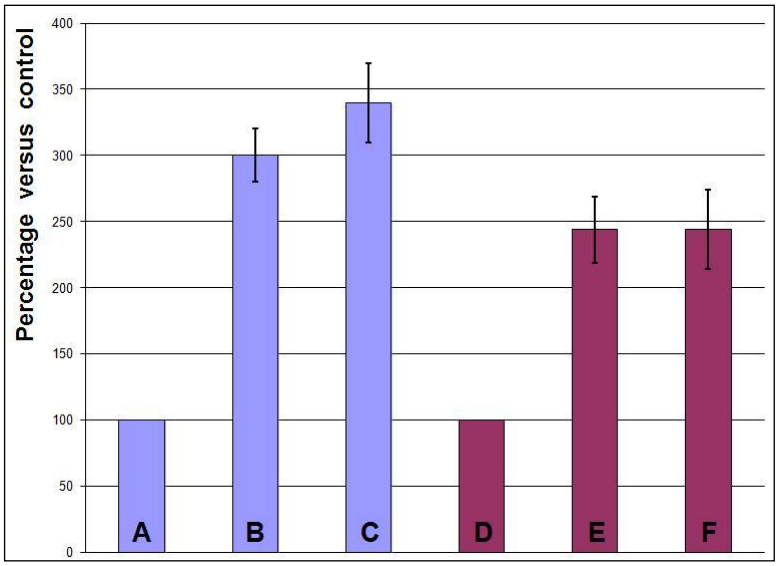

Fig.6: Proliferation rate of REN and MSTO-211H cell lines
A: REN cells – control (time 0, beginning of the test)
B: REN cells – 24 hours after beginning of the test
C: REN cells – 24 hours after the beginning of the test with cetuximab 0.1mM
D: MSTO-211H cells – control
E: MSTO-211H cells – 24 hours after beginning of the test
F: MSTO-211H cells – 24 hours after the beginning of the test with cetuximab 0.1mM

The proliferation rate of both REN and MSTO-211H cell lines 24 hours after the administration of cetuximab 0.1mM (respectively C and F) did not decrease compared to untreated REN and MSTO-211H cell lines (respectively B and F) examined at the same time point.

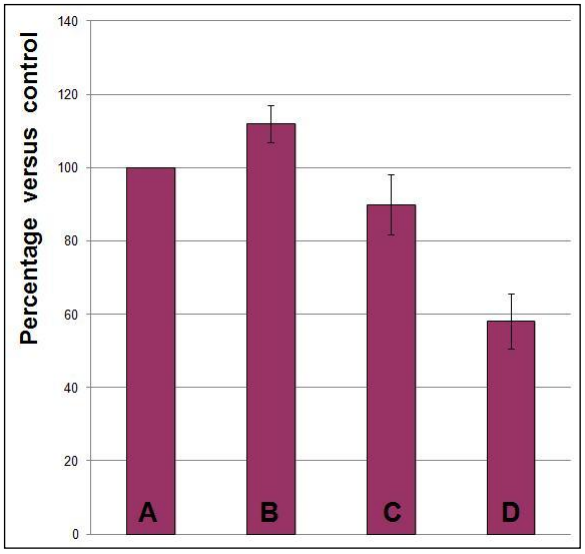

Fig.7: MSTO-211H cell lines - proliferation rate with EGF
A: MSTO-211H cells – control (time 0, beginning of the test)
B: MSTO-211H cells – 24 hours after beginning of the test with EGF 5ng/ml
C: MSTO-211H cells – 24 hours after the beginning of the test with cetuximab 0.1mM
D: MSTO-211H cells – 24 hours after the beginning of the test with cetuximab 0.1mM and EGF 5ng/ml

The proliferation rate of MSTO-211H cell line 24 hours after the administration of cetuximab 0.1mM slightly decreased when cetuximab was administered alone (C) but showed a more relevant decrease when it was supplemented with EGF 5ng/ml (D). A slight increase in the proliferation rate occurred when MSTO-211H cells were supplemented with EGF 5ng/ml alone (B).

Colony formation assay

The colony formation assay was tested on MSTO-211H cell line (Fig.8), to compare the inhibitory effect of cetuximab 0.1mM and Doxorubicin1mg/ml, alone or in combination.

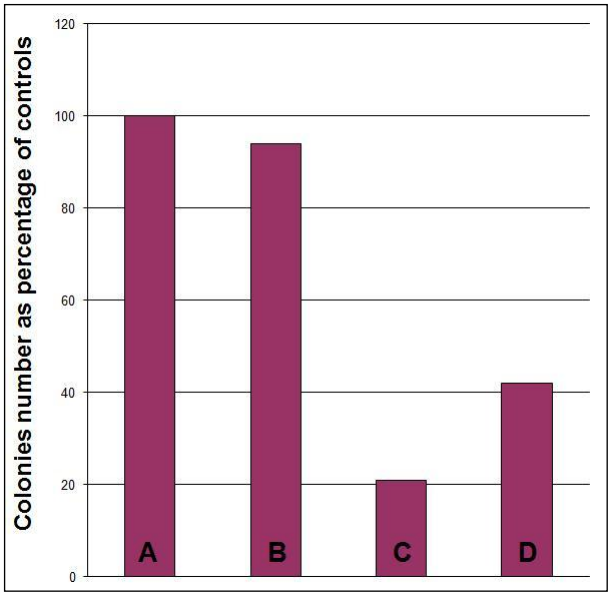

Fig.8: MSTO-211H cell lines - colony formation assay in soft agar
A: MSTO-211H cells – control (time 0, beginning of the test)
B: MSTO-211H cells – 14 days after beginning of the test with cetuximab 0.1mM
C: MSTO-211H cells – 14 days after beginning of the test with Doxorubicin 1 mg/ml
D: MSTO-211H cells – 14 days after beginning of the test with cetuximab 0.1mM and Doxorubicin 1 mg/ml

The number of MSTO-211H cell line colonies formed 14 days after the administration of cetuximab 0.1mM (B) did not significantly decrease compared to controls as has happened with the administration of Doxorubicin 1 mg/ml (C). The combination of the two compounds (D) did not improve the inhibition observed with administration of Doxorubicin alone.

Phosphorylation analysis

Analysis of pEGFR, pAkt and pERK phosphorylation in REN (Fig.9) and MSTO-211H (Fig.10) cell lines was performed 5 minutes after treatment with cetuximab 0.1mM alone or supplemented with EGF 5 ng/ml.

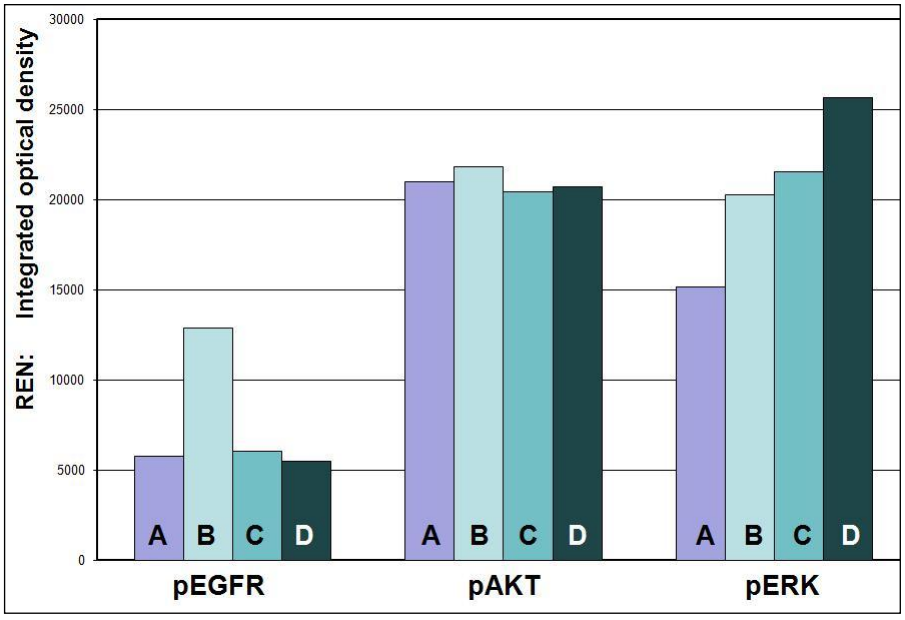

Fig.9: REN cell lines – western blot densitometric analysis
A: REN cells – control (time 0, beginning of the test)
B: REN cells – 5 minutes after beginning of the test with EGF 5ng/ml
C: REN cells – 5 minutes after the beginning of the test with cetuximab 0.1mM
D: REN cells – 5 minutes after the beginning of the test with cetuximab 0.1mM and EGF 5ng/ml

In REN cell lines cetuximab reduced ligand-induced EGFR phosphorylation, but did not affect AKT phosphorylation and, paradoxically, induced ERK activation.

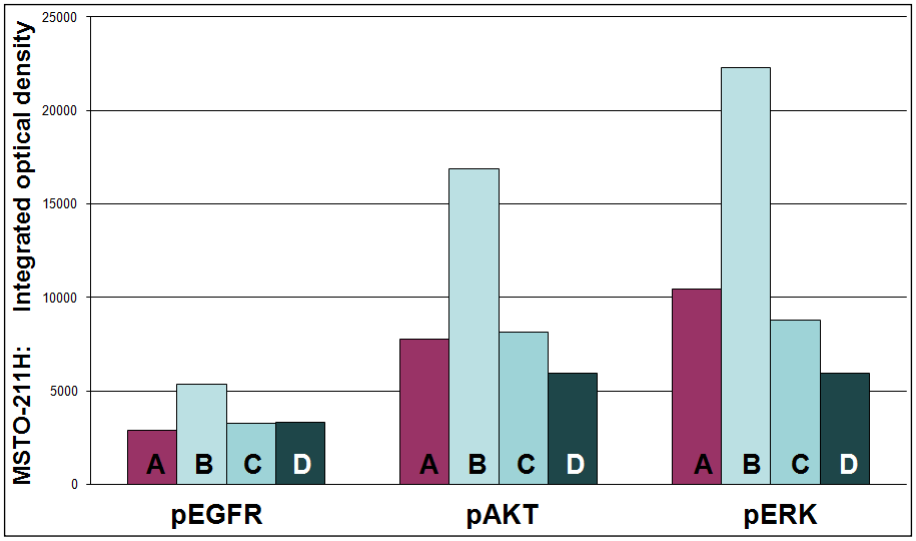

Fig.10: MSTO-211H cell lines – western blot densitometric analysis
A: MSTO-211H cells – control (time 0, beginning of the test)
B: MSTO-211H cells – 5 minutes after beginning of the test with EGF 5ng/ml
C: MSTO-211H cells – 5 minutes after the beginning of the test with cetuximab 0.1mM
D: MSTO-211H cells – 5 minutes after the beginning of the test with cetuximab 0.1mM and EGF 5ng/ml

In MSTO-211H cell lines cetuximab reduced ligand-induced EGFR phosphorylation and AKT and ERK signalling. Interestingly, upon cetuximab treatment in the presence of EGF, ERK and AKT, phosphorylation was reduced to levels lower than controls.

4.1.2 Bioluminescence Quantification (in vitro)

MSTO-211H luc$^{+/+}$ and REN luc$^{+/+}$ cells were dispensed in wells (30 thousand cells/well) to determine bioluminescence quantification after 10 minutes incubation with luciferin diluted in the culture medium (Fig.11).

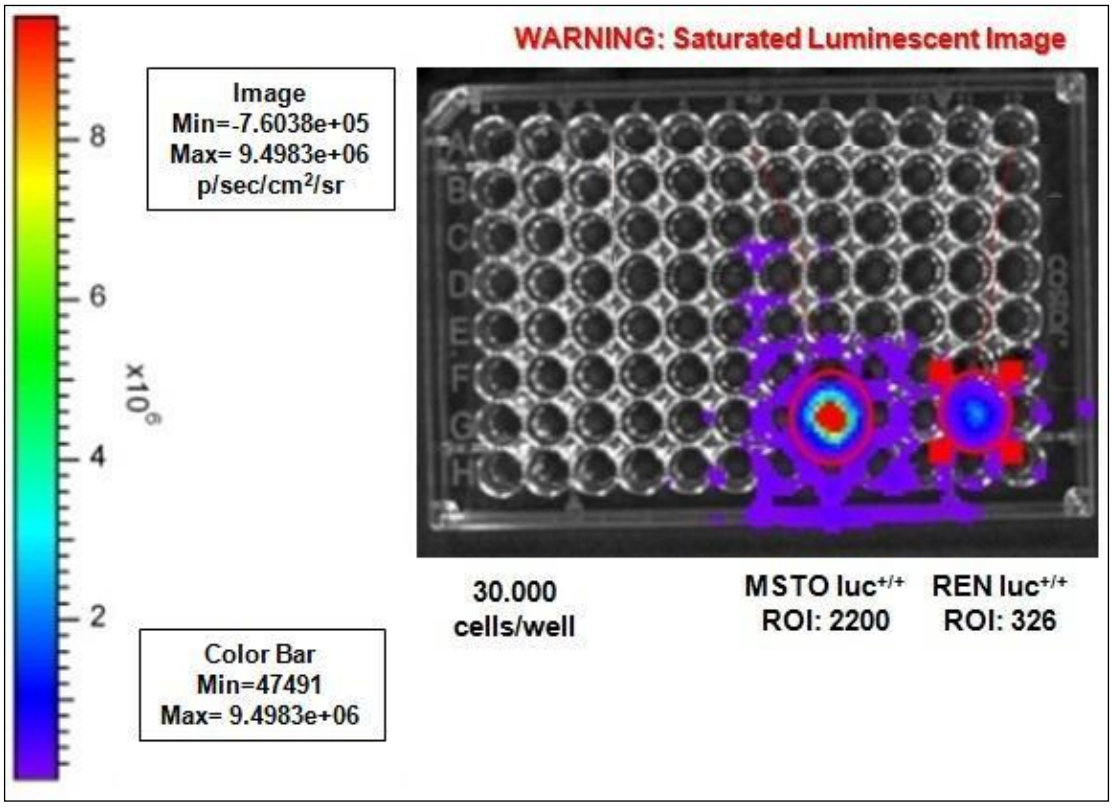

Fig.11: MSTO-211H and REN cell lines - in vitro bioluminescence quantification

Bioluminescence activity of REN luc$^{+/+}$ cells was 326 photons/sec/cell, in the average of other known cell lines; bioluminescence activity of MSTO-211H luc$^{+/+}$ was 2200 photons/sec/cell and the signal was extremely high, with the potential risk of saturation and loss of linearity, in respect of the number of the cells.

4.2 IN VIVO PILOT STUDY - First Phase

4.2.1 Bioluminescence Quantification (in vivo)

MSTO-211H luc$^{+/+}$ and REN luc$^{+/+}$ cells activity in xenograft mice injected 0.5, 1 and 5 million cells/animal was determined after 10 minutes incubation with luciferin injected intraperitoneally (Fig.12).

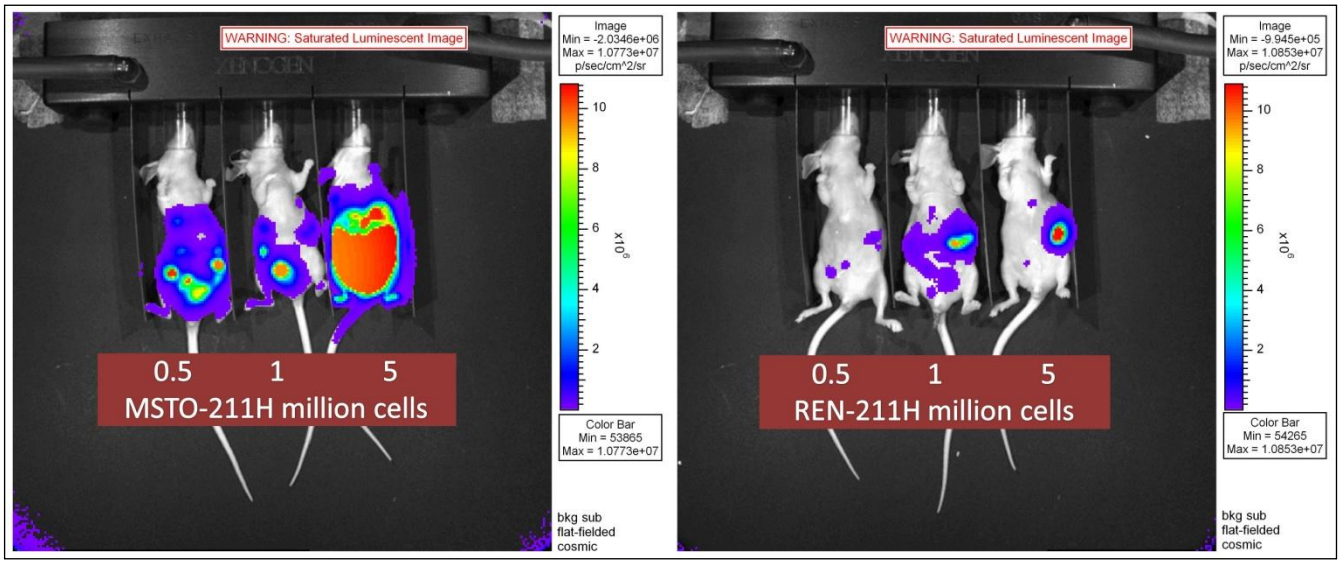

Fig.12: MSTO-211H and REN cell lines - *in vivo* bioluminescence quantification

Fifteen days after tumour cell inoculation, bioluminescence activity measured in animals injected with 5 million MSTO-211H luc$^{+/+}$ cells was 1.304e^{+09} extremely high, with the potential risk of signal saturation and loss of linearity, in respect of the number of the cells, whereas in those injected with 0.5 and 1 million MSTO-211H luc$^{+/+}$ cells the signal was respectively 2.374e^{+08} and 1.063e^{+08}, well comparable and within acceptable range. Bioluminescence activity measured in animals injected with both 1 and 5 million REN luc$^{+/+}$ cells was respectively 6.474e^{+07} and 7.128e^{+07} consider acceptable and the signal was well comparable in both animals; on the contrary the signal was weak, 2.354e^{+06}, when 0.5 million REN luc$^{+/+}$ cells were injected.

4.2.2 Cytological evaluation

May Grunwald Giemsa staining was performed on ascitic fluid collected at necropsy in all xenograft mice injected 0.5, 1 and 5 million cells/animal of MSTO-211H luc$^{+/+}$ and REN luc$^{+/+}$ cells (Fig.12).

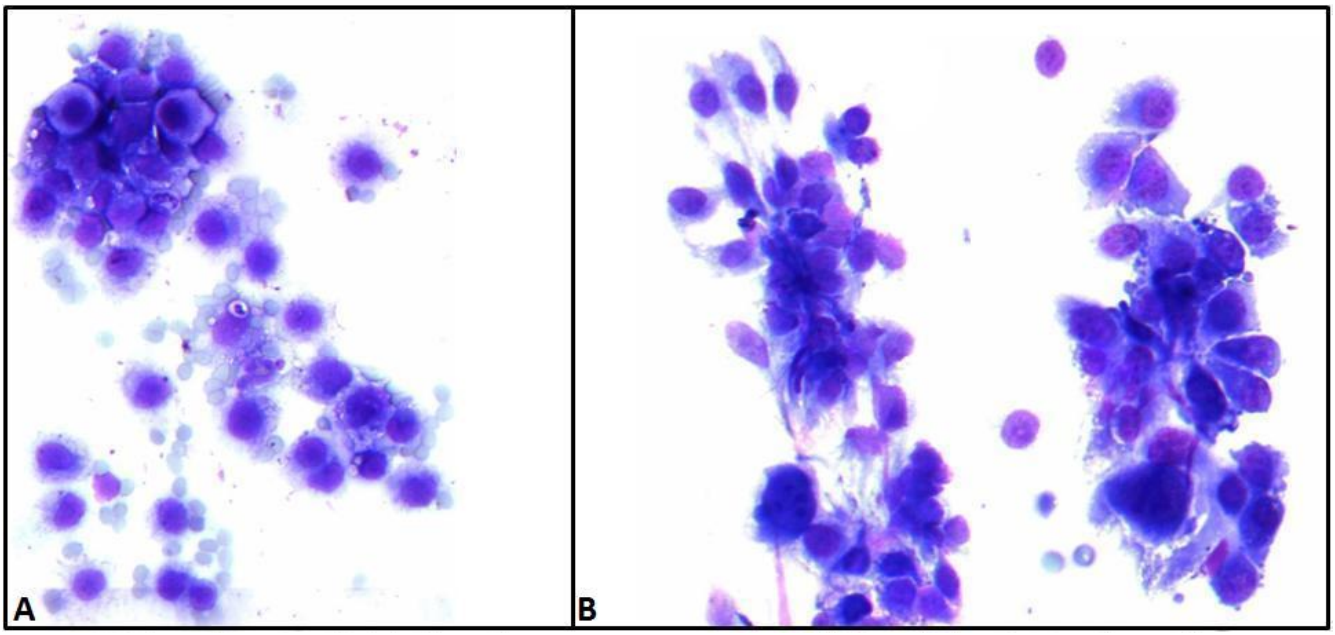

Fig.13: cyto-morphological differences between A) REN and B) MSTO-211H cell lines

The amount of fluid collection in the abdominal cavity was poor, requiring sampling by means of microcapillary tubes. Cytological evaluation showed a correspondence between the expected and the observed morphology of neoplastic cells (Fig.13): the epitheliod REN luc$^{+/+}$ cells consisting of polygonal or cylindrical cells and the biphasic MSTO-211H luc$^{+/+}$ cells consisting of polygonal but also spindled or stellate cells. Cellularity was adequate in mice injected with 0.5, 1 and 5 million REN luc$^{+/+}$ cells and with 5 million MSTO-211H luc$^{+/+}$ cells only, on the contrary it was not adequate in mice injected with 0.5 and 1 million MSTO-211H luc$^{+/+}$; this is in line with the greater tendency of tumoural cells to exfoliate in epithelioid compared to mesenchymal tumours.

4.2.3 Histological evaluation

Histological evaluation of selected organs and tissues (i.e. ovaries, uterus, vagina, kidneys, adrenals, diaphragmatic muscle, lungs, heart, stomach, small and large intestines, spleen, pancreas and liver), routinely trimmed and embedded in paraffin blocks according to the Registry of Industrial Toxicology Animal-data (RITA) and the North American Control Animal Database (NACAD) guidelines (Ruehl-Fehlert et al., 2003; Kittel et al., 2004; Morawietz et al., 2004) confirmed that “wholebody fixation” was adequate.

However, in mice injected with 5 million MSTO-211H luc$^{+/+}$ cells, tumour grew fast with presence of very large neoplastic masses, not suitable for testing the efficacy of treatments. On the contrary, in mice injected both with 1 and 5 million REN luc$^{+/+}$ cells, tumour grew more slowly and with neoplastic masses of similar dimension and adequate for our purposes.

Even though the quality of histological slides was excellent, the routine histotechnique used for slide preparation was not well suited to our purposes due to the high variability in tumour localization and dimension observed,

which did not permit an adequate evaluation of the smallest tumoural masses scattered around the peritoneum and unrelated to parenchymal structures, seen at necropsy and lost during slide preparation.

Based on all these considerations, trimming procedures and histotechnique were reconsidered and tested in the second phase of the pilot study and the amounts of cells to be injected were defined as 2 million for REN luc$^{+/+}$ cells and 1 million for MSTO-211H luc$^{+/+}$ cells.

4.3 IN VIVO PILOT STUDY - Second Phase

4.3.1 Histological evaluation

Histological evaluation of selected organs and tissues (i.e. liver, GI tracts, pancreas, spleen, mesentery and mesenteric lymph nodes) trimmed and embedded “en bloc” (wholebody histotechnique) well suited the high variability in tumour localization and dimension, enabling evaluation even of the smallest tumoural masses scattered around the peritoneum, even if unrelated to parenchymal structures (Fig.14).

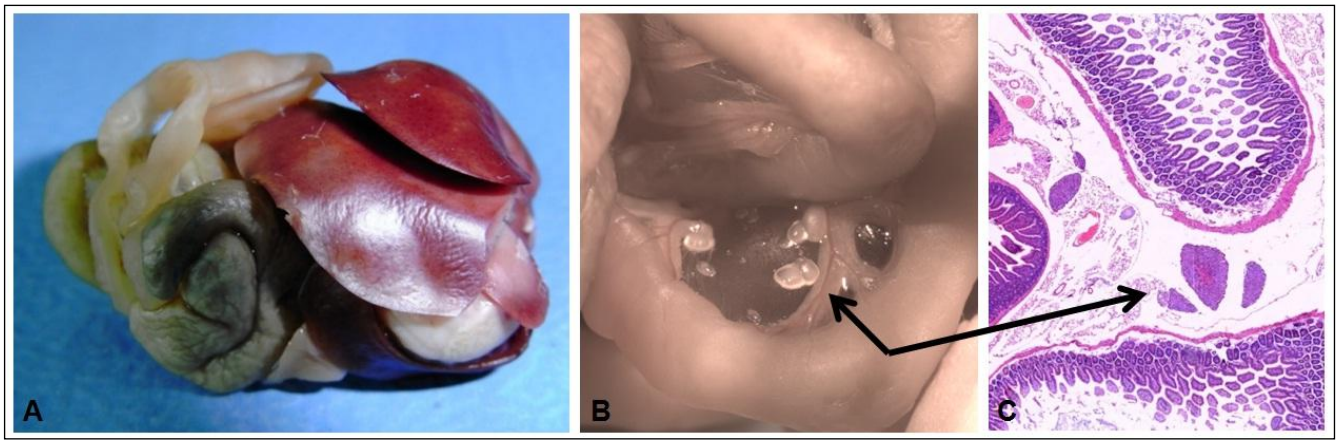

Fig.14: Appearance of small neoplastic masses in the peritoneal cavity. A) “wholebody” abdominal organs and tissues sampled en bloc; B) macroscopic neoplastic nodule (arrow); C) microscopic neoplastic nodule (arrow).

Tumoural masses in slides obtained at the first cut section level were observed in the majority of the animals, as shown in Tab.6:

Tab.6: Amount of neoplatic tissue in abominal cavity of mice sacrificed 28 days post injection

Animal #	MSTO-211H	REN
1	absent	absent
2	absent	absent
3	sufficient	absent
4	good	sufficient
5	good	good
6	excellent	good
7	excellent	excellent
8	excellent	excellent
9	excellent	excellent
10	excellent	excellent

All the slides examined showed excellent reproducibility of the tumoural lesions and of the organs' orientation with anatomical relations maintained (Fig.15). Tumour localization frequently occurred between the spleen, stomach, pancreas and diaphragmatic muscle. The ilar region of the spleen (lienorenal ligament) was always infiltrated by tumour masses (Fig.16). In conclusion, all these observations confirmed that the "wholemount histotechnique" could be useful for histological interpretation in the main study.

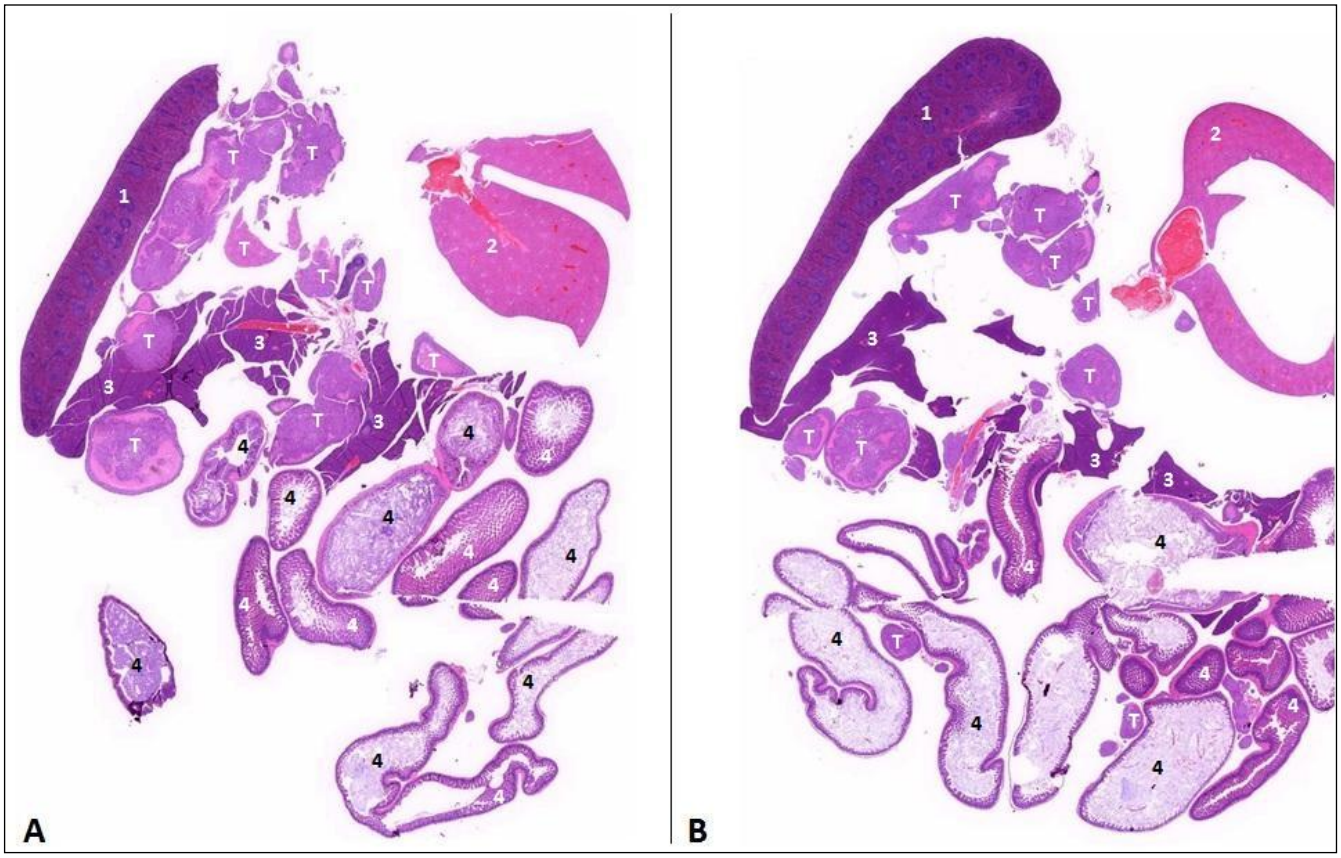

Fig.15: abdominal organs: "en bloc" section: 1) spleen; 2) liver; 3) pancreas; 4) intestine tract, T) neoplastic nodule

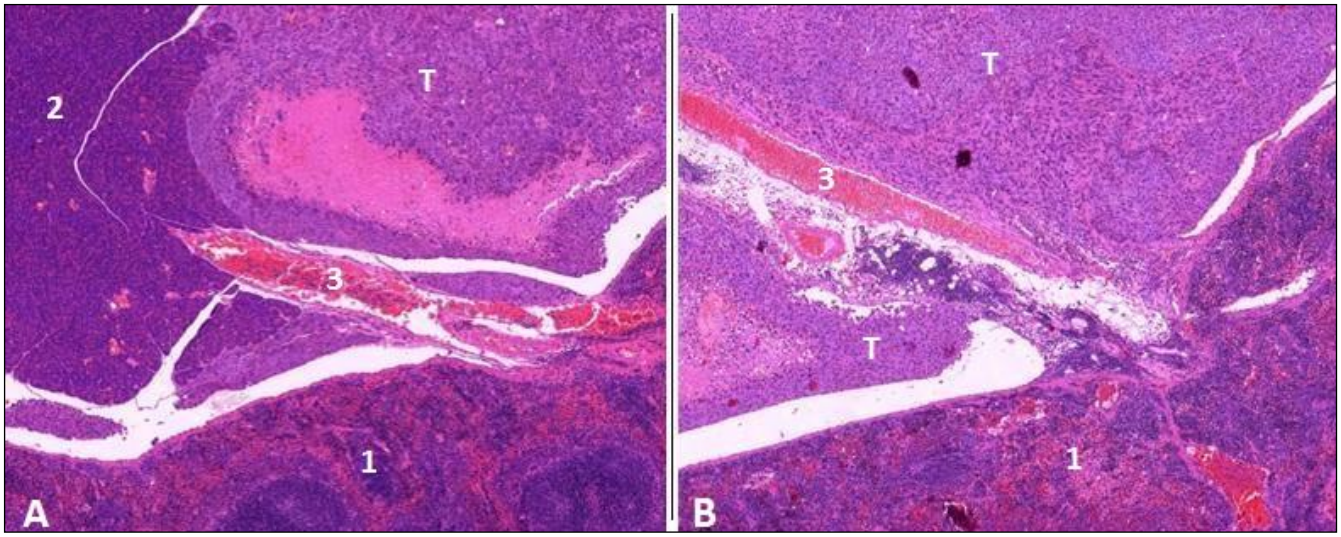

Fig.16: tumour growth surrounding the splenic ilus in both: A) MSTO-211H cell line; B) REN cell lines; 1) spleen; 2) pancreas; 3) blood vessel; T) neoplastic nodule

4.4 IN VIVO MAIN STUDY

Three mice injected with MSTO-211H luc$^{+/+}$ cell lines died during the experiment: animal No. 2-group1, animal No. 13-group3, and animal No. 24-group5. In the first two animals (Nos. 2 and 13) death occurred after the last IVIS monitoring on day 31 of the experiment. The last animal (No. 24) died before the last IVIS monitoring. These animals were not histologically examined.

4.4.1 Bioluminescence quantification (in vivo)

a) Confirmation of tumour growth: thirteen days after MSTO-211H luc$^{+/+}$ and REN luc$^{+/+}$ cell inoculation, bioluminescence quantification confirmed the presence of tumoural cells in the majority of the 74 mice examined.

b) Group randomization: sixty one mice were then selected from the 75 examined and allocated to the dose groups after being randomized based on ROI intensity to have homogeneous groups; each animal received a definitive identification number (IDd) to substitute the temporary one (IDt) (see appendix 1).

c) Tumour growth quantification: response to treatment was compared *i)* between the two cell lines and *ii)* between groups within each single cell line, as discussed below:

i) Comparison between cell lines: MSTO-211H luc$^{+/+}$ vs REN luc$^{+/+}$

Comparing the region of interest (ROI) for the MSTO-211H luc$^{+/+}$ and REN luc$^{+/+}$ cells generated in the respective untreated control group animals together, MSTO-211H luc$^{+/+}$ cell line showed a greater activity than REN luc$^{+/+}$ cell line, at all the selected time points: basal, interim and final.

Tab.7: region of interest raw data

Animal #	ROI Basal IVIS	ROI Interim IVIS	ROI Final IVIS
MSTO-211H			
1	1,779E+09	1,538E+10	6,567E+10
2	3,176E+09	1,619E+10	5,897E+10
3	3,705E+08	4,057E+09	1,833E+10
4	9,799E+08	8,347E+09	3,757E+10
5	1,033E+09	6,977E+08	4,814E+10
REN			
1	3,97E+07	1,42E+08	1,81E+08
2	1,45E+07	8,36E+07	2,12E+08
3	6,92E+07	3,87E+07	1,11E+08
4	4,23E+07	8,78E+07	2,01E+08
5	1,55E+08	7,70E+07	1,99E+08
	Average ROI	**Average ROI**	**Average ROI**
MSTO-211H	1,468E+09	8,934E+09	4,574E+10
REN	6,403E+07	8,573E+07	1,805E+08

Fig.17: region of interest curves (control groups only)

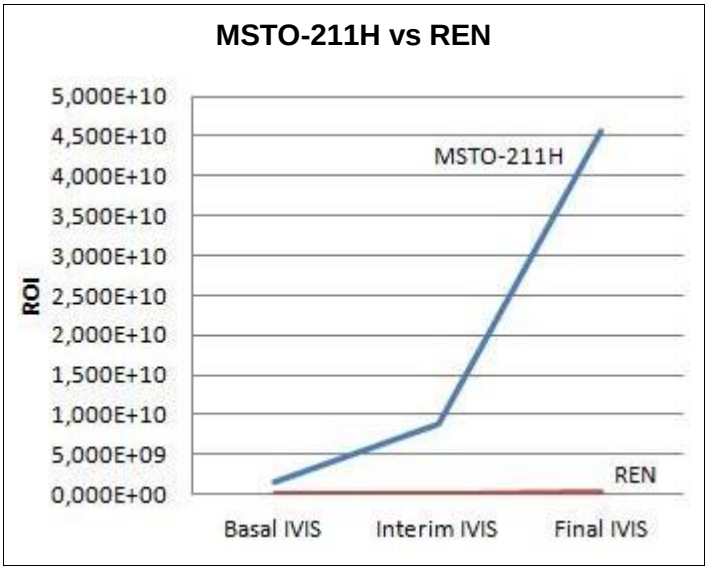

As shown in Tab.7 and Fig.17, the order of magnitude for the ROI of MSTO-211H luc$^{+/+}$ cells was x10^{9} in almost all animals at the basal IVIS reaching x10^{10} in all animals at the final IVIS, whereas the order of magnitude for the ROI of REN luc$^{+/+}$ cells was only x10^{7} in almost all animals at the basal IVIS, reaching at least x10^{8} in all animals at the final IVIS.

Based on these consideration, it was demonstrated that the two different cell lines both grew in mice after intraperitoneal injection even if their activity was quite different, MSTO-211H luc$^{+/+}$ cells being more aggressive than REN luc$^{+/+}$ cells.

ii) Comparison between groups within each cell line

By comparing the region of interest (ROI) in the six groups within each cell line (MSTO-211H luc$^{+/+}$ and REN luc$^{+/+}$) the interference of treatments on the tumour growth, in treated groups or versus untreated control animals were seen (Fig.18).

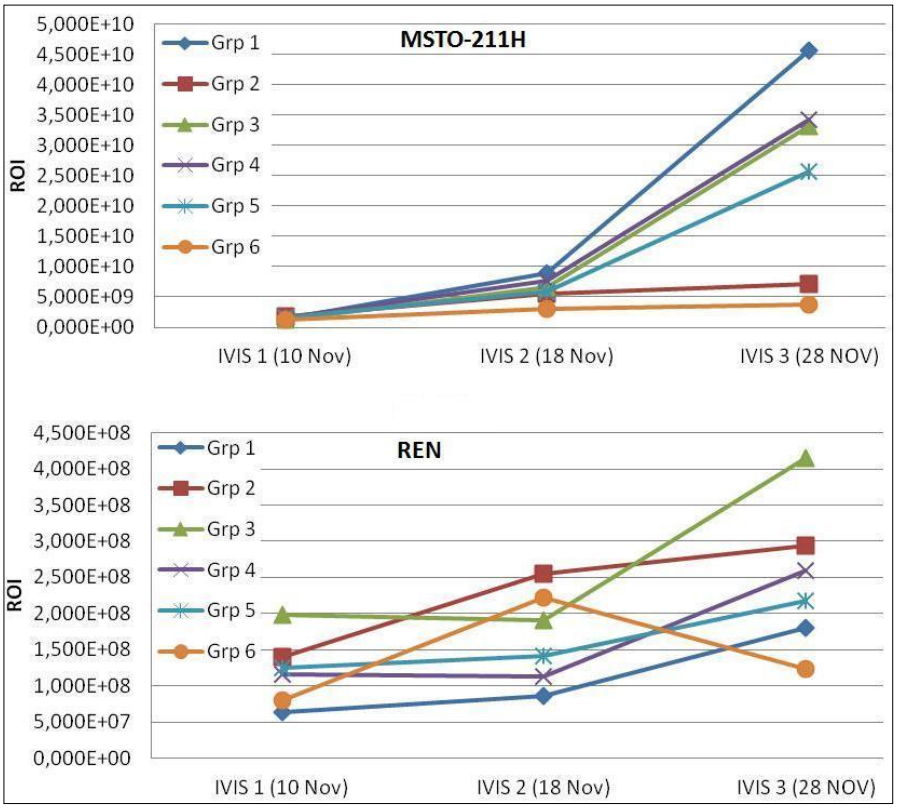

Legend (groups):

1: pbs

2: cisplatin and pemetrexed

3: cetuximab 3 mg/kg

4: cetuximab 10 mg/kg

5: cetuximab 30 mg/kg

6: cisplatin, pemetrexed, cetuximab

Fig.18: region of interest curves (all MSTO-211H and REN groups)

Within MSTO-211H luc$^{+/+}$ cell line, the region of interest (ROI) showed relevant differences, compared to untreated controls, in animals treated with pemetrexed and cisplatin alone (group 2) or in combination with cetuximab (group 6); statistically significance was only reported in group 6 versus the untreated control

group. Groups 3, 4 and 5, in which cetuximab was given as single agent at three increasing doses, no differences compared to untreated controls were observed.

Within REN luc$^{+/+}$ cell line no relevant changes among groups, treated or untreated control, were seen.

4.4.2 Histopathology

H&E - Morphological description

Differences in cell morphology and tumour growth patterns were observed: ***a)*** between the two cell lines, comparing untreated control animals injected MSTO-211H luc$^{+/+}$ and REN luc$^{+/+}$ cells, and ***b)*** between groups within the MSTO-211H luc$^{+/+}$ cell line, comparing untreated control (group 1) and treated animals, particularly in those given pemetrexed and cisplatin alone or in combination with cetuximab (groups 2 and 6), as discussed below and shown in Fig.19 a-b:

a) MSTO-211H luc$^{+/+}$ cell line grew in all untreated control and treated animals as nodules of solid tumour, multifocally distributed, extremely variable in size, densely cellular, widespread in the mesothelial lining of the coelomic cavity. Tumour cells infiltrated pancreas, mesenteric lymph nodes and the diaphragm muscle, with neoplastic invasion also of the thoracic cavity, the tracheobronchial lymph nodes and, in some cases, the pulmonary parenchyma. Necrotic areas were present, mainly in the centre of larger nodules. Neoplasia was characterized by nests of a single population of atypical cells admixed to a moderate amount of fibrovascular stroma.

In untreated control animals cell morphology was characterized by irregularly shaped, polygonal cells, 10-30 micron in size with poorly demarcated cell borders. A moderate amount of homogeneous basophilic cytoplasm and empty vacuoles sized 10 to 80 microns consistent with fatty change, were also present in some of the cells. Nuclei were large, 10-20 microns, oval shaped, and located centrally with coarsely stippled chromatin. Within the single nucleus there were often up to 3 large, prominent and distinct nucleoli, dark purple, round and located centrally. In treated animals severe cyto-karyomegaly as well diffuse anisocytosis and anisokaryosis were observed with evidence of bi-multinucleated cells. Furthermore, in all animals, bizarre mitoses were also observed, up to 5 per 40 HPF together with a higher number of apoptotic cells.

b) REN luc$^{+/+}$ cell line grew in all untreated control and treated animals as multifocally distributed nodules of solid tumour, extremely variable in size, densely cellular, widespread in the mesothelial lining of the coelomic cavity. In contrast to MSTO-211H, REN cells did not infiltrate the pancreas, mesenteric lymph nodes and diaphragm muscle, and where some neoplastic cells were also present in the thoracic cavity (in two animals only), did not infiltrate the tracheobronchial lymph nodes and pulmonary parenchyma.

Necrotic areas were present, mainly in the centre of larger nodules. Neoplasia was characterized by a closely packed island of a single population of atypical cells admixed to a small amount of fibrovascular stroma. Cells were round to oval shaped, 10-20 microns in size, without demarcated cell borders. A slight amount of homogeneous eosinophilic cytoplasm was present. No vacuolations consistent with fatty change were observed. Nuclei were large, 5-10 microns in size, round to oval shaped, located centrally/paracentrally and with clumped chromatin. Small nucleoli, mainly one per nucleus when present, were light purple, round and located centrally.

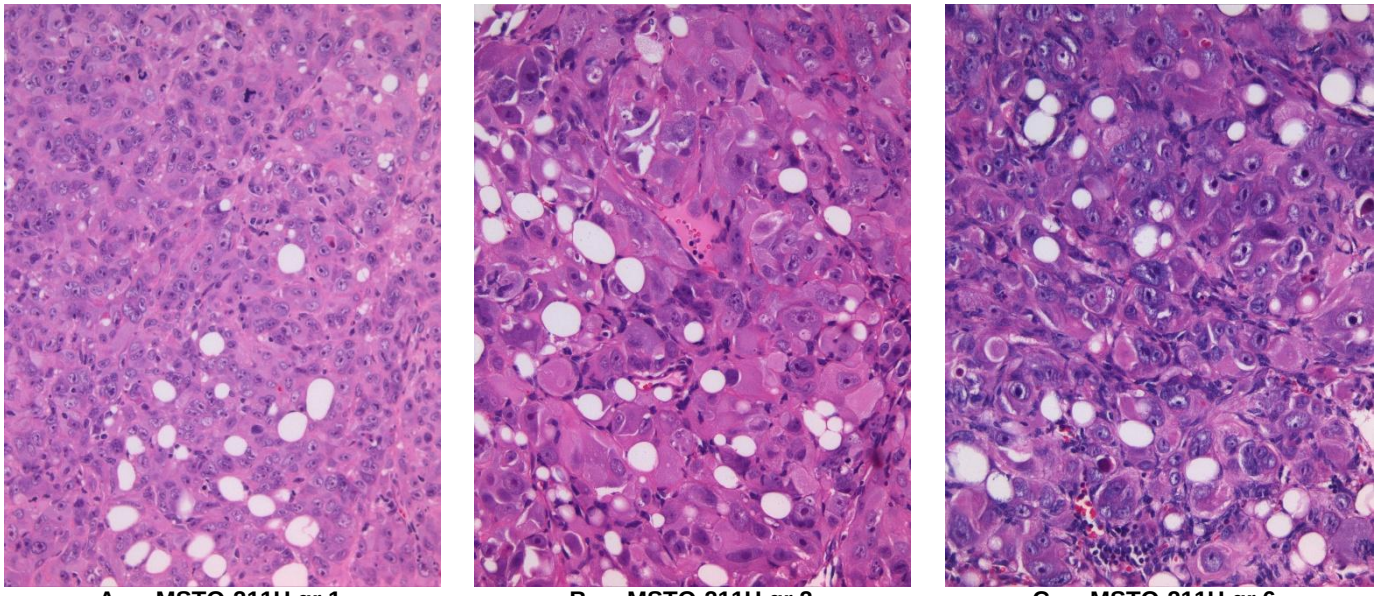

A. MSTO-211H gr.1 **B. MSTO-211H gr.2** **C. MSTO-211H gr.6**

Fig.19a: tumour growth patterns – MSTO-211H cell line

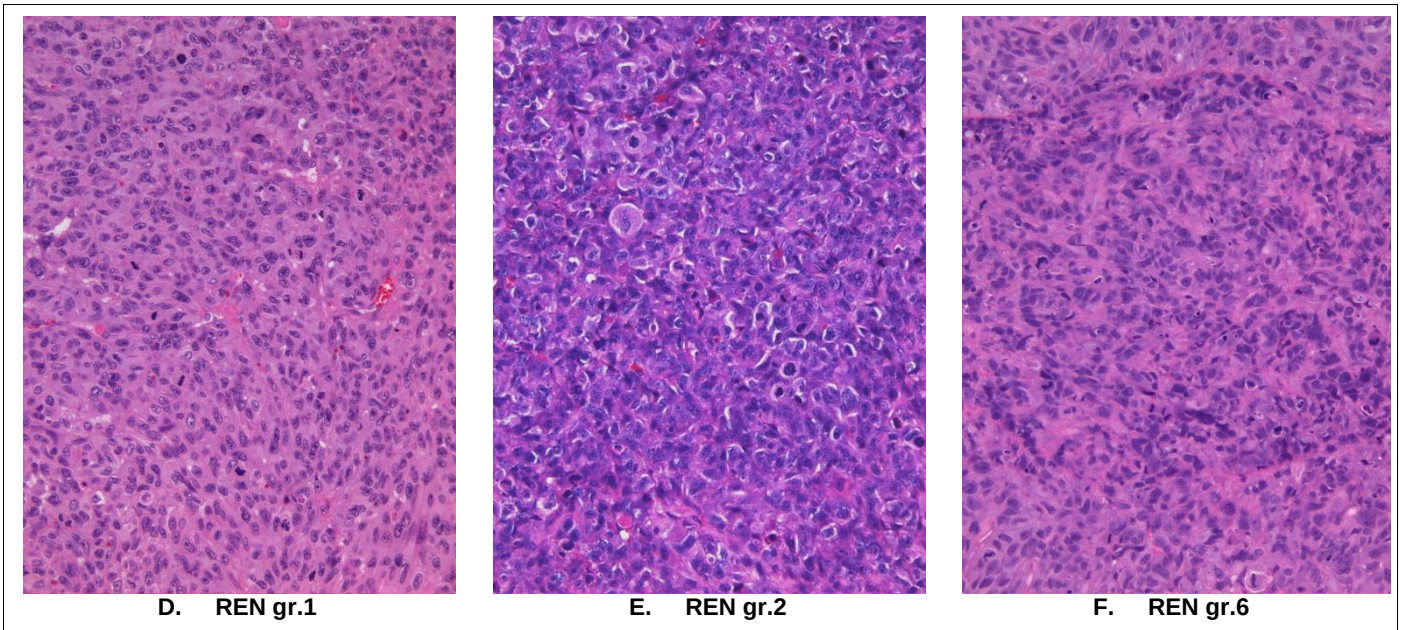

D. REN gr.1 **E. REN gr.2** **F. REN gr.6**

Fig.19b: tumour growth patterns – REN cell line

H&E - Tumour behaviour

A scoring system based on recording the presence/absence of neoplastic cells both in the abdominal and thoracic cavities, as isolated nodules or parenchymal organ infiltration, in the diaphragmatic muscle and in the mesenteric and tracheobronchial lymph nodes was used to better characterize the tumour growth and its tendency to spread within the abdominal cavity and its surroundings.

Differences in the behaviour of the tumour were observed: ***a)*** between the two cell lines, comparing untreated control animals (groups 1) injected MSTO-211H luc$^{+/+}$ or REN luc$^{+/+}$ cells and ***b)*** between groups within MSTO-211H luc$^{+/+}$ cell line, comparing untreated control (group1) and treated animals given pemetrexed and cisplatin alone (group 2) or in combination with cetuximab (group 6).

a) Comparison between cell lines: MSTO-211H luc$^{+/+}$ vs REN luc$^{+/+}$

Comparison of tumour behaviour in untreated control animals injected both with MSTO-211H luc$^{+/+}$ and REN luc$^{+/+}$ cells is shown in Tab.8 and some representative cases are illustrated in Fig.20-25:

Tab.8: tumour behaviour score (control groups only)

	MSTO-211H group1					REN group1				
Animal #	**1**	**2**	**3**	**4**	**5**	**1**	**2**	**3**	**4**	**5**
Abdominal cavity										
Organ Infiltration										
Abdominal LNs									M	M
Diaphragm										
Muscle Infiltration										
Thoracic cavity										
Lung parenchyma										
Thoracic LNs										

tumour presence | tumour absence | not examined | M missing

Neoplastic cells were observed in the abdominal cavity of all animals examined but only in those transplanted with MSTO-211H luc$^{+/+}$ cells did they infiltrate parenchymal organs, mainly the pancreas, and mesenteric lymph nodes. The abdominal surface of the diaphragm was lined by tumoural cells in all the animals transplanted with both cell lines but deep infiltration of the muscular fibres was mainly observed in those transplanted with MSTO-211H luc$^{+/+}$ cells. As a consequence of this greater tendency to infiltrate organs and tissues, neoplastic cells were observed in the thoracic cavity of all examined mice transplanted with MSTO-211H luc$^{+/+}$ cells, involving also the lung parenchyma and/or thoracic lymphnodes, in almost all cases. On the contrary, in REN luc$^{+/+}$ cells transplanted mice, the thoracic cavity was infiltrated only in two cases with no involvement of lungs or lymph nodes.

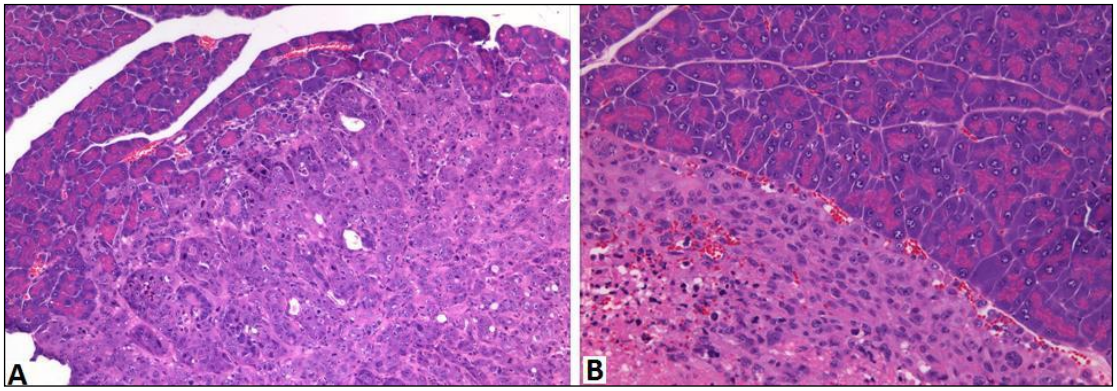

Fig.20: pancreas infiltration: A) MSTO-211H cell line; B) REN cell line

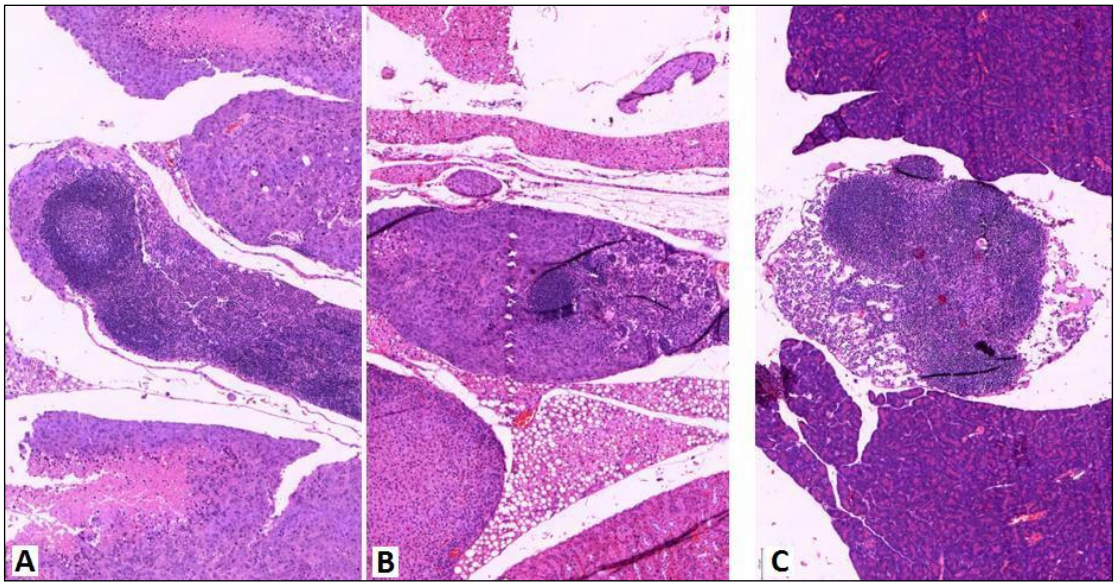

Fig.21: mesenteric lymph nodes infiltration: A) and B) MSTO-211H cell line; C) REN cell line

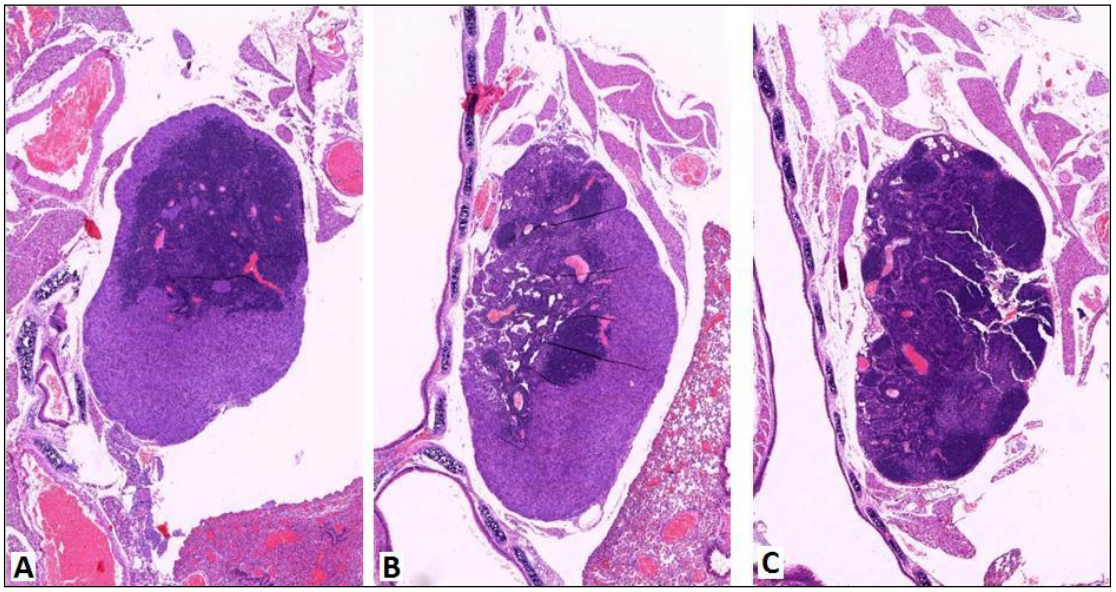

Fig.22: tracheobronchial lymph nodes infiltration: A) and B) MSTO-211H cell line; C) REN cell line

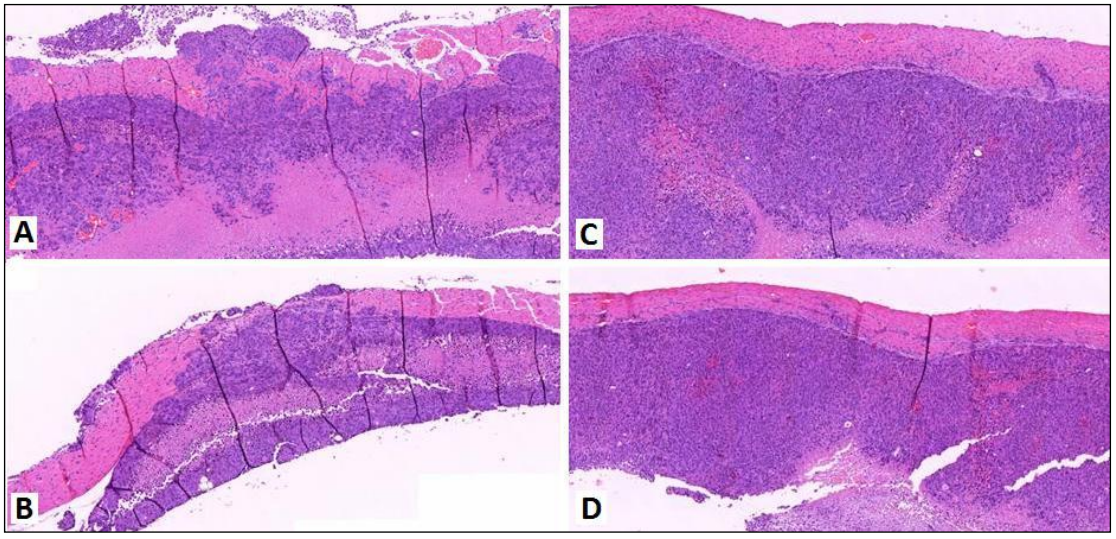

Fig.23: diaphragm infiltration: A) and B) MSTO-211H cell line; C) and D) REN cell line

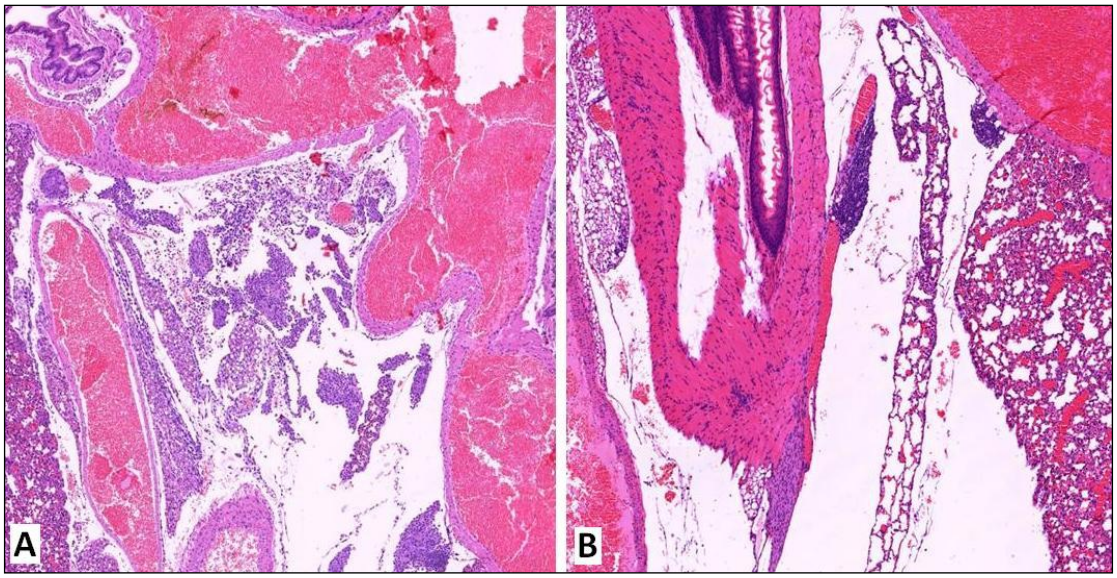

Fig.24: thoracic cavity infiltration: A) MSTO-211H cell line; B) REN cell line

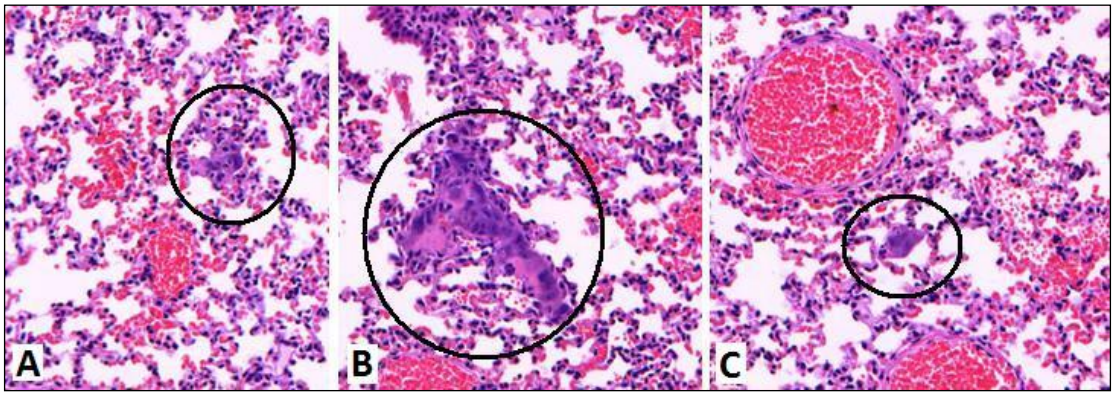

Fig.25: lung parenchyma neoplastic embolus (A and C) or metastasis (B)

b) Comparison between groups within cell lines

Tumour behavior in untreated control and treated animals injected both with MSTO-211H luc$^{+/+}$ and REN luc$^{+/+}$ cells, is shown in Tab.9-10:

Tab.9: tumour behaviour score (all MSTO-211H groups)

MSTO-211H	Group 1					Group 2					Group 3					Group 4					Group 5					Group 6					
Animal #	1	2	3	4	5	6	7	8	9	10	11	12	13	14	15	16	17	18	19	20	21	22	23	24	25	26	27	28	29	30	31
Abdominal cavity																															
Organ Infiltration																															
Abdominal LNs						M	M	M	M	M				M	M	M	M			M		M					M	M		M	
Diaphragm																															
Muscle Infiltration																															
Thoracic cavity																															
Lung parenchyma																															
Thoracic LNs						M			M																					M	M

tumour presence | tumour absence | not examined | M missing

Within the MSTO-211H cell line, relevant presence of tumoural cells in the abdominal cavity, their infiltration to parenchymal organs (e.g. pancreas and mesenteric lymph nodes) and involvement of diaphragm muscle were observed mainly in untreated control animals (group 1) and in those given cetuximab as a single agent (groups 3, 4 and 5). In animals given pemetrexed and cisplatin alone (group 2) or in combination with cetuximab (group 6), similar findings occurred in a small number of cases.

A higher incidence of tumoural cells in the thoracic cavity and their infiltration to lung parenchyma and tracheobronchial lymph nodes were also observed mainly in control, untreated animals (group 1), whereas in those given pemetrexed and cisplatin alone (group 2) and cetuximab alone (groups 3, 4 and 5), similar findings occurred in a small number of cases. Interestingly, in animals given pemetrexed and cisplatin combined with cetuximab (group 6), the thoracic cavity was almost free from tumours in the majority of the animals.

Tab.10: tumour behaviour score (all REN groups)

REN	Group 1					Group 2					Group 3					Group 4					Group 5					Group 6				
Animal #	1	2	3	4	5	6	7	8	9	10	11	12	13	14	15	16	17	18	19	20	21	22	23	24	25	26	27	28	29	30
Abdominal cavity																														
Organ Infiltration																														
Abdominal LNs				M	M					M		M	M	M	M	M	M			M		M	M	M				M	M	
Diaphragm																														
Muscle Infiltration																														
Thoracic cavity																														
Lung parenchyma																														
Thoracic LNs									M	M					M		M												M	

tumour presence tumour absence not examined M missing

No relevant differences in the incidence of tumoural cells in the abdominal cavity, diaphragm muscle and thoracic cavity were observed between untreated control and treated groups within the REN cell line.

IHC – Confirmation of mesothelial origin of the two cell lines

The panel of antibodies tested in two untreated control animals injected both with MSTO-211H luc$^{+/+}$ and REN luc$^{+/+}$ cell lines to confirm their mesothelial origin clearly showed that the two subtypes were negative for 2/2 markers with negative diagnostic value for mesothelioma and were positive for 2/3 markers with positive diagnostic value for mesothelioma (Tab.11).

Tab.11: IHC results to confirm mesothelial origin of MSTO-211H luc$^{+/+}$ or REN luc$^{+/+}$ cell lines

ANTIBODY		MSTO 211H		REN	
Mesothelial diagnostic marker		**animal #1 gr. 1**	**animal #5 gr 1**	**animal #2 gr 1**	**animal #4 gr 1**
Negative for mesothelioma	Carcinoembryonic antigen (CEA)	negative	negative	negative	negative
	Epithelial antigen (BerEP4)	negative	negative	negative	negative
Positive for mesothelioma	Calretinin	positive*	positive*	positive*	positive*
	Wilms' tumour protein (WT1)	positive	positive	positive	positive
	Cytokeratin 5/6	negative	negative	negative	negative

* patch distribution

According to the indication of the European Respiratory Society and the European Society of Thoracic Surgeons for the management of malignant pleural mesothelioma (Scherpereel, 2010), these results confirmed the mesothelial origin of the two cell lines used in the main experiment (Fig.26).

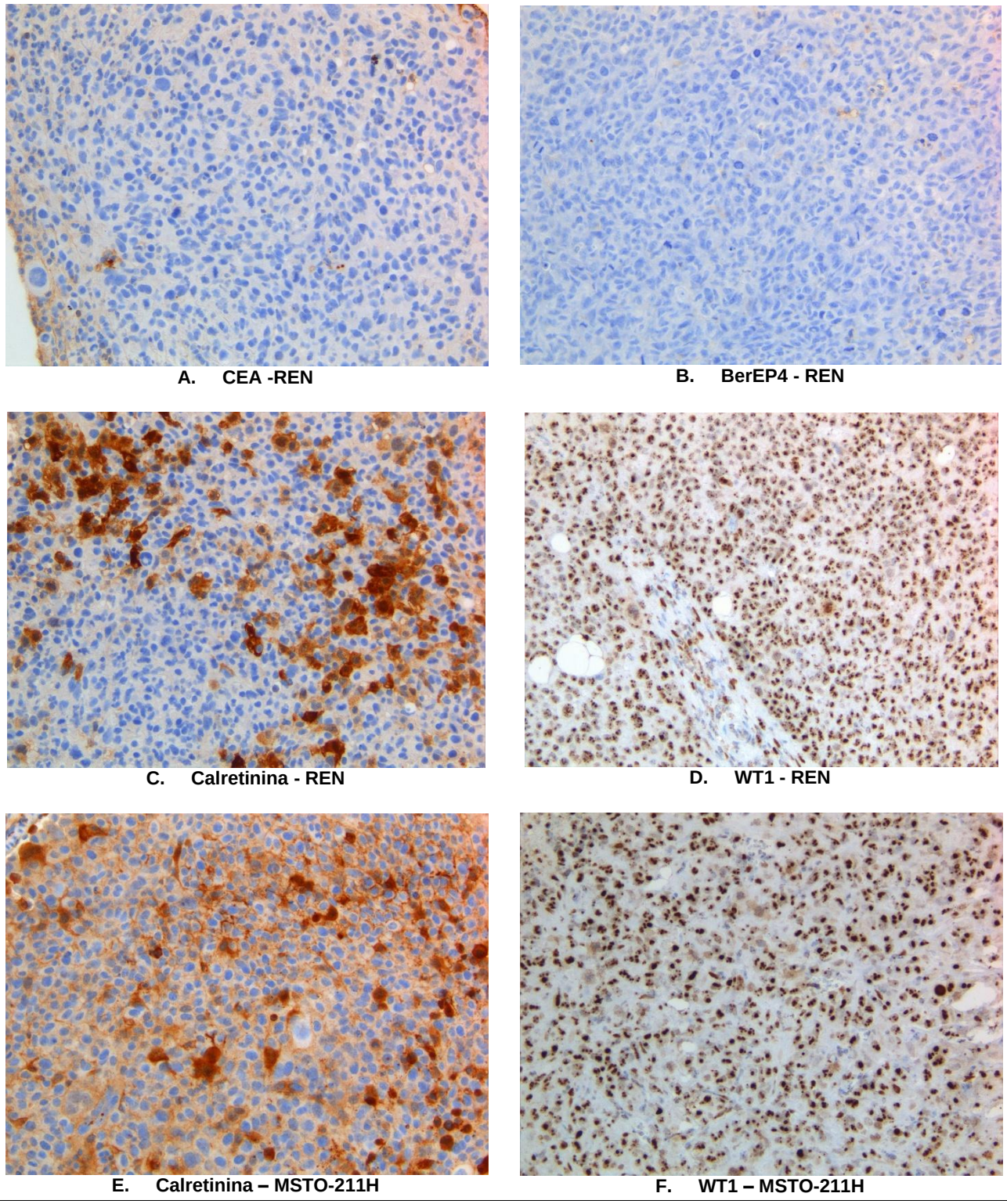

A. CEA -REN **B. BerEP4 - REN**

C. Calretinina - REN **D. WT1 - REN**

E. Calretinina – MSTO-211H **F. WT1 – MSTO-211H**

Fig.26: IHC diagnostic markers to confirm mesothelial origin of both REN and MSTO-211H cell lines

IHC – Apoptosis, proliferation, micro vessel density evaluation

a) Apoptosis

Three different fields (400x magnification) from each of the two animals examined in control untreated (group 1) and treated groups given pemetrexed and cisplatin alone (group 2) or combined to cetuximab, (group 6) were chosen, consisting of well representative neoplastic nodules. The number of immunopositive nuclei were counted over the total number of neoplastic cells and the mean percentages of the three fields were calculated in each untreated control and treated animal, as reported in Tab.12.

Tab.12: caspase 3 (apoptosis marker)

	Group	Animal #	Mean % positive cells
MSTO	Gr1	1 5	6,84 6,47
	Gr2	7 9	8,71 4,26
	Gr6	26 27	6,87 **10,66**

	Group	Animal #	Mean % positive cells
REN	Gr1	2 4	2,01 1,48
	Gr2	6 7	3,32 2,35
	Gr6	28 29	**5,78** **4,23**

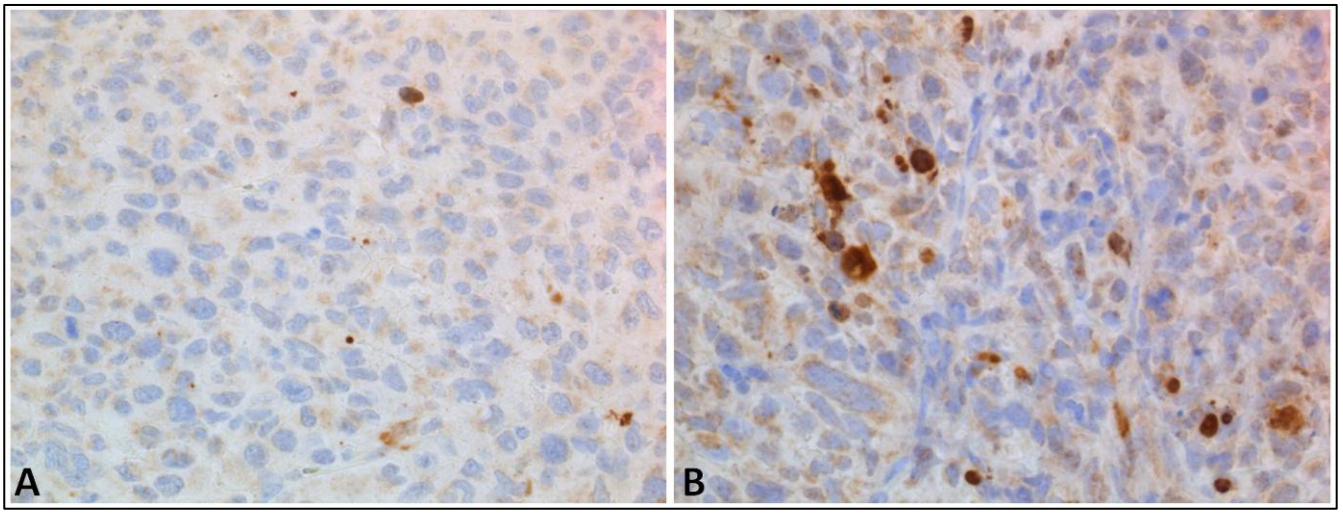

Fig.27: IHC apoptosis marker in REN cell line tumour: A) control untreated animal; B) treated animal

Compared to control untreated animals, a relevant trend towards an increased apoptosis was seen mainly in animals given pemetrexed and cisplatin in combination with cetuximab, as observed in one MSTO-211H xenograft mouse and in two REN xenograft mice.

b) Proliferation

Three different fields (400x magnification) from each of the two animals examined in control untreated (group 1) and treated groups given pemetrexed and cisplatin alone (group 2) or combined to cetuximab, (group 6) were chosen, consisting of well representative neoplastic nodules. The number of immunopositive nuclei were counted over the total number of neoplastic cells and the mean percentages of the three fields were calculated in each untreated control and treated animal, as reported in Tab.13.

Tab.13: KI67 (proliferation marker)

	Group	Animal #	Mean % positive cells
MSTO	Gr1	1	63,05
		5	79,93
	Gr2	7	**32,46**
		9	**33,98**
	Gr6	26	**32,34**
		27	**27,13**

	Group	Animal #	Mean % positive cells
REN	Gr1	2	80,04
		4	92,22
	Gr2	6	84,86
		7	83,62
	Gr6	28	73,31
		29	84,42

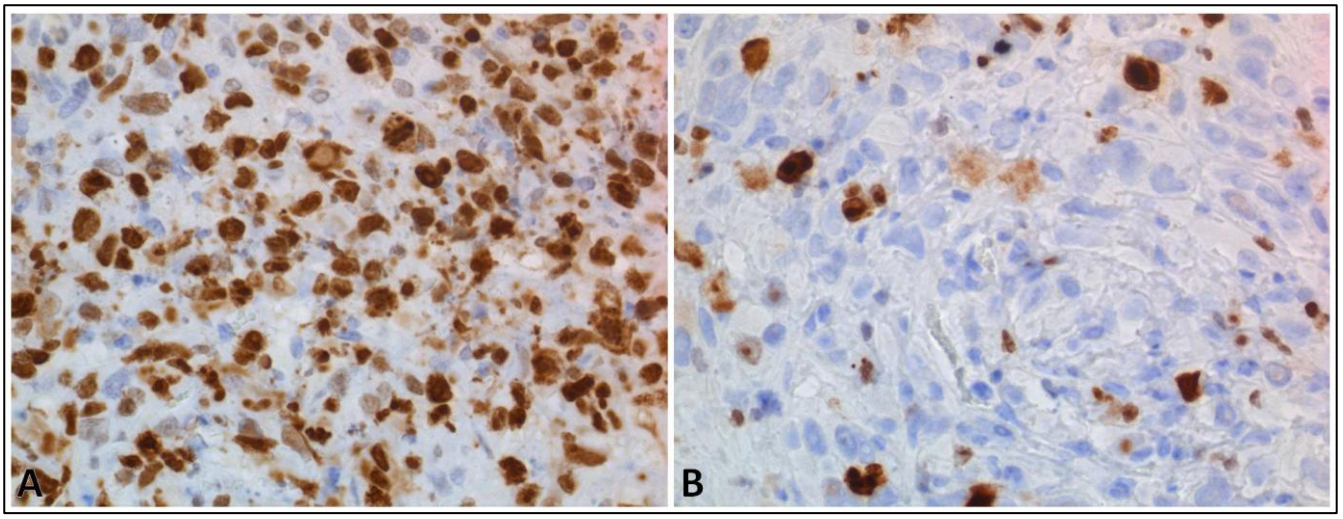

Fig.28: IHC proliferation marker in MSTO-211H cell line tumour: A) control untreated animal; B) treated animal

Compared to control untreated animals, a relevant trend towards a decreased proliferation was seen in animals given pemetrexed and cisplatin alone or in combination with cetuximab, mainly in MSTO-211H xenograft mice.

c) Micro vessel density

Three different fields (200x magnification) from each of the two animals examined in control untreated (group 1) and treated groups given pemetrexed and cisplatin alone (group 2) or combined to cetuximab, (group 6) were chosen, consisting of well representative neoplastic nodules. Each field had a maximum area of 198918.8 μm^2. The number of immunopositive newly-formed small vessels was determined and related to the total area of tumour examined, to finally calculate the number of vessels in 500μm^2 of tumour area, as reported in Tab.14.

Tab.14: CD31 (endothelial marker)

	Group	Animal #	vessel/500 µm2
MSTO	Gr1	1 5	0,23 0,26
	Gr2	7 9	**0,15** **0,16**
	Gr6	26 27	**0,13** **0,07**

	Group	Animal #	vessel/500 µm2
REN	Gr1	2 4	0,07 0,09
	Gr2	6 7	0,08 0,09
	Gr6	28 29	**0,02** 0,05

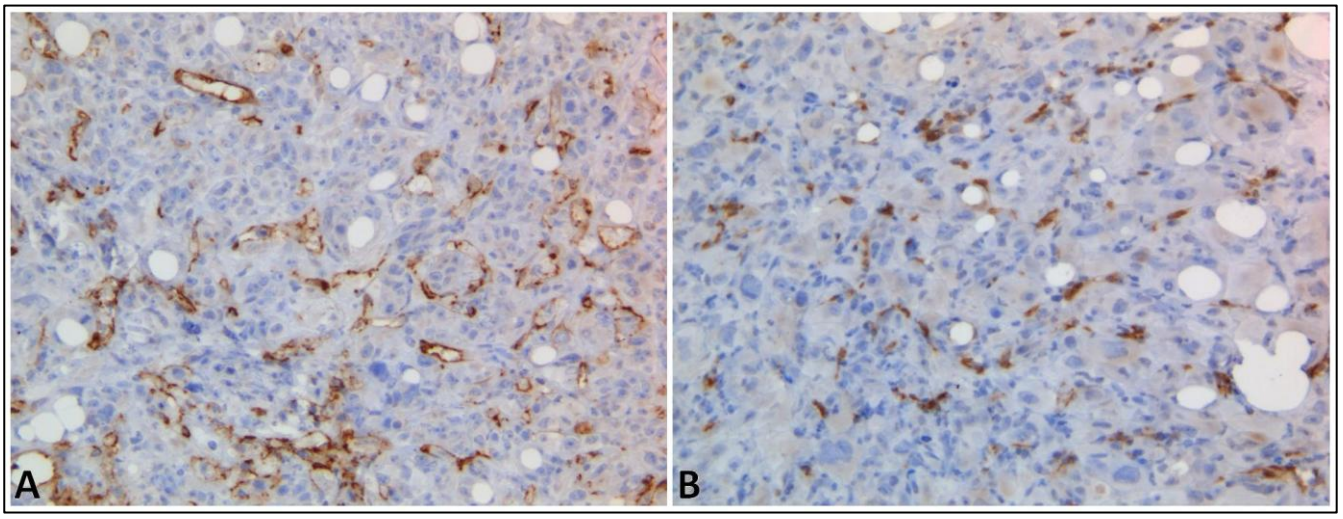

Fig.29: IHC proliferation marker in MSTO-211H cell line tumour: A) control untreated animal; B) treated animal

Compared to control untreated animals, a relevant trend towards a decreased number of newly-formed small vessels was seen in animals given pemetrexed and cisplatin alone or in combination with cetuximab in MSTO-211H xenograft mice. This was also seen in one REN xenograft mouse given the combination regimen.

Interestingly the basal level of newly-formed vessels in untreated animals was significantly lower in REN tumour xenograft mice, compared MSTO-211H tumour xenograft mice.

IHC – Signalling transduction patways evaluation: EGFR – AKT – ERK

Three to four different fields (400x magnification) from the selected animal examined in control untreated (group 1) and treated groups given pemetrexed and cisplatin alone (group 2) or combined to cetuximab, (group 6) were chosen, consisting of well representative neoplastic nodules. Each field had a maximum area of 198918.8 μm^2. A threshold of intensity for each marker was defined using a field from the untreated control animal as reference; the percentage of the total immunopositive area was then measured in control untreated and treated animals, as reported in Tab.15.

Tab.15: MSTO-211H cell line - EGF –AKT - ERK results

MARKER	Group	Animal #	% total positive area
EGF Receptor	Gr1	5	94,61
	Gr2	9	68,88
	Gr6	26	**27,03**
Phospho EGF Receptor	Gr1	5	27,52
	Gr2	9	17,63
	Gr6	26	22,89
MARKER	**Group**	**Animal #**	**% total positive area**
AKT pan	Gr1	5	74,80
	Gr2	9	21,13
	Gr6	26	51,60
Phospho AKT	Gr1	5	17,83
	Gr2	9	8,54
	Gr6	26	**3,03**
MARKER	**Group**	**Animal #**	**% total positive area**
ERK 1	Gr1	5	74,93
	Gr2	9	76,88
	Gr6	26	71,43
ERK 1/2	Gr1	5	22,95
	Gr2	9	26,95
	Gr6	26	**0,95**

The percentage of the total immunopositive areas measured in the selected control untreated and treated animals showed lower values in the MSTO-211H xenograft mouse given pemetrexed and cisplatin in combination with cetuximab, compared the others, as regard the amount of EGFR, phospho AKT and ERK 1/2 markers.

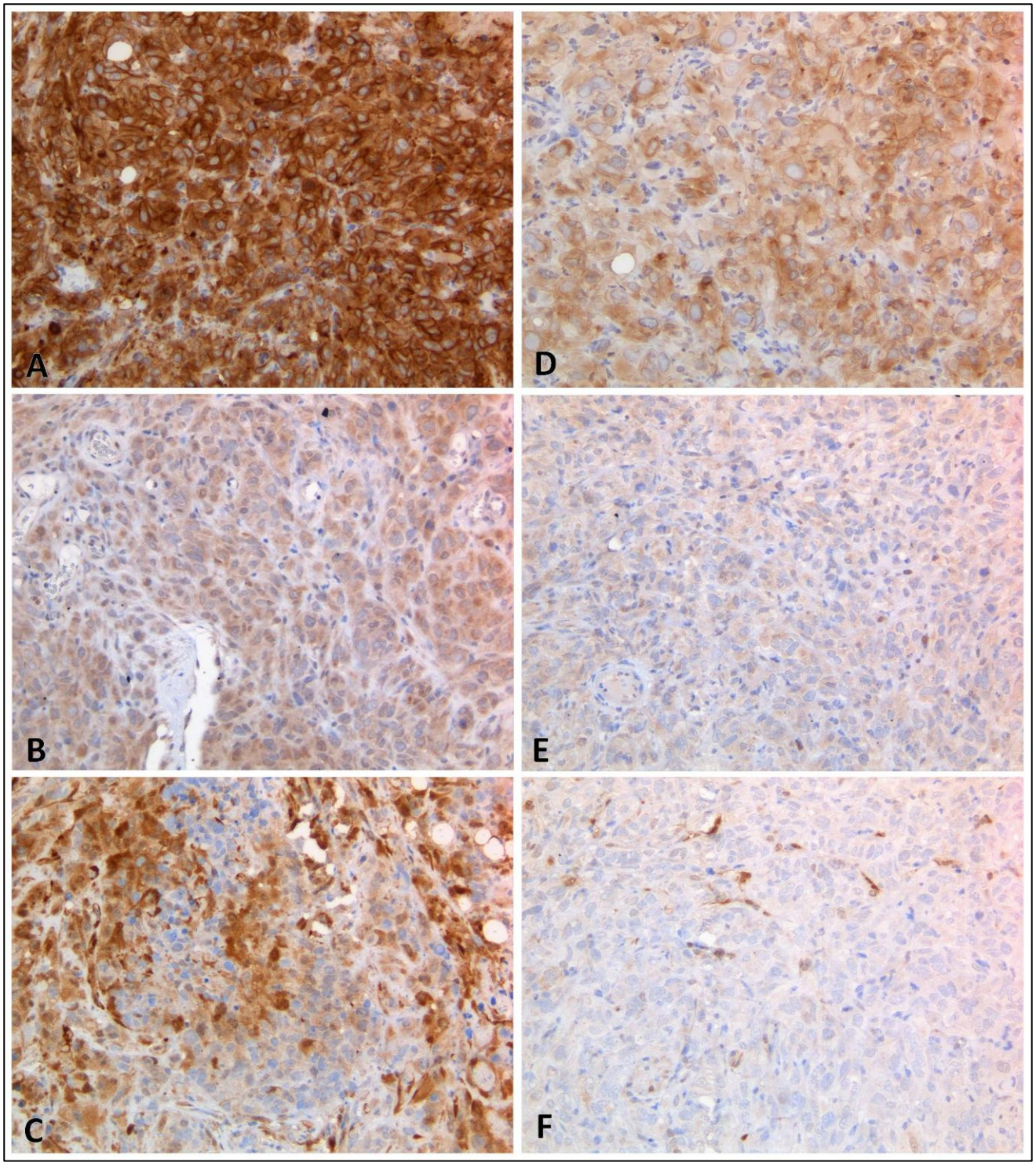

Fig.30: IHC signal transduction pathways marker in MSTO-211H cell line tumour:

A) control untreated animal	EGFR
B) control untreated animal	phosphor AKT
C) control untreated animal	ERK1/2
D) treated animal	EGFR
E) treated animal	phospho AKT
F) treated animal	ERK1/2

4.4.3 Statistical analyses on bioluminescence imaging

a) ROI in MSTO cell line (Tab.16)

Generalized estimated equation was used. A model was built with ROI as response variable, Gamma as distribution, “log” as link function and AR(1) as working correlation matrix. The independent variables were *time* (two observations points – beginning and end) and the category variable *group*. The latter had 6 categories.

Tab.16: MSTO-211H cell line bioluminescence - Statistical analysis for ROI quantification

Source	Type III		
	Wald chi square	df	Sig.
(Intercept)	47097.356	1	.000
group	20.135	5	.001
time	132.980	1	.000

(I) idgr	(J) idgr	Mean difference (I-J)	Standard Error Deviation	df	Sig Bonferroni.	95% Wald confidence limits for the difference Lower	Upper
1	2	.806	.360	1	.376	-.250	1.862
	3	.278	.357	1	1.000	-.771	1.327
	4	.176	.286	1	1.000	-.662	1.015
	5	.386	.318	1	1.000	-.546	1.318
	6	1.236	.301	1	**.001**	.352	2.121
2	1	-.806	.360	1	.376	-1.862	.250
	3	-.528	.431	1	1.000	-1.793	.737
	4	-.630	.374	1	1.000	-1.727	.468
	5	-.420	.401	1	1.000	-1.597	.757
	6	.430	.386	1	1.000	-.702	1.563
3	1	-.278	.357	1	1.000	-1.327	.771
	2	.528	.431	1	1.000	-.737	1.793
	4	-.102	.371	1	1.000	-1.192	.989
	5	.108	.396	1	1.000	-1.053	1.269
	6	.958	.384	1	.187	-.167	2.084
4	1	-.176	.286	1	1.000	-1.015	.662
	2	.630	.374	1	1.000	-.468	1.727
	3	.102	.371	1	1.000	-.989	1.192
	5	.209	.333	1	1.000	-.768	1.187
	6	1,060	.318	1	**.013**	.127	1.993
5	1	-.386	.318	1	1.000	-1.318	.546
	2	.420	.401	1	1.000	-.757	1.597
	3	-.108	.396	1	1.000	-1.269	1.053
	4	-.209	.333	1	1.000	-1.187	.768
	6	.850	.351	1	.231	-.180	1.880
6	**1**	-1.236	.301	1	**.001**	-2.121	-.352
	2	-.430	.386	1	1.000	-1.563	.702
	3	-.958	.384	1	.187	-2.084	.167
	4	-1.060	.318	1	**.013**	-1.993	-.127
	5	-.850	.351	1	.231	-1.880	.180

Legend groups:

1: pbs
2: cisplatin and pemetrexed
3: cetuximab 3 mg/kg
4: cetuximab 10 mg/kg
5: cetuximab 30 mg/kg
6: cisplatin, pemetrexed, cetuximab (high dose)

The *group* variable was found to be statistically significant (p = 0.001), as well as the *time* variable (p = 0.00001). In particular, pairwise comparisons with *Bonferroni* correction showed that Group 6 differed statistically from groups 1 and 4.

b) ROI in REN cell line (Tab.17)

Generalized estimated equation was used. A model was built with ROI as response variable, Gamma as distribution, “log” as link function and AR(1) as working correlation matrix. The independent variables were *time* (two observations points – beginning and end) and the category variable *group*. The latter had 6 categories.

Tab.17: REN cell line bioluminescence - Statistical analysis for ROI quantification

Source				Type III			
				Wald Chi-square	df	Sig.	
(Intercept)				61199.737	1	.000	
Group				33.405	5	.000	
Time				23.725	1	.000	
(I) idgr	(J) idgr	Mean difference (I-J)	Standard Error Deviation	df	Sig Bonferroni.	95% Wald confidence limits for the difference Lower	Upper
1	2	-.620	.309	1	.675	-1.527	.288
	3	-.970	.198	1	**.000**	-1.553	-.388
	4	-.468	.203	1	.316	-1.064	.128
	5	-.418	.255	1	1.000	-1.167	.331
	6	.086	.237	1	1.000	-.611	.783
2	1	.620	.309	1	.675	-.288	1.527
	3	-.351	.302	1	1.000	-1.237	.536
	4	.151	.305	1	1.000	-.744	1.047
	5	.202	.342	1	1.000	-.802	1.206
	6	.706	.329	1	.479	-.260	1.671
3	1	.970	.198	1	.000	.388	1.553
	2	.351	.302	1	1.000	-.536	1.237
	4	.502	.192	1	.134	-.062	1.066
	5	.552	.247	1	.376	-.171	1.276
	6	1.056	.228	1	.000	.387	1.726
4	1	.468	.203	1	.316	-.128	1.064
	2	-.151	.305	1	1.000	-1.047	.744
	3	-.502	.192	1	.134	-1.066	.062
	5	.050	.250	1	1.000	-.684	.785
	6	.554	.232	1	.254	-.127	1.235
5	1	.418	.255	1	1.000	-.331	1.167
	2	-.202	.342	1	1.000	-1.206	.802
	3	-.552	.247	1	.376	-1.276	.171
	4	-.050	.250	1	1.000	-.785	.684
	6	.504	.279	1	1.000	-.315	1.322
6	1	-.086	.237	1	1.000	-.783	.611
	2	-.706	.329	1	.479	-1.671	.260
	3	-1.056	.228	1	**.000**	-1.726	-.387
	4	-.554	.232	1	.254	-1.235	.127
	5	-.504	.279	1	1.000	-1.322	.315

Legend groups:

1: pbs
2: cisplatin and pemetrexed
3: cetuximab 3 mg/kg
4: cetuximab 10 mg/kg
5: cetuximab 30 mg/kg
6: cisplatin, pemetrexed, cetuximab (high dose)

The *group* variable was found to be statistically significant (p = 0.001), as was the *time* variable (p = 0.00001). In particular, pairwise comparisons with *Bonferroni* correction showed that Group 3 differed statistically from groups 1 and 6

5 DISCUSSION

The results obtained in the research project carried out during the doctoral programme successfully achieved the aim of the work, making a certain contribution to increasing our knowledge in the biology and behaviour of the selected human malignant pleural mesothelioma (hMPM) cell lines.

In the first phase of the project, a preclinical investigative platform, consisting of *in vitro* and *in vivo* models, bioluminescence imaging and histopathology investigations, was defined with the aim of creating an easily usable "tool" to investigate the response of hMPM cells to drug compounds. The two selected hMPM cell lines are REN, an epithelioid cell line and MSTO-211H, a bi-phasic cell line, being the most common variant of the tumour occurring in humans (the epithelioid subtypes alone comprises 50–60% of all mesotheliomas). Other variants are the sarcomatoid type and the desmoplastic mesothelioma, considered extremely rare (Greillier and Astoul, 2008).

In the second phase of the project, this newly set up platform was used to assess the efficacy of cetuximab, a monoclonal antibody at present used for the treatment of metastatic colorectal cancer and head and neck cancer, on the selected hMPM cell lines, both as a single agent and in combination with first line drugs used in therapeutic protocols, with the aim of testing its potential inhibitory activity on tumours.

Platform setup

The diagnostic platform was defined and characterized during the first phase of the project by carefully assessing the data obtained in the single in vitro and in vivo studies conducted. The temporal sequence with which the activities progressed allowed useful technical/scientific suggestions to be taken into account to create an efficient experimental protocol.

This was able to show a good correlation between the in vitro and in vivo results for the two tumour lines examined, as well as between the bioluminescence and histopathology results. This enables molecules to be screened progressively, based on a step-wise approach, making a first selection on the basis of the in vitro results, then testing the molecules of potential interest in vivo, and deciding whether to continue with histopathology investigations depending on the bioluminescence results. This approach therefore allows efficient time management and a lower number of animals to be used, in line with current ethical and scientific considerations regarding animal testing and research, as regards the 3R's (Ferdowsian and Beck, 2011), reducing both the number of studies and the number of tests to those effectively needed.

The first studies conducted were those in vitro, which showed that MSTO-211H cells had greater biological activity than REN cells, as demonstrated by the higher bioluminescence activity measured, and were more sensitive to treatment with cetuximab, as demonstrated in the tumour growth assay by partial inhibition of tumoural growth, especially following addition of epidermal growth factor (EGF) to the culture. Again in the presence of EGF, it was observed that in the MSTO-211H cell line cetuximab reduced ligand-induced EGFR

phosphorylation as well as reducing ERK and AKT phosphorylation to levels lower than untreated controls. This peculiar effectiveness in presence of EGF supplementation spurred us to proceed with the program, as it is well known in the literature the role of EGF-dependent autocrine loop in malignant tumours with related EGFR over expression in the response proliferative effect induced (Ciardiello and Tortora, 2003).

On the basis of these first in vitro results and of the significant biological differences between the two cell lines, we decided to assess their behaviour in an animal model. Since in order to know a patient's tumour response to a specific therapeutic regimen, the best approach is to examine the response of that human tumour to the therapy, the human malignant mesothelioma xenograft model on athymic nude mice was considered appropriate, being potentially able to reproduce the organ environment in which the tumour grows, including tumour stroma, and the effect of the tumour on its microenvironment, albeit with the exception of certain T-cell populations, as athymic mice (Richmond, 2008).

A challenge presented with orthotopic intraperitoneal models was the difficulty of following tumour growth *in vivo* and to this end bioluminescent imaging, a non-invasive and highly sensitive analytical method, was found to be useful for our experimental needs.

In an initial stage of the pilot study, bioluminescence allowed tumoural growth of both cell lines to be confirmed without having to euthanize the animals, and also in this case the measurement of bioluminescence activity showed greater biological activity of MSTO-211H cell line than REN. This new information obtained *in vivo*, in line with that already shown *in vitro*, provided guidance on the choice of the dose of tumour cells to be inoculated into main study animals, the quantity varying depending on the cell line used.

Even though the problem of assessing tumour growth *in vivo* had been solved thanks to the use of bioluminescence imaging, during the first phase of the study we realized that tissue sampling for histology investigations in accordance with international guidance proposed by the RITA and NACAD groups (Ruehl-Fehlert et al., 2003; Kittel et al., 2004; Morawietz et al., 2004), resulted in the loss of some of the smaller tumoural masses not adhering to abdominal organs but scattered among the peritoneal ligaments.

To avoid this, in the second phase of the pilot study a method was set up in order to sample organs in the abdominal cavity without losing any information. This technique for sampling together all the abdominal organs and subsequent whole body histotechnique was found to be useful, allowing histological examination of a sufficient quantity of tumoural tissue, even if the masses themselves were small and unattached to the parenchymal organs. The slides produced using this technique also allow many serial cuts to be made, for use with the desired histochemical and immunohistochemical staining. Furthermore this technique also allowed the preservation of the natural anatomical relationships among the organs populating the abdominal cavity. This gave an insight on how tumor cells growth and disseminate within the peritoneal cavity.

A final platform setup step was performed during the main study, with the comparison of bioluminescence and histopathology results in control untreated animals injected both with MSTO-211H and REN cells. In line with the bioluminescence results in *in vitro* studies and in the *in vivo* pilot study, also in this case greater biological activity

of the MSTO-211H cell line was seen compared to REN, as demonstrated by the greater bioluminescence activity measured. Interestingly, the histopathology examination similarly showed a more aggressive growth pattern for the MSTO-211H cell line than REN. In fact, in animals of the untreated control group in the main study, MSTO-211H cells inoculated into the abdominal cavity tended to infiltrate the organs contained, in particular the pancreas, mesenteric lymph nodes and diaphragm, passing through the latter to the thoracic cavity, in some animals involving the tracheobronchial lymph nodes and the lung parenchyma itself.

Cetuximab efficacy

Even though data from *in vitro* tests and the *in vivo* hMPM xenograft main study suggest that cetuximab was not effective on REN cell lines, either as a single agent or in combination with pemetrexed and cisplatin, on the contrary, however, cetuximab efficacy was interestingly observed on MSTO-211H cell lines, as shown both *in vitro* and *in vivo*.

The *in vitro* tumour growth assays showed partial inhibition of tumour growth and reduced ligand-induced EGFR phosphorylation as well as reduced ERK and AKT phosphorylation to levels lower than untreated controls, especially following addition of EGF to the culture.

In the in vivo study on MSTO-211H xenograft mice cetuximab, when in combination with pemetrexed and cisplatin, decreased bioluminescence activity with evidence of statistical significance compared to the untreated control group. A similar trend was seen in animals given pemetrexed and cisplatin alone, however without statistical significance. Likewise, at histology, a less pronounced tendency to infiltrate organs in the abdominal cavity and to expand to the thoracic cavity was observed when cetuximab was given in combination with pemetrexed and cisplatin, compared to untreated controls, showing also a minimal improvement compared to animals given pemetrexed and cisplatin alone.

Based on these results we can conclude that cetuximab induced enhanced tumour growth inhibiting effect on MSTO-211H cell line when it was given in combination with first line chemotherapeutics such as pemetrexed and cisplatin; however since the inhibiting effects on tumour growth induced by the first line treatment alone, were only slightly less evident, it is our opinion that further investigations could better explain the real contribute of cetuximab in addition to the first line agents used in the current therapeutic protocols for malignant mesothelioma.

In this direction are here only introduced some preliminary data obtained by immunohistochemistry evaluation on tumours coming from three MSTO-211H xenograft mice, a control untreated animal and two treated animals, one given pemetrexed and cisplatin alone and the other in combination with cetuximab. Preliminary results showed a relevant trend towards a decreased proliferative effect and a decreased number of newly-formed small vessels in the tumours examined in animals given pemetrexed and cisplatin alone or combined to cetuximab. Moreover a clear reduction of AKT and ERK 1/2 phosphorylation was seen mainly in the combination regimen, showing a potential effect of cetuximab on the signaling downstream of EGFR pathway in MSTO-211H cell line.

In conclusion, it is important to acknowledge the value of having set up a preclinical diagnostic platform to use in screening molecules potentially effective against tumours (i.e. human malignant mesothelioma) strictly connected with the possibility of carrying out experimental preclinical investigations based on a step-wise approach, with a well-defined rationale that brings together the information obtained at different times, from early studies that can be conducted quickly and tend to be less costly in less complex cell systems, to studies in more complex animal models, with consequent time-saving and use of fewer animals.

6 REFERENCES

Altomare DA, Vaslet CA, Skele KL et al. (2005) A mouse model recapitulating molecular features of human mesothelioma. *Cancer Res* 65: 8090–8095

Au JT, Gonzalez L, Chen CH et al. (2012) Bioluminescence imaging serves as a dynamic marker for guiding and assessing thermal treatment of cancer in a preclinical model. *Ann Surg Oncol.* 19(9): 3116-3122

Bertino P, Piccardi F, Porta C et al. (2008) Imatinib mesylate enhances therapeutic effects of gemcitabine in human malignant mesothelioma xenografts. *Clin Cancer Res* 14(2): 541-548

Bianchi C and Bianchi T (2007) Estimated annual crude incidence rates of malignant mesothelioma in the world. *Industrial Health* 45: 379-387

Ciardiello F, Tortora G (2003) Epidermal growth factor receptor (EGFR) as a target in cancer therapy: understanding the role of receptor expression and other molecular determinants that could influence the response to anti-EGFR drugs. *European Journal of Cancer* 39(10): 1348-1354

Ferdowsian HR, Beck N (2011) Ethical and scientific considerations regarding animal testing and research. *PLoS ONE* 6(9): e24059

Ferrante D, Bertolotti M, Todesco A et al. (2007) Cancer mortality and incidence of mesothelioma in a cohort of wives of asbestos workers in Casale Monferrato, Italy. *Environmental Health Perspectives* 115(10): 1401-1405

Greillier L, Astoul P (2008) Mesothelioma and Asbestos-Related Pleural Diseases. *Respiration* 76 :1–15

Iwatsubo Y, Pairon JC, Boutin C, et al. (1998) Pleural mesothelioma: dose-response relation at low levels of asbestos exposure in a French population-based case-control study. *Am J Epidemiol* 148(2): 133–142

Jackaman C, Bundell CS, Kinnear BF et al. (2003) IL-2 intratumoral immunotherapy enhances CD8+ T cells that mediate destruction of tumour cells and tumor-associated vasculature: a novel mechanism for IL-2. *J Immunol* 171: 5051–5063

Kittel B, Ruehl-Fehlert C, Morawietz G et al. (2004) Revised guides for organ sampling and trimming in rats and mice - Part 2. *Exp Toxicol Pathol* 55(6): 413–431

Magnani C, Agudo A, González CA, et al. (2000) Multicentric study on malignant pleural mesothelioma and non-occupational exposure to asbestos. *British Journal of Cancer* 83(1): 104–111

Magnani C, Dalmasso P, Biggeri A et al. (2001) Increased risk of malignant mesothelioma of the pleura after residential or domestic exposure to asbestos: a case–control study in Casale Monferrato, Italy. *Environmental Health Perspectives* 109 (9): 915-919

Magnani C, Ferrante D, Barone-Adesi F et al. (2008) Cancer risk after cessation of asbestos exposure: a cohort study of italian asbestos cement workers. *Occup. Environ. Med.* 65: 164-170

Mingqian F, Jingli Z, Miriam A et al. (2011) *In vivo* imaging of human malignant mesothelioma grown orthotopically in the peritoneal cavity of nude mice. *J Cancer* 2:123-131

Morawietz G, Ruehl-Fehlert C, Kittel B et al. (2004) Revised guides for organ sampling and trimming in rats and mice - Part 3. *Exp Toxicol Pathol* 55(6): 433–449

Ruehl-Fehlert C, Kittel B, Morawietz G et al. (2003) Revised guides for organ sampling and trimming in rats and mice - Part 1. *Exp Toxicol Pathol* 55(2): 91–106

Richmond A, Su Y (2008) Mouse xenograft models vs GEM models for human cancer therapeutics. *Dis Model Mech* 1(2-3): 78-82

Scherpereel A, Astoul P, Baas P et al. (2010) Guidelines of the European Respiratory Society and the European Society of Thoracic Surgeons for the management of malignant pleural mesothelioma. *Eur Respir J* 35: 479–495

Shi Y, Hollenstein A, Felley-Bosco E et al. (2011) Bioluminescence imaging for *in vivo* monitoring of local recurrence mesothelioma model. *Lung Cancer* 71: 370–373

Silberhumer GR, Brader P, Wong J et al. (2010) Genetically engineered oncolytic newcastle disease virus effectively induces sustained remission of malignant pleural mesothelioma. *Mol Cancer Ther* 9(10): 2761- 2769

Smythe WR, Kaiser LR, Hwang HC et al. (1994) Successful adenovirus-mediated gene transfer in an *in vivo* model of human malignant mesothelioma. *Ann Thorac Surg* 57: 1395-1401

The Mesothelioma Center (Dec. 2012) *Asbestos and Mesothelioma Around the World.* Available at: www.asbestos.com/mesothelioma/related-issues.php

Vaslet CA, Messier NJ and Kane AB (2002) Accelerated progression of asbestos-induced mesotheliomas in heterozygous $p53^{+/-}$ mice. *Toxicol Sci* 68: 331–338

Wagner JC and Berry G (1969) Mesotheliomas in rats following inoculation with asbestos. *Br J Cancer* 23(3): 567–581

Wagner JC, Sleggs CA and Marchand P (1960) Diffuse pleural mesothelioma and asbestos exposure in the North Western Cape Province. *Br J Ind Med* 17: 260–271

Yanagihara K, Tsumuraya M, Takigahira M et al. (2010) An orthotopic implantation mouse model of human malignant pleural mesothelioma for *in vivo* photon counting analysis and evaluation of the effect of S-1 therapy. *Int. J. Cancer* 126: 2835–2846

7 APPENDICES

Appendix 1: Main study randomization

On day 0 of the main experiment, thirty five CD1-Foxn1$^{nu/nu}$ mice received i.p. injections of 1 million/animal MSTO-211H luc$^{+/+}$ cells and other forty CD1-Foxn1$^{nu/nu}$ mice received i.p. injections of 2 million/animal REN luc$^{+/+}$ cells; mice were kept in groups of 5 animals each cage and a temporary identification number (IDt) was given. Thirteen days after cell inoculation, sixty one mice were selected and allocated to the dose groups by randomization based on region of interest (ROI) intensity. Each animal received a definitive identification number (IDd) to substitute the temporary one.

MSTO-211H luc^{++} - Assigned numbers before randomization

CAGE 1		CAGE 2		CAGE 3		CAGE 4		CAGE 5		CAGE 6		CAGE 7	
IDt	ROI	IDt	ROI	IDt	ROI	IDt	ROI	IDt	ROI	IDt	ROI	IDt	ROI
0	+++	5	-	24	++++	5	+++	36	-	124	++++	234	-
1	++++	6	++++	25	+	13	++	23	+	126	++++	235	++++
2	-	14	++++	26	-	46	++++	12	+++	136	+++	236	+++
3	++++	15	++	34	++++	134	++++	145	+++	45	+++	345	++
4	+++	16	+++	35	+++	135	+++	56	++++	125	++++	156	+++

MSTO-211H luc^{++} - Assigned numbers after randomization

Group 1		Group 2		Group 3		Group 4		Group 5		Group 6	
IDt	IDd	IDt	IDd	IDt	IDd	IDt	IDd	IDt	IDd	IDt	IDd
6	1	**0**	6	**5**	11	**12**	16	**36**	21	**24**	26
14	2	**1**	7	**13**	12	**56**	17	**45**	22	**25**	27
15	3	**2**	8	**124**	13	**126**	18	**46**	23	**26**	28
16	4	**3**	9	**134**	14	**136**	19	**125**	24	**34**	29
235	5	**4**	10	**135**	15	**145**	20	**236**	25	**35**	30
										156	31

REN luc^{++} - Assigned numbers before randomization

CAGE 1		CAGE 2		CAGE 3		CAGE 4		CAGE 5		CAGE 6		CAGE 7		CAGE 8	
IDt	ROI	IDt	ROI	IDt	ROI	IDt	ROI	IDt	ROI	IDt	ROI	IDt	ROI	IDt	ROI
0	++	5	++	24	-	0	-	36	++	124	+++	3	-	145	+++
1	+	6	+++	25	+++	13	+++	23	++	2	-	234	+	125	+++
2	+++	14	-	26	++	46	++	12	+++	126	++	235	+++	4	-
3	+	15	-	34	++	134	+++	1	-	136	+++	236	+++	346	+++
4	+++	16	+++	35	+++	135	++	56	+++	45	++	345	++	156	-

REN luc^{++} - Assigned numbers after randomization

Group 1		Group 2		Group 3		Group 4		Group 5		Group 6	
IDt	IDd	IDt	IDd	IDt	IDd	IDt	IDd	IDt	IDd	IDt	IDd
0	1	**5**	6	**12**	11	**13**	16	**26**	21	**125**	26
1	2	**6**	7	**23**	12	**45**	17	**234**	22	**135**	27
2	3	**14**	8	**36**	13	**124**	18	**235**	23	**145**	28
3	4	**16**	9	**46**	14	**126**	19	**236**	24	**156**	29
4	5	**34**	10	**56**	15	**136**	20	**345**	25	**346**	30

Legenda for ROI intensity interpretation:

- : signal absent or weak
+ : signal single spot
++ : signal blue
+++ : signal some red
++++ : signal extremely red

Appendix 2: Raw data for bioluminescence imaging (MSTO-211H luc^{++})

Pilot study

Image Number MSTO	ROI	Mouse injected	Image Layer	Total Flux [p/s]	Avg Radiance [p/s/cm²/sr]	Stdev Radiance	Min Radiance	Max Radiance
MC20110531131054	ROI 1	0.5 million cells	Overlay	2.374e+08	1.414e+06	2.207e+06	5.931e+03	1.050e+07
MC20110531131054	ROI 2	1 million cells	Overlay	1.063e+08	7.597e+05	1.822e+06	5.487e+03	9.512e+06
MC20110531131054	ROI 3	5 million cells	Overlay	1.304e+09	6.853e+06	3.885e+06	3.870e+04	1.077e+07

Main study

Image Number MSTO group 1	ROI	Mouse # IDt	Mouse # IDd	Image Layer	Total Flux [p/s]	Avg Radiance [p/s/cm²/sr]	Stdev Radiance	Min Radiance	Max Radiance
EMI20111110144220A	ROI 1	6	**1**	Overlay	1.779e+09	9.193e+06	1.778e+07	1.692e+03	8.683e+07
EMI20111110144220A	ROI 2	14	**2**	Overlay	3.176e+09	1.810e+07	2.734e+07	2.158e+03	1.048e+08
EMI20111110144939A	ROI 1	15	**3**	Overlay	3.705e+08	1.914e+06	3.356e+06	-1.082e+04	3.080e+07
EMI20111110144939A	ROI 2	16	**4**	Overlay	9.799e+08	5.644e+06	1.078e+07	-8.819e+03	9.278e+07
EMI20111110161454A	ROI 2	235	**5**	Overlay	1.033e+09	5.279e+06	7.627e+06	-1.288e+03	5.702e+07
EMI20111118113959A	ROI 1	6	**1**	Overlay	1.538e+10	8.976e+07	1.291e+08	1.026e+05	5.839e+08
EMI20111118113959A	ROI 2	14	**2**	Overlay	1.619e+10	9.555e+07	1.288e+08	9.142e+04	5.197e+08
EMI20111118113959A	ROI 3	15	**3**	Overlay	4.057e+09	2.432e+07	3.902e+07	3.591e+04	2.997e+08
EMI20111118114916A	ROI 1	16	**4**	Overlay	8.347e+09	4.927e+07	7.730e+07	-4.019e+04	3.923e+08
EMI20111118114916A	ROI 2	235	**5**	Overlay	6.997e+08	4.083e+06	8.068e+06	-5.279e+04	5.967e+07
EMI20111128115859A	ROI 1	6	**1**	Overlay	6.567e+10	3.393e+08	4.096e+08	7.164e+05	1.202e+09
EMI20111128115859A	ROI 2	14	**2**	Overlay	5.897e+10	3.396e+08	3.780e+08	5.715e+05	1.051e+09
EMI20111128115859A	ROI 3	15	**3**	Overlay	1.833e+10	9.802e+07	1.443e+08	3.593e+05	9.801e+08
EMI20111128120345A	ROI 1	16	**4**	Overlay	3.757e+10	1.913e+08	2.713e+08	2.529e+05	1.164e+09
EMI20111128120345A	ROI 2	235	**5**	Overlay	4.814e+10	2.819e+08	3.336e+08	2.384e+05	1.170e+09

Image Number MSTO group 2	ROI	Mouse # IDt	Mouse # IDd	Image Layer	Total Flux [p/s]	Avg Radiance [p/s/cm²/sr]	Stdev Radiance	Min Radiance	Max Radiance
EMI20111110142648A	ROI 1	0	**6**	Overlay	1.602e+09	8.157e+06	1.623e+07	1.094e+04	9.362e+07
EMI20111110142648A	ROI 2	1	**7**	Overlay	3.683e+09	2.121e+07	2.860e+07	3.097e+04	9.028e+07
EMI20111110142648A	ROI 3	2	**8**	Overlay	1.229e+08	6.572e+05	1.775e+06	-1.382e+03	3.016e+07
EMI20111110143058A	ROI 1	3	**9**	Overlay	2.156e+09	1.215e+07	1.911e+07	1.763e+03	9.526e+07
EMI20111110143058A	ROI 2	4	**10**	Overlay	1.055e+09	6.179e+06	1.587e+07	-6.253e+03	1.124e+08
EMI20111118120617A	ROI 1	0	**6**	Overlay	1.517e+09	8.955e+06	1.745e+07	-2.495e+04	2.120e+08
EMI20111118120617A	ROI 2	1	**7**	Overlay	1.162e+10	6.856e+07	1.044e+08	8.335e+03	5.190e+08
EMI20111118120617A	ROI 3	2	**8**	Overlay	6.346e+09	3.804e+07	5.725e+07	-3.278e+04	3.588e+08
EMI20111118121321A	ROI 1	3	**9**	Overlay	5.367e+09	3.168e+07	5.734e+07	-7.244e+04	4.257e+08
EMI20111118121321A	ROI 2	4	**10**	Overlay	2.914e+09	1.747e+07	4.073e+07	-5.950e+04	3.114e+08
EMI20111128122419A	ROI 1	0	**6**	Overlay	7.065e+09	3.598e+07	1.091e+08	-1.056e+05	9.812e+08
EMI20111128122419A	ROI 2	1	**7**	Overlay	1.748e+10	1.007e+08	1.967e+08	-3.333e+04	1.043e+09
EMI20111128122419A	ROI 3	2	**8**	Overlay	4.456e+09	2.396e+07	3.781e+07	-1.457e+05	2.118e+08
EMI20111128123029A	ROI 1	3	**9**	Overlay	4.908e+09	3.347e+07	6.055e+07	-1.891e+04	4.197e+08
EMI20111128123029A	ROI 2	4	**10**	Overlay	1.772e+09	1.037e+07	3.128e+07	-7.428e+04	3.579e+08

Image Number MSTO group 3	ROI	Mouse # IDt	Mouse # IDd	Image Layer	Total Flux [p/s]	Avg Radiance [p/s/cm²/sr]	Stdev Radiance	Min Radiance	Max Radiance
EMI20111110151510A	ROI 1	5	**11**	Overlay	1.039e+09	5.369e+06	9.713e+06	-3.477e+03	9.155e+07
EMI20111110151510A	ROI 2	13	**12**	Overlay	3.001e+08	1.728e+06	4.348e+06	-5.407e+03	6.032e+07
EMI20111110155938A	ROI 1	124	**13**	Overlay	3.161e+09	1.610e+07	2.524e+07	1.837e+04	9.759e+07
EMI20111110151742A	ROI 1	134	**14**	Overlay	1.042e+09	5.385e+06	9.451e+06	-4.773e+03	5.930e+07
EMI20111110151742A	ROI 2	135	**15**	Overlay	5.971e+08	3.496e+06	1.037e+07	-1.228e+04	1.043e+08
EMI20111118125303A	ROI 1	5	**11**	Overlay	1.052e+08	6.139e+05	9.076e+05	-1.989e+04	5.817e+06
EMI20111118125303A	ROI 2	13	**12**	Overlay	2.802e+09	1.654e+07	2.231e+07	-3.334e+04	1.629e+08
EMI20111118125303A	ROI 3	124	**13**	Overlay	1.745e+10	1.030e+08	1.339e+08	-1.096e+04	5.928e+08
EMI20111118130016A	ROI 1	134	**14**	Overlay	4.633e+09	2.703e+07	3.792e+07	-1.981e+04	2.488e+08
EMI20111118130016A	ROI 2	135	**15**	Overlay	8.245e+09	4.866e+07	6.880e+07	-3.229e+04	3.562e+08
EMI20111128133532A	ROI 1	5	**11**	Overlay	1.740e+10	8.861e+07	1.354e+08	1.713e+05	7.930e+08
EMI20111128133532A	ROI 2	13	**12**	Overlay	7.945e+09	4.576e+07	7.092e+07	1.700e+04	4.251e+08
EMI20111128133532A	ROI 3	124	**13**	Overlay	6.963e+10	3.560e+08	3.855e+08	3.911e+05	1.213e+09
EMI20111128134232A	ROI 1	134	**14**	Overlay	3.750e+10	1.890e+08	2.490e+08	3.459e+04	1.130e+09
EMI20111128134232A	ROI 2	135	**15**	Overlay	3.348e+10	1.928e+08	2.304e+08	1.240e+05	9.311e+08

Image Number MSTO group 4	ROI	Mouse # IDt	IDd	Image Layer	Total Flux [p/s]	Avg Radiance [p/s/cm²/sr]	Stdev Radiance	Min Radiance	Max Radiance
EMI20111110153104A	ROI 3	12	**16**	Overlay	1.133e+09	6.156e+06	1.015e+07	-7.556e+03	7.434e+07
EMI20111110153425A	ROI 2	56	**17**	Overlay	1.487e+09	8.619e+06	1.613e+07	-4.136e+03	9.657e+07
EMI20111110155938A	ROI 2	126	**18**	Overlay	3.140e+09	1.809e+07	2.735e+07	1.864e+04	8.712e+07
EMI20111110155938A	ROI 3	136	**19**	Overlay	6.938e+08	3.769e+06	7.640e+06	6.356e+03	1.005e+08
EMI20111110153425A	ROI 1	145	**20**	Overlay	1.325e+09	6.846e+06	1.309e+07	-2.490e+03	9.266e+07
EMI20111118142426A	ROI 1	12	**16**	Overlay	5.165e+09	3.048e+07	3.761e+07	1.032e+04	1.854e+08
EMI20111118142426A	ROI 2	56	**17**	Overlay	3.824e+09	2.257e+07	4.117e+07	-3.380e+04	2.849e+08
EMI20111118142426A	ROI 3	126	**18**	Overlay	1.436e+10	8.475e+07	1.334e+08	-2.659e+04	5.822e+08
EMI20111118143109A	ROI 1	136	**19**	Overlay	1.907e+09	1.125e+07	1.935e+07	-5.173e+04	1.531e+08
EMI20111118143109A	ROI 2	145	**20**	Overlay	1.319e+10	7.786e+07	1.193e+08	-3.598e+04	5.910e+08
EMI20111128140125A	ROI 1	12	**16**	Overlay	3.826e+10	1.956e+08	2.566e+08	3.406e+05	1.182e+09
EMI20111128140125A	ROI 2	56	**17**	Overlay	1.769e+10	1.019e+08	1.622e+08	1.510e+05	7.602e+08
EMI20111128140125A	ROI 3	126	**18**	Overlay	6.026e+10	3.240e+08	3.948e+08	4.564e+05	1.206e+09
EMI20111128140520A	ROI 1	136	**19**	Overlay	1.491e+10	7.511e+07	1.113e+08	-3.426e+04	5.316e+08
EMI20111128140520A	ROI 2	145	**20**	Overlay	4.033e+10	2.337e+08	3.018e+08	8.848e+04	1.218e+09

Image Number MSTO group 5	ROI	Mouse # IDt	IDd	Image Layer	Total Flux [p/s]	Avg Radiance [p/s/cm²/sr]	Stdev Radiance	Min Radiance	Max Radiance
EMI20111110153104A	ROI 1	36	**21**	Overlay	5.280e+07	2.660e+05	7.854e+05	-1.470e+04	7.857e+06
EMI20111110160353A	ROI 1	45	**22**	Overlay	1.001e+09	5.046e+06	1.220e+07	-3.770e+03	9.598e+07
EMI20111110151510A	ROI 3	46	**23**	Overlay	1.827e+09	9.927e+06	1.602e+07	1.877e+03	1.046e+08
EMI20111110160353A	ROI 2	125	**24**	Overlay	3.820e+09	2.200e+07	2.960e+07	-2.381e+03	1.111e+08
EMI20111110161454A	ROI 3	236	**25**	Overlay	9.071e+08	5.312e+06	7.912e+06	-7.325e+03	6.298e+07
EMI20111118144923A	ROI 1	36	**21**	Overlay	4.090e+09	2.414e+07	4.476e+07	-1.749e+04	2.502e+08
EMI20111118144923A	ROI 2	45	**22**	Overlay	4.635e+09	2.705e+07	4.495e+07	-2.590e+04	3.088e+08
EMI20111118144923A	ROI 3	46	**23**	Overlay	8.850e+09	5.164e+07	6.232e+07	-1.053e+04	3.697e+08
EMI20111118145348A	ROI 1	125	**24**	Overlay	8.680e+09	5.065e+07	7.812e+07	0.000e+00	4.326e+08
EMI20111118145348A	ROI 2	236	**25**	Overlay	3.550e+09	2.071e+07	2.652e+07	-5.148e+04	1.721e+08
EMI20111128142416A	ROI 1	36	**21**	Overlay	1.369e+10	7.071e+07	9.868e+07	1.029e+05	4.574e+08
EMI20111128142416A	ROI 2	45	**22**	Overlay	1.128e+10	6.495e+07	8.525e+07	-3.329e+04	4.124e+08
EMI20111128142416A	ROI 3	46	**23**	Overlay	4.614e+10	2.443e+08	2.861e+08	1.737e+05	1.248e+09
-	-	125	**24**	-	-	-	-	-	-
EMI20111128142730A	ROI 2	236	**25**	Overlay	3.157e+10	1.818e+08	2.038e+08	1.264e+05	8.565e+08

Image Number MSTO group 6	ROI	Mouse # IDt	IDd	Image Layer	Total Flux [p/s]	Avg Radiance [p/s/cm²/sr]	Stdev Radiance	Min Radiance	Max Radiance
EMI20111110145738A	ROI 1	24	**26**	Overlay	2.682e+09	1.352e+07	2.466e+07	2.472e+02	1.009e+08
EMI20111110145738A	ROI 2	25	**27**	Overlay	1.530e+08	8.811e+05	2.626e+06	-1.313e+04	2.771e+07
EMI20111110145738A	ROI 3	26	**28**	Overlay	7.947e+07	4.317e+05	1.028e+06	-1.512e+04	1.533e+07
EMI20111110150132A	ROI 1	34	**29**	Overlay	2.209e+09	1.129e+07	2.046e+07	-9.116e+02	9.700e+07
EMI20111110150132A	ROI 2	35	**30**	Overlay	1.048e+09	6.075e+06	1.368e+07	-4.161e+03	1.028e+08
EMI20111110161929A	ROI 2	156	**31**	Overlay	9.507e+08	5.661e+06	9.465e+06	-6.175e+03	6.173e+07
EMI20111118150225A	ROI 1	24	**26**	Overlay	2.103e+09	1.227e+07	2.220e+07	-7.918e+04	1.592e+08
EMI20111118150225A	ROI 2	25	**27**	Overlay	6.122e+09	3.572e+07	5.409e+07	-3.363e+04	3.407e+08
EMI20111118150225A	ROI 3	26	**28**	Overlay	6.476e+09	3.882e+07	6.161e+07	-5.035e+04	3.842e+08
EMI20111118150852A	ROI 1	34	**29**	Overlay	3.430e+09	2.001e+07	3.263e+07	-7.998e+04	2.269e+08
EMI20111118150852A	ROI 2	35	**30**	Overlay	2.552e+08	1.489e+06	3.047e+06	-8.604e+04	2.680e+07
EMI20111118150852A	ROI 3	156	**31**	Overlay	3.065e+08	1.809e+06	5.463e+06	-8.928e+04	6.871e+07
EMI20111128143957A	ROI 1	24	**26**	Overlay	7.022e+08	4.200e+06	1.137e+07	-2.697e+04	1.269e+08
EMI20111128143957A	ROI 2	25	**27**	Overlay	8.252e+09	4.704e+07	8.695e+07	-8.744e+03	5.188e+08
EMI20111128143957A	ROI 3	26	**28**	Overlay	8.118e+09	4.342e+07	9.260e+07	-6.410e+04	5.959e+08
EMI20111128144646A	ROI 1	34	**29**	Overlay	5.637e+09	2.870e+07	5.637e+07	-5.760e+04	4.503e+08
EMI20111128144646A	ROI 2	35	**30**	Overlay	5.916e+06	3.372e+04	6.769e+04	-1.162e+05	7.999e+05
EMI20111128144646A	ROI 3	156	**31**	Overlay	2.152e+08	1.295e+06	4.009e+06	-8.154e+04	5.148e+07

Appendix 3: Raw data bioluminescence imaging REN luc^{++} cell lines

Pilot study

Image Number REN	ROI	Mouse injected	Image Layer	Total Flux [p/s]	Avg Radiance [p/s/cm²/sr]	Stdev Radiance	Min Radiance	Max Radiance
MC20110531130114	ROI 1	0.5 million cells	Overlay	2.354e+06	1.713e+04	3.316e+04	-1.650e+03	3.107e+05
MC20110531130114	ROI 2	1 million cells	Overlay	6.474e+07	4.010e+05	1.235e+06	-1.729e+03	9.443e+06
MC20110531130114	ROI 3	5 million cells	Overlay	7.128e+07	5.125e+05	1.817e+06	-2.226e+03	1.085e+07

Main study

Image Number REN group 1	ROI	Mouse # IDt	Mouse # IDd	Image Layer	Total Flux [p/s]	Avg Radiance [p/s/cm²/sr]	Stdev Radiance	Min Radiance	Max Radiance
EMI20111110100320A	ROI 1	0	**1**	Overlay	3.967e+07	1.938e+05	3.761e+05	-1.649e+04	3.453e+06
EMI20111110100320A	ROI 2	1	**2**	Overlay	1.453e+07	6.926e+04	1.390e+05	-1.617e+04	1.852e+06
EMI20111110100320A	ROI 3	2	**3**	Overlay	6.920e+07	3.330e+05	9.902e+05	-1.422e+04	9.630e+06
EMI20111110101204A	ROI 1	3	**4**	Overlay	4.226e+07	2.014e+05	6.807e+05	-1.253e+04	9.449e+06
EMI20111110101204A	ROI 2	4	**5**	Overlay	1.545e+08	7.473e+05	3.550e+06	-1.559e+04	4.135e+07
EMI20111118161112A	ROI 1	0	**1**	Overlay	1.415e+08	8.350e+05	1.515e+06	-1.104e+04	1.659e+07
EMI20111118161112A	ROI 2	1	**2**	Overlay	8.360e+07	4.934e+05	6.398e+05	-1.054e+04	4.527e+06
EMI20111118161112A	ROI 3	2	**3**	Overlay	3.874e+07	2.286e+05	4.719e+05	-1.350e+04	5.714e+06
EMI20111118161520A	ROI 1	3	**4**	Overlay	8.780e+07	5.123e+05	1.223e+06	-1.569e+04	1.381e+07
EMI20111118161520A	ROI 2	4	**5**	Overlay	7.702e+07	4.546e+05	1.112e+06	-1.266e+04	1.151e+07
EMI20111128155042A	ROI 1	0	**1**	Overlay	1.805e+08	9.095e+05	1.601e+06	-8.733e+03	1.278e+07
EMI20111128155042A	ROI 2	1	**2**	Overlay	2.120e+08	1.221e+06	1.403e+06	-1.156e+04	9.780e+06
EMI20111128155042A	ROI 3	2	**3**	Overlay	1.108e+08	6.019e+05	7.927e+05	-1.163e+04	6.398e+06
EMI20111128155759A	ROI 1	3	**4**	Overlay	2.005e+08	1.021e+06	1.689e+06	-1.066e+04	1.288e+07
EMI20111128155759A	ROI 2	4	**5**	Overlay	1.989e+08	1.146e+06	2.236e+06	-1.135e+04	1.583e+07

Image Number REN group 2	ROI	Mouse # IDt	Mouse # IDd	Image Layer	Total Flux [p/s]	Avg Radiance [p/s/cm²/sr]	Stdev Radiance	Min Radiance	Max Radiance
EMI20111110104135A	ROI 1	5	**6**	Overlay	2.009e+08	1.023e+06	3.208e+06	-1.243e+04	2.799e+07
EMI20111110104135A	ROI 2	6	**7**	Overlay	2.831e+08	1.630e+06	5.254e+06	-8.782e+03	4.288e+07
EMI20111110104135A	ROI 3	14	**8**	Overlay	1.653e+07	8.842e+04	3.362e+05	-1.787e+04	3.463e+06
EMI20111110105117A	ROI 2	16	**9**	Overlay	5.261e+07	3.030e+05	1.064e+06	-1.304e+04	1.811e+07
EMI20111110110031A	ROI 1	34	**10**	Overlay	1.422e+08	6.878e+05	1.463e+06	-1.228e+04	1.650e+07
EMI20111118163808A	ROI 1	5	**6**	Overlay	2.549e+08	1.487e+06	3.825e+06	-6.314e+03	3.377e+07
EMI20111118163808A	ROI 2	6	**7**	Overlay	1.695e+08	1.000e+06	1.026e+06	-6.739e+03	6.770e+06
EMI20111118163808A	ROI 3	14	**8**	Overlay	2.491e+08	1.476e+06	3.416e+06	-1.042e+04	2.921e+07
EMI20111118164145A	ROI 1	16	**9**	Overlay	8.008e+07	4.727e+05	7.378e+05	-1.102e+04	4.695e+06
EMI20111118164145A	ROI 2	34	**10**	Overlay	5.183e+08	3.024e+06	4.164e+06	-6.925e+03	3.347e+07
EMI20111128161527A	ROI 1	5	**6**	Overlay	1.147e+08	6.107e+05	8.898e+05	-9.416e+03	6.254e+06
EMI20111128161527A	ROI 2	6	**7**	Overlay	1.925e+08	1.035e+06	1.102e+06	-1.762e+04	6.439e+06
EMI20111128161527A	ROI 3	14	**8**	Overlay	9.046e+07	4.864e+05	7.697e+05	-1.256e+04	7.639e+06
EMI20111128162013A	ROI 1	16	**9**	Overlay	2.273e+08	1.174e+06	3.376e+06	-1.058e+04	4.062e+07
EMI20111128162013A	ROI 2	34	**10**	Overlay	8.463e+08	4.670e+06	7.173e+06	-6.288e+03	5.893e+07

Image Number REN group 3	ROI	Mouse # IDt	Mouse # IDd	Image Layer	Total Flux [p/s]	Avg Radiance [p/s/cm²/sr]	Stdev Radiance	Min Radiance	Max Radiance
EMI20111110111706A	ROI 3	12	**11**	Overlay	2.987e+08	1.598e+06	5.231e+06	-1.083e+04	4.696e+07
EMI20111110111706A	ROI 2	23	**12**	Overlay	1.352e+08	7.919e+05	2.787e+06	-1.102e+04	2.683e+07
EMI20111110111706A	ROI 1	36	**13**	Overlay	1.713e+08	8.853e+05	2.982e+06	-1.178e+04	3.321e+07
EMI20111110110652A	ROI 3	46	**14**	Overlay	9.621e+07	5.146e+05	1.194e+06	-1.793e+04	1.408e+07
EMI20111110112210A	ROI 1	56	**15**	Overlay	2.910e+08	1.640e+06	6.512e+06	-9.756e+03	7.434e+07
EMI20111118165652A	ROI 1	12	**11**	Overlay	2.289e+08	1.351e+06	2.072e+06	-1.106e+04	1.798e+07
EMI20111118165652A	ROI 2	23	**12**	Overlay	1.283e+08	7.571e+05	8.386e+05	-6.448e+03	5.207e+06
EMI20111118165652A	ROI 3	36	**13**	Overlay	2.499e+08	1.475e+06	3.257e+06	-8.125e+03	3.851e+07
EMI20111118170002A	ROI 1	46	**14**	Overlay	1.852e+08	1.081e+06	1.707e+06	-1.719e+04	1.379e+07
EMI20111118170002A	ROI 2	56	**15**	Overlay	1.579e+08	9.466e+05	2.179e+06	-1.846e+04	1.939e+07
EMI20111128163445A	ROI 1	12	**11**	Overlay	5.642e+08	2.915e+06	2.988e+06	1.069e+03	2.129e+07
EMI20111128163445A	ROI 2	23	**12**	Overlay	2.586e+08	1.489e+06	1.838e+06	-3.361e+03	1.214e+07
EMI20111128163445A	ROI 3	36	**13**	Overlay	6.306e+08	3.373e+06	6.111e+06	-4.884e+03	4.404e+07
EMI20111128163948A	ROI 1	46	**14**	Overlay	3.747e+08	1.908e+06	2.647e+06	-6.306e+03	2.583e+07
EMI20111128163948A	ROI 2	56	**15**	Overlay	2.508e+08	1.468e+06	2.059e+06	-6.695e+03	1.875e+07

Image Number REN group 4	ROI	Mouse # IDt	IDd	Image Layer	Total Flux [p/s]	Avg Radiance [p/s/cm²/sr]	Stdev Radiance	Min Radiance	Max Radiance
EMI20111110110652A	ROI 2	13	**16**	Overlay	6.388e+07	3.679e+05	1.653e+06	-1.200e+04	1.958e+07
EMI20111110113610A	ROI 2	45	**17**	Overlay	1.179e+08	6.905e+05	2.213e+06	-1.339e+04	2.975e+07
EMI20111110113232A	ROI 1	124	**18**	Overlay	9.137e+07	4.652e+05	1.607e+06	-1.525e+04	1.717e+07
EMI20111110113232A	ROI 2	126	**19**	Overlay	4.936e+07	2.843e+05	8.485e+05	-1.205e+04	1.227e+07
EMI20111110113610A	ROI 1	136	**20**	Overlay	2.577e+08	1.437e+06	4.971e+06	-1.379e+04	4.838e+07
EMI20111118171509A	ROI 1	13	**16**	Overlay	2.639e+07	1.557e+05	3.847e+05	-1.628e+04	4.307e+06
EMI20111118171509A	ROI 2	45	**17**	Overlay	1.863e+08	1.099e+06	1.414e+06	-1.251e+04	9.258e+06
EMI20111118171509A	ROI 3	124	**18**	Overlay	1.621e+08	9.532e+05	2.397e+06	-1.562e+04	2.352e+07
EMI20111118171845A	ROI 1	126	**19**	Overlay	1.087e+08	6.418e+05	1.087e+06	-1.083e+04	8.722e+06
EMI20111118171845A	ROI 2	136	**20**	Overlay	7.856e+07	4.709e+05	6.260e+05	-1.271e+04	5.071e+06
EMI20111128165303A	ROI 1	13	**16**	Overlay	2.407e+08	1.386e+06	2.252e+06	-9.239e+03	1.528e+07
EMI20111128165303A	ROI 2	45	**17**	Overlay	3.409e+08	1.815e+06	1.800e+06	-4.861e+03	1.221e+07
EMI20111128165303A	ROI 3	124	**18**	Overlay	1.580e+08	8.450e+05	1.238e+06	-1.487e+04	7.835e+06
EMI20111128165805A	ROI 1	126	**19**	Overlay	3.290e+08	1.700e+06	2.264e+06	-7.477e+03	1.392e+07
EMI20111128165805A	ROI 2	136	**20**	Overlay	2.318e+08	1.335e+06	1.850e+06	-9.363e+03	1.928e+07

Image Number REN group 5	ROI	Mouse # IDt	IDd	Image Layer	Total Flux [p/s]	Avg Radiance [p/s/cm²/sr]	Stdev Radiance	Min Radiance	Max Radiance
EMI20111110105441A	ROI 3	26	**21**	Overlay	8.211e+07	4.729e+05	1.537e+06	-1.603e+04	1.698e+07
EMI20111110114221A	ROI 1	234	**22**	Overlay	7.458e+07	4.597e+05	1.504e+06	-8.707e+03	1.669e+07
EMI20111110114221A	ROI 2	235	**23**	Overlay	3.214e+08	1.851e+06	5.174e+06	-1.070e+04	4.094e+07
EMI20111110114615A	ROI 1	236	**24**	Overlay	9.503e+07	5.565e+05	2.201e+06	-1.469e+04	2.044e+07
EMI20111110114615A	ROI 2	345	**25**	Overlay	5.219e+07	3.161e+05	8.442e+05	-1.478e+04	1.099e+07
EMI20111118172858A	ROI 1	26	**21**	Overlay	2.196e+08	1.296e+06	2.196e+06	-9.650e+03	2.258e+07
EMI20111118172858A	ROI 2	234	**22**	Overlay	8.060e+07	4.757e+05	6.691e+05	-9.731e+03	5.090e+06
EMI20111118172858A	ROI 3	235	**23**	Overlay	2.302e+08	1.343e+06	4.264e+06	-1.229e+04	3.838e+07
EMI20111118173205A	ROI 1	236	**24**	Overlay	1.158e+08	6.836e+05	2.412e+06	-1.485e+04	2.436e+07
EMI20111118173205A	ROI 2	345	**25**	Overlay	6.117e+07	3.569e+05	7.642e+05	-1.181e+04	6.909e+06
EMI20111128170903A	ROI 1	26	**21**	Overlay	2.729e+08	1.375e+06	1.910e+06	-1.854e+04	1.905e+07
EMI20111128170903A	ROI 2	234	**22**	Overlay	2.295e+08	1.322e+06	1.786e+06	-5.713e+03	1.376e+07
EMI20111128170903A	ROI 3	235	**23**	Overlay	2.423e+08	1.296e+06	2.015e+06	-9.224e+03	1.562e+07
EMI20111128172615A	ROI 1	236	**24**	Overlay	1.687e+08	8.499e+05	1.821e+06	-8.889e+03	1.638e+07
EMI20111128172615A	ROI 2	345	**25**	Overlay	1.719e+08	9.898e+05	1.616e+06	-9.180e+03	1.416e+07

Image Number REN group 6	ROI	Mouse # IDt	IDd	Image Layer	Total Flux [p/s]	Avg Radiance [p/s/cm²/sr]	Stdev Radiance	Min Radiance	Max Radiance
EMI20111110115108A	ROI 2	125	**26**	Overlay	1.527e+08	8.939e+05	1.962e+06	-7.427e+03	1.624e+07
EMI20111110111014A	ROI 2	135	**27**	Overlay	3.880e+07	1.976e+05	3.075e+05	-1.447e+04	3.668e+06
EMI20111110115108A	ROI 1	145	**28**	Overlay	6.081e+07	3.109e+05	1.261e+06	-1.535e+04	1.597e+07
EMI20111110115509A	ROI 2	156	**29**	Overlay	2.575e+07	1.645e+05	4.199e+05	-1.339e+04	7.581e+06
EMI20111110115509A	ROI 1	346	**30**	Overlay	1.193e+08	6.983e+05	2.763e+06	-1.292e+04	3.577e+07
EMI20111118174323A	ROI 1	125	**26**	Overlay	4.485e+08	2.647e+06	6.969e+06	-7.715e+03	9.333e+07
EMI20111118174323A	ROI 2	135	**27**	Overlay	1.300e+08	7.674e+05	1.149e+06	-9.286e+03	1.274e+07
EMI20111118174323A	ROI 3	145	**28**	Overlay	2.266e+08	1.322e+06	2.274e+06	-1.322e+04	2.141e+07
EMI20111118174743A	ROI 1	156	**29**	Overlay	9.951e+07	5.806e+05	1.641e+06	-1.607e+04	1.381e+07
EMI20111118174743A	ROI 2	346	**30**	Overlay	2.063e+08	1.217e+06	3.439e+06	-1.199e+04	3.298e+07
EMI20111128173408A	ROI 1	125	**26**	Overlay	1.356e+08	6.833e+05	1.372e+06	-1.029e+04	1.838e+07
EMI20111128173408A	ROI 2	135	**27**	Overlay	1.332e+08	7.669e+05	1.137e+06	-1.146e+04	1.038e+07
EMI20111128173408A	ROI 3	145	**28**	Overlay	4.971e+07	2.701e+05	6.238e+05	-1.224e+04	5.562e+06
EMI20111128173835A	ROI 1	156	**29**	Overlay	1.306e+08	6.652e+05	2.000e+06	-1.402e+04	1.927e+07
EMI20111128173835A	ROI 2	346	**30**	Overlay	1.665e+08	9.590e+05	1.444e+06	-1.063e+04	9.457e+06

Appendix 4: Wholebody fixation

With the application of this simple and practical method, mice that are suppressed in the context of an experimental study or that spontaneously die in cage can be preserved *in toto* for a long period of time pending complete necropsy, adequate tissues sampling and histopathological examination.

This procedure is of particular advantage for all those investigators that do not have enough experience with interpretation of gross lesions, adequate organ dissection and standardized tissue sampling for histopathology. In this situation, the entire animal can be easily fixed and any further pathological examination deferred to laboratories with specific expertise in the field.

General considerations

In order to avoid the progression of post-mortem degenerative processes (i.e. putrefaction and autolysis), the following steps must be carried out as soon possible after animal death.

The necessary instruments are: tables of cork, expanded polystyrene or rubber; pins or adhesive tape; scissors and pliers, enough volume of fixative (10% NBF or 4% PFA), containers of adequate size.

Procedures

Lay down the mouse on an appropriate surface (i.e. tables of cork, expanded polystyrene or rubber), extended on the back, with the limbs spread and held firmly with pins or adhesive tape (Fig. 1 and 2)

Abdominal cavity opening

1. Using plier and scissor, open the abdominal cavity through a straight cut along the midline (Fig. 1, blue arrow; Fig. 2). This first cut of the abdominal wall should start approx at the umbilical level (in the caudal third of the abdomen) and end at the level of the xiphoid cartilage (the caudal extremity of the sternum) (Fig. 3).
2. Having reached the caudal extremity of the sternum, extend the cut of the abdominal wall laterally along the right and left costal arches (Fig. 1, green arrows; Fig. 4). When the mouse is placed in the bath of 10% NBF (or 4% PFA), these further two lateral cuts along the costal arches allow a wider exposure of the intra-abdominal organs to the fixative (Fig. 5).
3. During these operations pay attention not to damage the underlying abdominal organs with the scissors.

Thoracic cavity opening

4. At this point, pull-up the xiphoid cartilage with the pliers (Fig. 6) and create a wide breach in the diaphragm (i.e. the thin muscular membrane that separates the abdominal and thoracic cavity).
5. Cut the chest cage along a parasternal axis reaching the cranial extremity of the sternum (Fig. 1, red arrows; Fig. 7). Repeat the same procedure on both sides of the sternum to ensure a wider exposure of the intra-thoracic organs to the fixative when the mouse is placed in the bath of 10% NBF (or 4% PFA) (Fig. 8).
6. During these operations pay attention not to damage the underlying thoracic organs with the scissors.

Put the entire animal in a tank containing an adequate amount of fixative (10% NBF or 4% PFA) and shake gently for a couple of minutes to let out any residual air bubbles trapped in the opened body cavities. The ratio between the amount of tissue to be fixed and the volume of fixative should be at least 1/15. Once put in the bath of 10% NBF or 4% PFA, the mouse can be stored and/or shipped either at room temperature or at +4 °C.

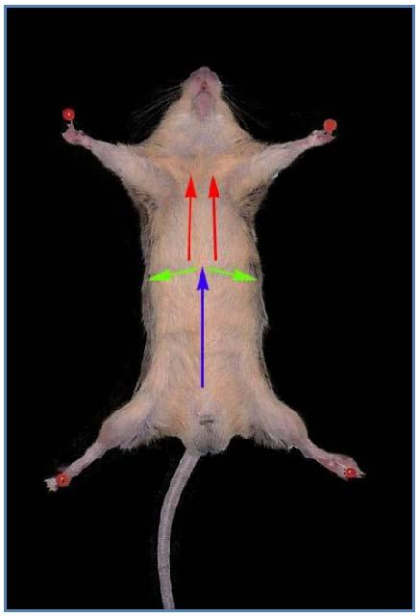

Fig. 1 – Schematic diagram showing the orientation of the main cuts: midline abdominal cut (blue arrow); lateral abdominal cuts along the costal arches (green arrows); parasternal cuts of the chest cage (red arrows).

Fig. 2 – Approach to the midline abdominal cut.

Fig. 3 – Midline abdominal cut with opening of the abdominal cavity.

Fig. 4 – Approach to the lateral abdominal cuts along the costal arches.

Fig. 5 – Lateral abdominal cuts along the costal arches with completely opened abdominal cavity (black arrow pointing at the xiphoid cartilage).

Fig. 6 – Pull-up of the xiphoid cartilage to approach the parasternal cuts of the chest cage.

Fig. 7 – Parasternal cut of the chest cage with opening of the thoracic cavity.

Fig. 8 – Completely opened thoracic cavity.

Major disadvantages

1. Slow and inadequate fixation of specific organs/tissues that consequently undergo autolytic/putrefactive changes. These post-mortal changes greatly affects gastrointestinal tract, CNS, enlarged organs and tumour or tumour-like lesions with a thickness exceeding 8-9 mm.

2. Tissue overfixation if gross examination with sampling and processing for histopathology are delayed beyond 72 hours from animal death and fixation. Since overfixation may compromise tissue antigenicity, this is a primary concern only when immunohistochemistry is specifically required on sampled organs/tissues.

Document produced by
Dr. E Radaelli and Dr. M. Losa
February, 2011

Mouse & Animal Pathology Laboratory (MAPLab)
Animal Model Systems - FONDAZIONE FILARETE
Viale Ortles, 22/4 – 20139 Milano (MI), Italy

Appendix 5: Wholebody histotechnique

Wholemount" histotechnique is conducted sampling abdominal organs "en bloc" after "wholemount fixation" and embedding them in paraffin blocks.

1. Open the abdominal cavity to visualize the entire content (Fig.1A).
2. Pull up the mass of abdominal organs consisting of liver, stomach, small and large intestinal tracts with mesenteric lymph nodes, spleen and pancreas ("en bloc" mass).
3. Using scissors, dissect the rectum, the mesenteric ligament, the epato-diaphragmatic ligament and the abdominal portion of the aesophagus (Fig.1B, 1C, 1D). Now the "en bloc" mass is disengaged.
4. Gently pull out the "en bloc" mass from the abdominal cavity by rolling it from cranial through caudal portion of the cavity.
5. Now the "en bloc" mass is fully disengaged and ready to be embedded (Fig.1E).

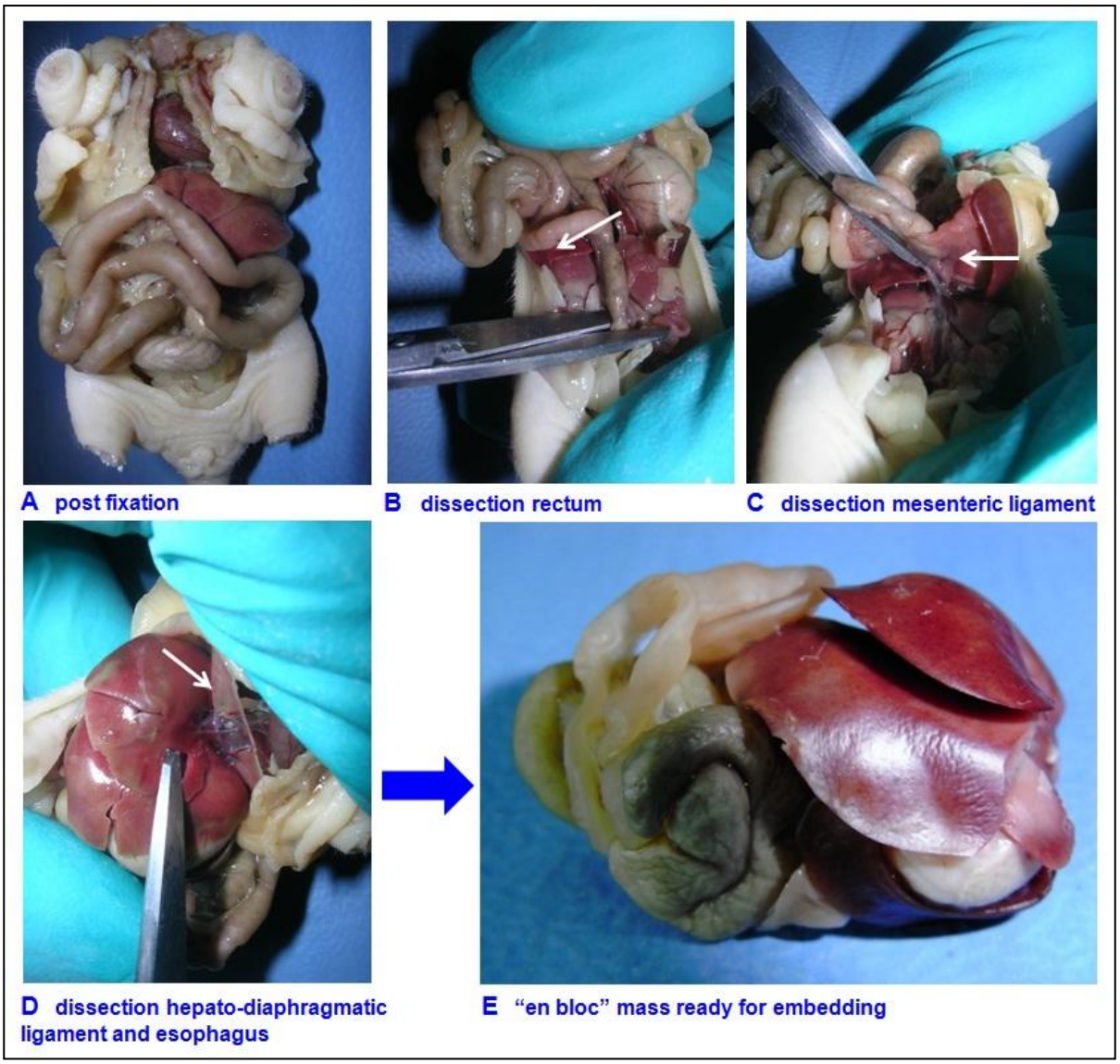

Fig.1: wholebpdy histotechnique

Appendix 6: Immunohistochemistry protocols

EGF Receptor (D38B1) XP – Cell Signaling								
Dilution	**Endogenous peroxidase inhibition**	**Ag retrieval**	**Serum blocking**	**Primary Ab diluent**	**Primary Ab incubation**	**Secondary Ab**	**Reveal System**	**Development**
1:150	3% H_2O_2	HIER citrate pH6	10% goat serum	specific Ab-diluent	1h room temperature	biotinylate anti-rabbit (Vectorlab) diluited in serum goat 10% (incubation 30 minutes RT)	ABC (30 min)	DAB (8 min)
Rabbit mAb: detects endogenous levels of total EGF receptor protein. This antibody does not cross-react with other proteins of the ErbB family.								

Phospho-EGF Receptor (Tyr1173) (53A5) – Cell Signaling								
Dilution	**Endogenous peroxidase inhibition**	**Ag retrieval**	**Serum blocking**	**Primary Ab diluent**	**Primary Ab incubation**	**Secondary Ab**	**Reveal System**	**Development**
1:150	3% H_2O_2	HIER citrate pH6	10% goat serum	specific Ab-diluent	1h room temperature	biotinylate anti-rabbit (Vectorlab) diluited in serum goat 10% (incubation 30 minutes RT)	ABC (30 min)	DAB (8 min)
Rabbit mAb: detects endogenous EGF receptors only when phosphorylated at Tyr1173. This antibody may cross-react with other activated receptor tyrosine kinases.								

Phospho-EGF Receptor (Tyr1068) (D7A5) XP – Cell Signaling								
Dilution	**Endogenous peroxidase inhibition**	**Ag retrieval**	**Serum blocking**	**Primary Ab diluent**	**Primary Ab incubation**	**Secondary Ab**	**Reveal System**	**Development**
1:200	3% H_2O_2	HIER EDTA pH8	10% goat serum	specific Ab-diluent	1h room temperature	biotinylate anti-rabbit (Vectorlab) diluited in serum goat 10% (incubation 30 minutes RT)	ABC (30 min)	DAB (8 min)
Rabbit mAb: detects endogenous EGF receptor only when phosphorylated at Tyr1068. This antibody may cross-react weakly with other tyrosinephosphorylated proteins.								

Akt (pan) (11E7) – Cell Signaling								
Dilution	**Endogenous peroxidase inhibition**	**Ag retrieval**	**Serum blocking**	**Primary Ab diluent**	**Primary Ab incubation**	**Secondary Ab**	**Reveal System**	**Development**
1:350	3% H_2O_2	HIER citrate pH6	10% goat serum	specific Ab-diluent	1h room temperature	biotinylate anti-rabbit (Vectorlab) diluited in serum goat 10% (incubation 30 minutes RT)	ABC (30 min)	DAB (8 min)
Rabbit mAb: detects endogenous levels of total Akt protein. This antibody does not cross-react with other related proteins.								

Phospho-Akt (Ser473) (D9E) XP – Cell Signaling								
Dilution	**Endogenous peroxidase inhibition**	**Ag retrieval**	**Serum blocking**	**Primary Ab diluent**	**Primary Ab incubation**	**Secondary Ab**	**Reveal System**	**Development**
1:50	3% H_2O_2	HIER citrate pH6	10% goat serum	specific Ab-diluent	1h room temperature	biotinylate anti-rabbit (Vectorlab) diluited in serum goat 10% (incubation 30 minutes RT)	ABC (30 min)	DAB (8 min)
Rabbit mAb: detects endogenous levels of Akt only when phosphorylated at Ser473								

p44 MAPK (Erk1) (N-Term) - Epitomics								
Dilution	**Endogenous peroxidase inhibition**	**Ag retrieval**	**Serum blocking**	**Primary Ab diluent**	**Primary Ab incubation**	**Secondary Ab**	**Reveal System**	**Development**
1:150	3% H_2O_2	HIER citrate pH6	10% goat serum	10% goat serum	1h room temperature	biotinylate anti-rabbit (Vectorlab) diluited in serum goat 10% (incubation 30 minutes RT)	ABC (30 min)	DAB (8 min)
Rabbit mAb: detects endogenous levels of p44 MAP Kinase (Erk1)which activation occurs through phosphorylation of threonine 202 and tyrosine 204 of human MAP kinase. Erk1 is also known to autophosphorylate on tyrosine. This antibody does not cross-react with other MAP kinases.								

Phospho-p44/42 MAPK (Erk1/2) (thr202/Tyr204) – Cell Signaling								
Dilution	**Endogenous peroxidase inhibition**	**Ag retrieval**	**Serum blocking**	**Primary Ab diluent**	**Primary Ab incubation**	**Secondary Ab**	**Reveal System**	**Development**
1:350	3% H_2O_2	HIER citrate pH6	10% goat serum	specific Ab-diluent	1h room temperature	biotinylate anti-rabbit (Vectorlab) diluited in serum goat 10% (incubation 30 minutes RT)	ABC (30 min)	DAB (8 min)
Rabbit mAb: detects endogenous levels of p44 and p42 MAP Kinase (Erk1 and Erk2) when dually phosphorylated at Thr202 and Tyr204 of Erk1 (Thr185 and Tyr187 of Erk2), and singly phosphorylated at Thr202. This antibody does not cross-react with the corresponding phosphorylated residues of either JNK/SAPK or p38 MAP kinases.								

Cleaved Caspase-3 (Asp175) – Cell Signaling								
Dilution	**Endogenous peroxidase inhibition**	**Ag retrieval**	**Serum blocking**	**Primary Ab diluent**	**Primary Ab incubation**	**Secondary Ab**	**Reveal System**	**Development**
1:2000	3% H_2O_2	HIER citrate pH6	10% goat serum	10% goat serum	1h room temperature	biotinylate anti-rabbit (Vectorlab) diluited in serum goat 10% (incubation 30 minutes RT)	ABC (30 min)	DAB (8 min)
Rabbit polyAb: detects endogenous levels of the large fragment (17/19 kDa) of activated caspase-3 resulting from cleavage adjacent to Asp175. This antibody does not recognize full length caspase-3 or other cleaved caspases.								

Anti-mouse CD31 clone SZ31 – Dianova								
Dilution	**Endogenous peroxidase inhibition**	**Ag retrieval**	**Serum blocking**	**Primary Ab diluent**	**Primary Ab incubation**	**Secondary Ab**	**Reveal System**	**Development**
1:50	3% H_2O_2	HIER citrate pH6	10% rabbit serum	10% rabbit serum	1h room temperature	biotinylate anti-rabbit (Vectorlab) diluited in serum goat 10% (incubation 30 minutes RT)	ABC (30 min)	DAB (8 min)
Rat mAb: detects endogenous levels of CD31, an integral membrane glycoprotein expressed on the surface of embryonic and adult endothelial cells, which play a major role in angiogenesis.								

Ki67 clone SP6 – Thermo Scientific								
Dilution	**Endogenous peroxidase inhibition**	**Ag retrieval**	**Serum blocking**	**Primary Ab diluent**	**Primary Ab incubation**	**Secondary Ab**	**Reveal System**	**Development**
1:150	3% H_2O_2	HIER citrate pH6	10% goat serum	10% goat serum	1h room temperature	not applicable	Dako EnVision rabbit	DAB (8 min)
Rabbit mAb: detects Ki-67, a nuclear protein, which is expressed in proliferating cells, preferentially during late G1-, S-, M-, and G2-phases of the cell cycle, while cells in the G0 (quiescent) phase are negative for this protein.								

Wilm's Tumour Antigen 1 - Epitomics								
Dilution	**Endogenous peroxidase inhibition**	**Ag retrieval**	**Serum blocking**	**Primary Ab diluent**	**Primary Ab incubation**	**Secondary Ab**	**Reveal System**	**Development**
1:100	3% H_2O_2	HIER citrate pH6	10% goat serum	10% goat serum	1h room temperature	biotinylate anti-rabbit (Vectorlab) diluited in serum goat 10% (incubation 30 minutes RT)	ABC (30 min)	DAB (8 min)
Rabbit mAb: detects human Wilms tumour WT1 gene product.								

Appendix 7: Raw data for Caspase 3, KI67 and CD31

MSTO IDt	IDd	KI67 field	Negative cells	Positive cells	Total cells	% positive cells	Negative cells Σ	Positive cells Σ	Total cells Σ	Mean % positive cells
Gr1-6	1	400x	84	171	255	**67,05882**	279	476	755	**63,04635762**
		400x0001	98	140	238	**58,82353**				
		400x0002	97	165	262	**62,9771**				
Gr1-235	5	400x	45	244	289	**84,42907**	173	689	862	**79,93039443**
		400x0001	52	226	278	**81,29496**				
		400x0002	76	219	295	**74,23729**				
Gr2-1	7	400x	88	43	131	**32,82443**	283	136	419	**32,45823389**
		400x0001	89	45	134	**33,58209**				
		400x0002	106	48	154	**31,16883**				
Gr2-3	9	400x	129	45	174	**25,86207**	305	157	462	**33,98268398**
		400x0001	86	45	131	**34,35115**				
		400x0002	90	67	157	**42,67516**				
Gr6-24	26	400x	132	39	171	**22,80702**	362	173	535	**32,3364486**
		400x0001	144	86	230	**37,3913**				
		400x0002	86	48	134	**35,8209**				
Gr6-25	27	400x	108	42	150	**28**	376	140	516	**27,13178295**
		400x0001	89	65	154	**42,20779**				
		400x0002	179	33	212	**15,56604**				

MSTO IDt	IDd	CASPASE field	Negative cells	Positive cells	Total cells	% positive	Negative cells Σ	Positive cells Σ	Total cells Σ	Mean % positive cells
Gr1-6	1	400x	190	22	212	**10,37736**	640	47	687	**6,841339156**
		400x0001	216	7	223	**3,139013**				
		400x0002	234	18	252	**7,142857**				
Gr1-235	5	400x	279	24	303	**7,920792**	780	54	834	**6,474820144**
		400x0001	268	10	278	**3,597122**				
		400x0002	233	20	253	**7,905138**				
Gr2-1	7	400x	95	4	99	**4,040404**	304	29	333	**8,708708709**
		400x0001	84	16	100	**16**				
		400x0002	125	9	134	**6,716418**				
Gr2-3	9	400x	166	12	178	**6,741573**	404	18	422	**4,265402844**
		400x0001	121	1	122	**0,819672**				
		400x0002	117	5	122	**4,098361**				
Gr6-24	26	400x	180	17	197	**8,629442**	488	36	524	**6,870229008**
		400x0001	143	7	150	**4,666667**				
		400x0002	165	12	177	**6,779661**				
Gr6-25	27	400x	111	8	119	**6,722689**	335	40	375	**10,66666667**
		400x0001	122	6	128	**4,6875**				
		400x0002	102	26	128	**20,3125**				

MSTO IDt	IDd	CD31 field	Partial Area µm²	Positive vessels	Vessel/500 µm2	Total Area µm²	Positive vessels	Vessel/500 µm2
Gr1-6	1	200x	198918,8	118	**0,296603513**	596756,3	279	**0,233764**
		200x0001	198918,8	94	**0,236277375**			
		200x0002	198918,8	67	**0,168410469**			
Gr1-235	5	200x	198918,8	85	**0,213655073**	596756,3	313	**0,262251**
		200x0001	198918,8	172	**0,432337324**			
		200x0002	198918,8	56	**0,140760989**			
Gr2-1	7	200x	198918,8	53	**0,133220222**	486133,4	148	**0,152222**
		200x0001	193855,9	47	**0,121224064**			
		200x0002	93358,71	48	**0,257072961**			
Gr2-3	9	200x	198918,8	49	**0,123165865**	554945,3	182	**0,16398**
		200x0001	157107,8	63	**0,200499326**			
		200x0002	198918,8	70	**0,175951236**			
Gr6-24	26	200x	198918,8	66	**0,16589688**	596756,3	161	**0,134896**
		200x0001	198918,8	41	**0,103057153**			
		200x0002	198918,8	54	**0,135733811**			
Gr6-25	27	200x	198918,8	28	**0,070380495**	469319,7	72	**0,076707**
		200x0001	110577,3	22	**0,099477931**			
		200x0002	159823,7	22	**0,068825855**			

REN IDt	IDd	KI67 field	Negative cells	Positive cells	Total cells	% positive	Negative cells Σ	Positive cells Σ	Total cells Σ	Mean % positive cells
		400x	56	266	322	**82,6087**				
Gr1-1	**2**	400x0001	60	269	329	**81,76292**	194	778	972	**80,04115226**
		400x0002	78	243	321	**75,70093**				
		400x	24	305	329	**92,70517**				
Gr1-3	**4**	400x0001	26	303	329	**92,09726**	78	925	1003	**92,22333001**
		400x0002	28	317	345	**91,88406**				
		400x	37	226	263	**85,93156**				
Gr2-5	**6**	400x0001	67	280	347	**80,69164**	132	740	872	**84,86238532**
		400x0002	28	234	262	**89,31298**				
		400x	125	254	379	**67,01847**				
Gr2-6	**7**	400x0001	22	332	354	**93,78531**	168	858	1026	**83,62573099**
		400x0002	21	272	293	**92,83276**				
		400x	87	223	310	**71,93548**				
Gr6-145	**28**	400x0001	54	207	261	**79,31034**	221	607	828	**73,30917874**
		400x0002	80	177	257	**68,8716**				
		400x	49	293	342	**85,67251**				
Gr6-156	**29**	400x0001	16	294	310	**94,83871**	131	710	841	**84,42330559**
		400x0002	66	123	189	**65,07937**				

REN IDt	IDd	CASPASE field	Negative cells	Positive cells	Total cells	% positive	Negative cells Σ	Positive cells Σ	Total cells Σ	Mean % positive cells
		400x	324	6	330	**1,818182**				
Gr1-1	**2**	400x0001	291	5	296	**1,689189**	926	19	945	**2,010582011**
		400x0002	311	8	319	**2,507837**				
		400x	320	1	321	**0,311526**				
Gr1-3	**4**	400x0001	324	6	330	**1,818182**	999	15	1014	**1,479289941**
		400x0002	355	8	363	**2,203857**				
		400x	272	8	280	**2,857143**				
Gr2-5	**6**	400x0001	307	8	315	**2,539683**	814	28	842	**3,325415677**
		400x0002	235	12	247	**4,8583**				
		400x	235	7	242	**2,892562**				
Gr2-6	**7**	400x0001	306	8	314	**2,547771**	790	19	809	**2,348578492**
		400x0002	249	4	253	**1,581028**				
		400x	246	15	261	**5,747126**				
Gr6-145	**28**	400x0001	252	15	267	**5,617978**	766	47	813	**5,781057811**
		400x0002	268	17	285	**5,964912**				
		400x	221	13	234	**5,555556**				
Gr6-156	**29**	400x0001	255	11	266	**4,135338**	725	32	757	**4,227212682**
		400x0002	249	8	257	**3,11284**				

REN IDt	IDd	CD31 field	Partial Area μm^2	Positive vessels	Vessel /500 µm2	Total Area μm^2	Positive vessels	Vessel/500 µm2
		200x	198918,8	26	**0,065353316**			
Gr1-1	**2**	200x0001	198918,8	15	**0,037703836**	596756,3	88	**0,073732**
		200x0002	198918,8	47	**0,118138687**			
		200x	198918,8	35	**0,087975618**			
Gr1-3	**4**	200x0001	198918,8	45	**0,113111509**	596756,3	108	**0,090489**
		200x0002	198918,8	28	**0,070380495**			
		200x	198918,8	39	**0,098029975**			
Gr2-5	**6**	200x0001	198918,8	27	**0,067866905**	596756,3	96	**0,080435**
		200x0002	198918,8	30	**0,075407673**			
		200x	198918,8	32	**0,080434851**			
Gr2-6	**7**	200x0001	198918,8	38	**0,095516385**	596756,3	115	**0,096354**
		200x0002	198918,8	45	**0,113111509**			
		200x	198918,8	21	**0,052785371**			
Gr6-145	**28**	200x0001	127636,7	7	**0,027421572**	525474,2	31	**0,029497**
		200x0002	198918,8	3	**0,007540767**			
		200x	198918,8	0	**0**			
Gr6-156	**29**	200x0001	198918,8	31	**0,077921262**	565487,1	61	**0,053936**
		200x0002	167649,6	30	**0,089472355**			

Appendix 8: Raw data for EGFR, AKT and ERK

	MARKER		TOTAL AREA	POSITIVE AREA	% POSITIVE AREA	Σ total area	Σ positive area	%total positive area
	IDt	IDd						
EGFR	panEGFR-235	5	198918,7	187058,03	94,04	596756,1	564594,39	**94,61057709**
	panEGFR-235a		198918,7	185816,92	93,41			
	panEGFR-235b		198918,7	191719,44	96,38			
	panEGFR-3	9	198918,7	113104,18	56,86	475771,14	327745,05	**68,88712291**
	panEGFR-3a		198918,7	156937,38	78,9			
	panEGFR-3b		77933,74	57703,49	74,04			
	panEGFR-24	26	198918,7	69684,3	35,03	596756,1	161311,9	**27,03146227**
	panEGFR-24a		198918,7	31784,85	15,98			
	panEGFR-24b		198918,7	59842,75	30,08			
	pEGFR-235	5	198918,7	23321,57	11,72	543971,34	149724,14	**27,52426994**
	pEGFR-235a		198918,7	24320,22	12,23			
	pEGFR-235b		146133,94	102082,35	69,86			
	pEGFR-3	9	198918,7	34760,23	17,47	579915,53	102258,37	**17,63332153**
	pEGFR-3a		182078,13	7584,8	4,17			
	pEGFR-3b		198918,7	59913,34	30,12			
	pEGFR-24	26	198918,7	8344,3	4,19	596756,1	136610,93	**22,89225531**
	pEGFR-24a		198918,7	38992,8	19,6			
	pEGFR-24b		198918,7	89273,83	44,88			
AKT	panAKT-235	5	198918,7	154441,8	77,64	596756,1	446411,46	**74,80635053**
	panAKT-235a		198918,7	156640,19	78,75			
	panAKT-235b		198918,7	135329,47	68,03			
	panAKT-3	9	198918,7	59943,66	30,13	546149,52	115420,02	**21,1334105**
	panAKT-3a		198918,7	34304,24	17,25			
	panAKT-3b		148312,12	21172,12	14,28			
	panAKT-24	26	198918,7	106221,59	53,4	795674,8	410599,68	**51,60395679**
	panAKT-24a		198918,7	139157,4	69,96			
	panAKT-24b		198918,7	124158,89	62,42			
	panAKT-24c		198918,7	41061,8	20,64			
	pAKT-235	5	198918,7	13869,82	6,97	554675,18	98929,12	**17,8355051**
	pAKT-235a		198918,7	25241,49	12,69			
	pAKT-235b		156837,78	59817,81	38,14			
	pAKT-3	9	93906,18	11337,37	12,07	491743,58	42030,88	**8,547316469**
	pAKT-3a		198918,7	21793,73	10,96			
	pAKT-3b		198918,7	8899,78	4,47			
	pAKT-24	26	198918,7	6950,05	3,49	596756,1	18082,89	**3,030197764**
	pAKT-24a		198918,7	10420,71	5,24			
	pAKT-24b		198918,7	712,13	0,36			
ERK	ERK1-235	5	198918,7	164173,75	82,53	668299,03	500780,76	**74,93363562**
	ERK1-235a		198918,7	121319,03	60,99			
	ERK1-235b		114921,82	100633,54	87,57			
	ERK1-235c		155539,81	114654,44	73,71			
	ERK1-3	9	198918,7	170200,43	85,56	596756,1	458796,06	**76,88167075**
	ERK1-3a		198918,7	117341,32	58,99			
	ERK1-3b		198918,7	171254,31	86,09			
	ERK1-24	26	198918,7	133182,98	66,95	596756,1	426300,51	**71,43630539**
	ERK1-24a		198918,7	127846,24	64,27			
	ERK1-24b		198918,7	165271,29	83,08			
	ERK12-235	5	198918,7	58317,95	29,32	536134,16	123067,97	**22,95469664**
	ERK12-235a		198918,7	22508,89	11,32			
	ERK12-235b		138296,76	42241,13	30,54			
	ERK12-3	9	198918,7	26515,14	13,33	503301,71	135688,59	**26,95969183**
	ERK12-3a		170821,92	69190,64	40,5			
	ERK12-3b		133561,09	39982,81	29,94			
	ERK12-24	26	198918,7	207,96	0,1	596756,1	5710	**0,956839821**
	ERK12-24a		198918,7	4960,45	2,49			
	ERK12-24b		198918,7	541,59	0,27			